UNCLASSIFIED

SLL 80 487/AO/M

~~Porter~~ RLP
Sepucha RCS
File: Rockwell; misc.

NASA CONTRACTOR REPORT

NASA CR-159630

C76-1555/501

Bob- didn't the Lewis laser get closed down? Any work still going on?
Ron

NASA CR-159630

HIGH POWER PHASE LOCKED LASER OSCILLATORS

LASER
AO, M,

Prepared By:

C.L. Hayes, C. L. Telk, J. Soohoo, and W. C. Davis

Prepared for:

National Aeronautics and Space Administration
Lewis Research Center
Cleveland, Ohio

u3982

NATIONAL AERONAUTICS AND SPACE ADMINISTRATION • WASHINGTON, D.C. • MAY 1979

UNCLASSIFIED

Accession Number: 3982

Publication Date: May 01, 1979

Title: High Power Phase Locked Laser Oscillators

Personal Author: Hayes, C.L.; Telk, C.L.; SooHoo, J.; Davis, W.C.

Corporate Author Or Publisher: Rockwell International, 3370 Miraloma Avenue, Anaheim, CA 92803 Report Number: C76-1555/01

Report Prepared for: NASA Lewis Research Center, 21000 Brookpark Road, Cleveland, OH 44135 Report Number Assigned by Contract Monitor: SLL 80 487

Comments on Document: Archive, RRI, DEW

Descriptors, Keywords: High Power Phase Locked Laser Oscillator Adaptive Effect Beam Atmosphere Physics Satellite Tracking Optics

Pages: 00099

Cataloged Date: Dec 03, 1992

Contract Number: NAS3-20376

Document Type: HC

Number of Copies In Library: 000001

Record ID: 25409

Source of Document: DEW

1. Report No.	2. Government Accession No.	3. Recipient's Catalog No.
CR159630		

4. Title and Subtitle	5. Report Date
High Power Phase Locked Laser Oscillators	May 1979
	6. Performing Organization Code

7. Author(s)	8. Performing Organization Report No.
C. L. Hayes, C. L. Telk, J. SooHoo, W. C. Davis	C76-1555/501
	10. Work Unit No.

9. Performing Organization Name and Address	11. Contract or Grant No.
Rockwell International 3370 Miraloma Avenue Anaheim, CA 92803	NAS3-20376
	13. Type of Report and Period Covered
	FINAL REPORT

12. Sponsoring Agency Name and Address	14. Sponsoring Agency Code
NASA Lewis Research Center 21000 Brookpark Road Cleveland, Ohio 44135	

15. Supplementary Notes

None

16. Abstract

The feasibility of mechanizing an adaptive array of independent laser oscillators for generation of a high power coherent output was experimentally investigated. Tests were structured to evaluate component/system requirements for delivery of energy to a low-earth orbit satellite. Initial experiments addressed the control issues of phase locking unstable resonators at low power levels. A successful phase lock demonstration formed the basis for the design and fabrication of the high power, water-cooled, control mirror subsequently installed in the NASA LeRC high power laser.

Tests were then performed to characterize the operational limits of the laser system and included quantitative assessment of the frequency stability, "noise" sources, and optical properties of the beam. Phase lock operation by cavity length control was demonstrated when augmented with a wideband control loop. Results of these tests positively indicate the feasibility and practicality of generating large quantities of power by combining multiple laser cavities. Delivery of the energy to a remote station with an adaptive array can now be considered.

17. Key Words (Suggested by Author(s))	18. Distribution Statement
High Power Laser Systems Adaptive Effects on Laser Beams Atmospheric Physics Satellite Tracking Adaptive Optics	Unclassified - Unlimited

19. Security Classif. (of this report)	20. Security Classif. (of this page)	21. No. of Pages	22. Price*
Unclassified	Unclassified	99	

* For sale by the National Technical Information Service, Springfield, Virginia 22161

TABLE OF CONTENTS

LIST OF ILLUSTRATIONS

LIST OF ILLUSTRATIONS (CONT.)

LIST OF ILLUSTRATIONS (CONT.)

LIST OF TABLES

I. INTRODUCTION AND SUMMARY

For several years Rockwell International has been developing a new and unique laser control technique. This new method uses automatic servo control of laser resonator parameters to achieve stabilization and control of the absolute temporal phase of the output of individual laser oscillators. With this approach, high power systems are possible by coherently combining the outputs of a number of lower power devices. This concept has been previously demonstrated experimentally and put on a sound theoretical foundation on the basis of the following:

- Lock of the absolute phase of a pair of 5-watt low pressure CO_2 lasers to a precision of $< 1°$ rms.
- Loss free combination of the outputs of multiple locked CO_2 laser oscillators.
- Phase lock of multiple high pressure CO_2 waveguide oscillators operating at equally spaced frequencies to produce a pulse train output from CW laser oscillators.
- Assembly of multiple phase locked CO_2 laser oscillators into an adaptive array.

In parallel with this effort, studies have been conducted to assess the significant technical problems involved in transmitting substantial quantities (up to 5 MW) of laser power to a satellite in low altitude circular orbit. This work was performed under Contract No. NAS3-18937, sponsored by the NASA Lewis Research Center (Final Report NASA CR-134952). That effort was directed toward a detailed assessment of atmospheric effects, and estab-

lished the adaptive optics system parameters necessary to achieve efficient power transfer in the presence of atmospheric turbulence, thermal blooming, and other perturbations to the optical system. A number of conceptual optical systems to perform the required energy transfer were evaluated on the basis of efficiency, reliability, size and weight, advanced technology requirements, and potential cost. The phase locked array of lasers showed very substantial advantages in four of these five evaluation criteria, and only a slight disadvantage in the fifth. Perhaps surprisingly, one of the primary advantages turned out to be substantial reductions in the size, cost, and weight of the beam pointing system that resulted from the use of individual pointing systems in a hexagonal close packed array, as opposed to a single (Mt. Palomar class) pointing system for a single laser beam. These results provided the motivation for extending phase lock control techniques into the high power region.

Over the last several years, research workers at NASA Lewis have developed a very carefully engineered and instrumented transverse flow, transverse discharge, CO_2 laser facility (Figure 1). Because of its unique operating characteristics and specific gain region dimensions, this laser is ideally configured for experiments in high power laser phase locking. The configuration is such that five individual unstable resonator cavities could be arranged in the existing gain region with a minimum of required hardware changes (Figure 2). The vibration environment is quite reasonable, in contrast to the $\sim$ 120 db noise level which must be dealt with in many high energy laser sources. This program was directed toward obtaining specific design data on this high power laser facility and answering certain key feasibility questions with respect to high energy laser phase locking with unstable

NASA
C-76-2845

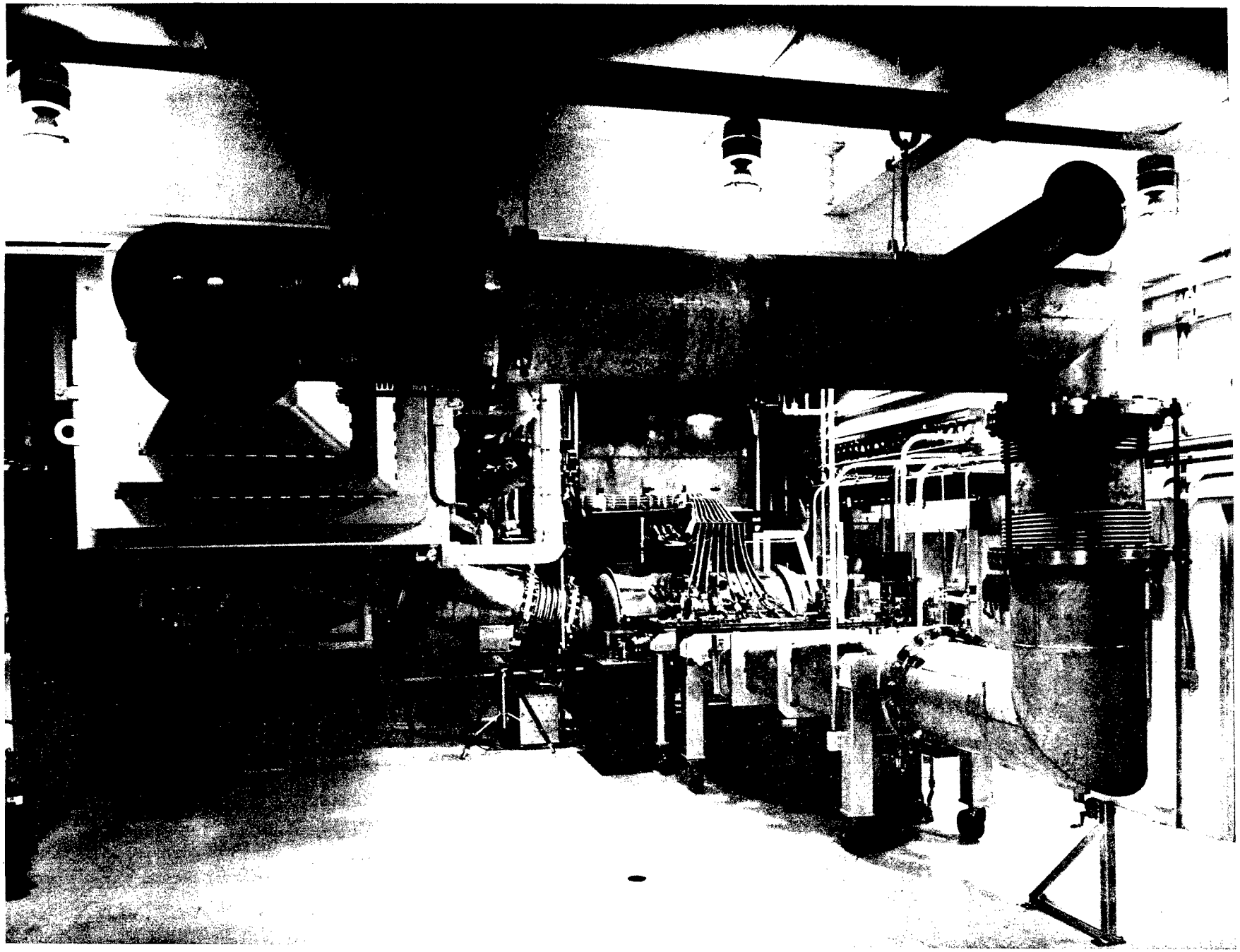

Figure 1. NASA Lewis Laser

LASER TEST CAVITY

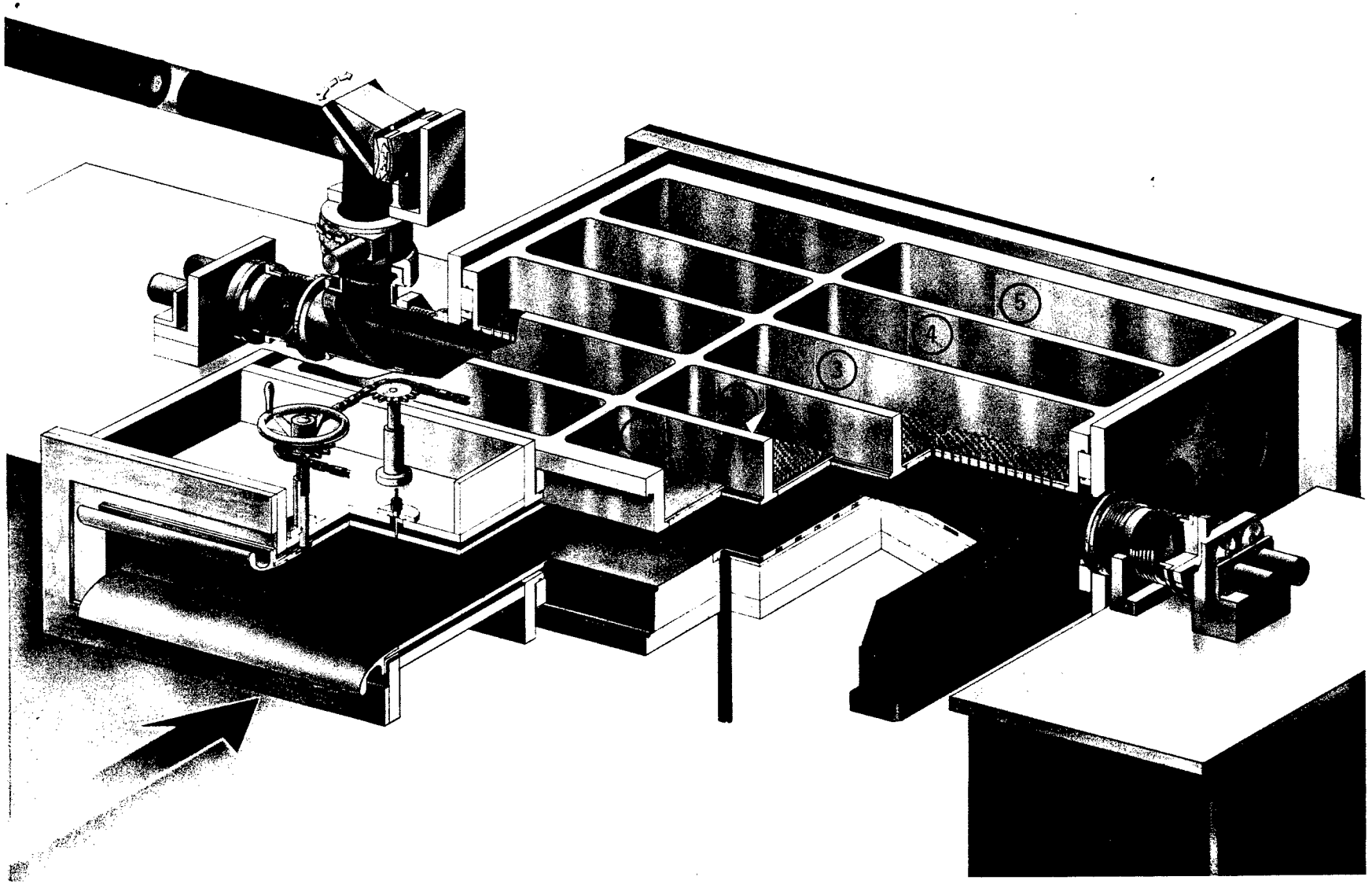

Figure 2. Concept Photo of Oscillator Configuration

resonator cavities. Thus, this program represents a first step toward a very important technological development - the capability to phase lock multiple high energy laser sources and assemble them into adaptive arrays.

The effort, as performed, was divided into five technical tasks. The first consisted of computer modeling of the phase distribution sensitivity for unstable resonator configuration changes; the second was an experimental demonstration of phase locking with low power unstable resonators; the third was measurements of the frequency stability of the NASA laser; the fourth was the design and fabrication of the cavity length control mirror for phase locking an unstable resonator; and the fifth task involved experiments conducted to demonstrate the potential of the phase locking process when applied to the high energy laser. Each task is reported individually in Section II through VI, respectively.

At the onset of this program, there was very little data available on the frequency stability of unstable laser resonators. In addition, because of the larger size end mirrors and the extreme angular alignment sensitivity associated with unstable resonators, it was not apparent that the methodology used in phase locking stable configuration lasers was acceptable. The measurements made in Task II, however, clearly indicated that there were no extraordinary frequency instabilities associated with unstable resonators for either a flowing or nonflowing gain medium, at least not for the low pressures used. The results obtained also indicated that while the angular alignment sensitivity of the resonator was a problem, we could achieve a good phase lock to a reference laser using control techniques very similar to those applied to stable laser configurations.

For the most part, experimental observations with fast-flow high power CO_2 lasers have been characterized by complex output wavefronts produced by temporal and spatial changes in the gain medium of the laser. When the Task III measurements started, it was feared that conditions such as these would produce not only rapid changes in the transition line the NASA laser was running on, but also large frequency changes in the output when the laser was operating in a single line. The results of the frequency stability measurements made with the NASA laser have shown that the initial concern was unwarranted. The data collected indicated that when the resonator optics were properly aligned, the laser operated on only the P(20) transition. In addition, it was found that while the total bandwidth of the output frequency instability was about a factor of 10 greater than had been measured with the low pressure unstable resonator, it was not so great that a different methodology of phase locking would have to be considered. As part of Task III, subsequent interferometric measurements were made to determine the cause of the observed frequency instabilities. These results clearly indicated that, except for some thermal wedging, which was nearly constant with input power, the laser gain medium exhibited no index changes that would result in frequency variations of the resonator output. In fact, it was learned that acoustic vibrations transmitted through the floor from three different sources could account for the frequency instabilities observed. Fortunately, it is possible to remove two of the sources during laser operation and it may be further possible to reduce to insignificance the effects of the third vibration source by some straightforward mechanical techniques.

Based on the LeRC laser cavity dimensions and the results of the preceding frequency instability measurements, modification of the resonator mirrors

were made to provide cavity length control for adjusting the laser frequency as part of a servo system. Design goals were established as 0.5 micrometers of piston motion at rates up to 500 Hz and a dynamic range of 5.0 micrometers at rates up to 5 Hz. A power density of 1000 watts/cm^2 was assumed which required water cooling of the copper assembly. Complete design details are presented in Section V.

Finally, as described in Section VI, tests were conducted at the NASA Lewis facility to ascertain the limits of system/component performance. Both single channel and two-channel operational tests were performed. Phase locked operation was achieved initially by controlling the cavity of a low power laser with respect to the NASA laser. Analysis of the control signals indicated several "noise" sources exceeded the originally observed frequency/bandwidth criteria. Changes were made to reduce the "noise" and tests conducted with control signals being applied to the high energy cavity. Phase lock operation was established by a combination of signals; low frequency/wide dynamic range was compensated by the water-cooled mirror and high frequency response furnished by the low power reference laser control circuitry.

In summary, the research effort performed was designed to determine the potential for phase locking multiple cavities of a laser system for the purpose of generating a large power output for use in an adaptive-array transmitter. Results of these tests indicate the feasibility and practicality of such an approach have been established. Several areas, however, require further development and investigation. Foremost is the requirement for a control mirror assembly with a greater deformation bandwidth product. With a parallel reduction in perturbing sources of frequency instability, high power array outputs can be demonstrated.

II. UNSTABLE RESONATOR MODELING

A. Introduction

As the basis for subsequent design and experimental tasks, an analysis of the NASA cavity configuration to be used in the phase lock experiment was the initial thrust of this program. Its purpose was to provide a means of estimating the laser output parameters in terms of phase (frequency) and power quantities. For reference purposes, the cavity mode structure in the absence of any perturbations was calculated. Small tilt and focus errors were then introduced on the otherwise ideal characteristics of the mode structure. Phase errors of this kind are usually present in real HEL cavities, as a result of cavity misalignment, gain-medium inhomogeneities, etc. Although phase errors of orders higher than tilt and focus could exist, their effects are usually much less dominating than that of the latter and therefore were not considered. The numerical results to be presented were obtained using the fast Fourier transform method, the formulation of which is discussed elsewhere.[1]

B. Numerical Results

The circular, unstable, positive branch-confocal cavity of the NASA laser device is depicted in Figure 3. The scraper mirror, which directs the output beam, is properly placed so that the effective diameter of mirror 1 is about 3.2 cm. Other relevant configuration parameter values are included in Figure 3.

1. Mode structure of Passive Cavity

The results of Figure 4 through 6 are for the passive cavity case, where there are no cavity perturbations present. Figure 4 and 5 are, respec-

1. J. SooHoo and G. E. Mevers, "Cavity Mode Analysis Using the Fourier Transform Method," Proc. IEEE, Vol. 62, No. 12, December 1974.

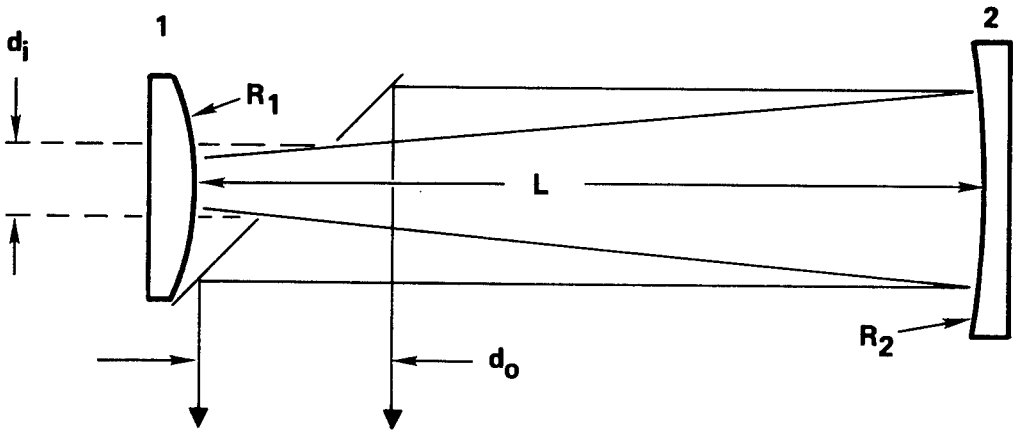

$R_1 = 17.5\ M$

$R_2 = 22\ M$

$d_i = 3.28\ cm$

$d_o = \left|\frac{R_2}{R_1}\right| d_i = 4.12\ cm$

$L = 2.25\ M$

$\lambda = 10.6\ \mu m$

Figure 3. NASA Cavity Configuration (Positive Branch Confocal)

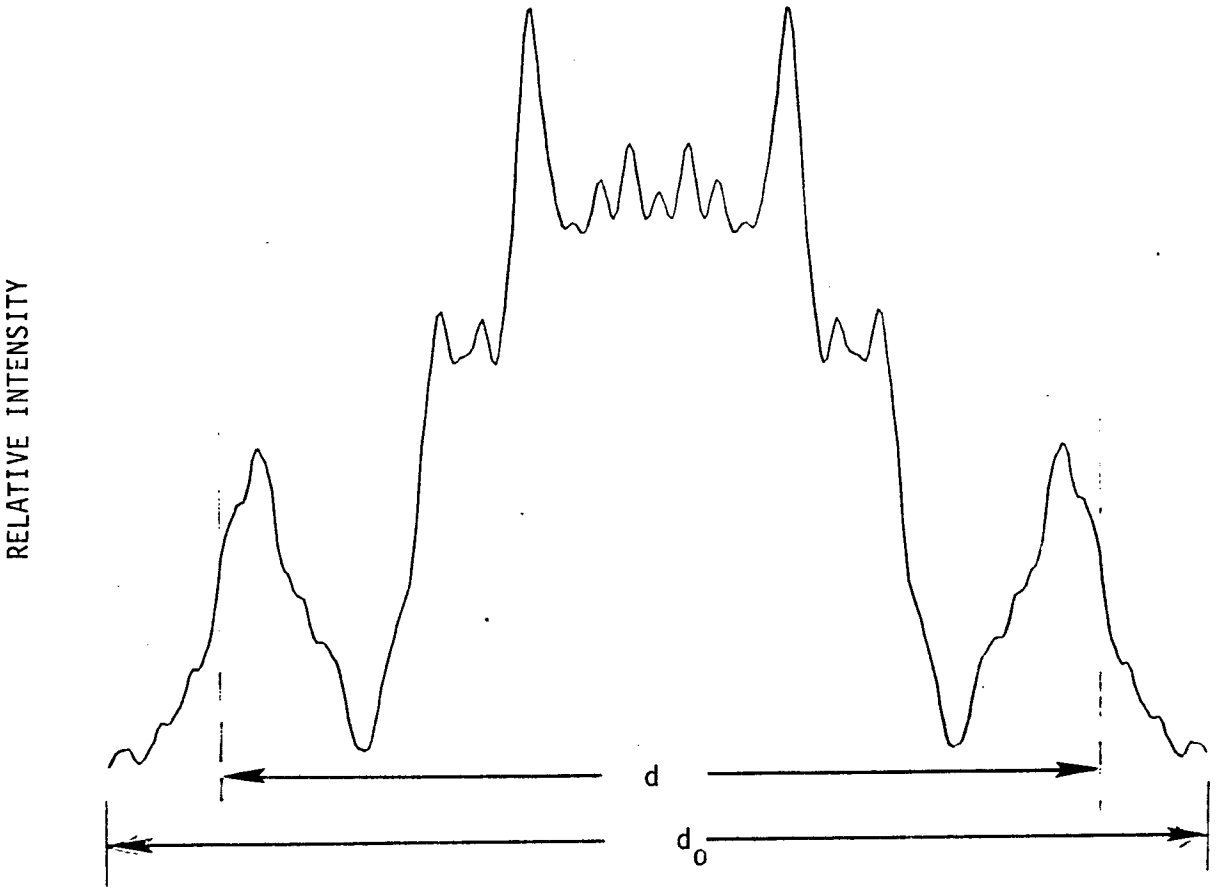

Figure 4. Near Field Intensity Distribution of Passive Cavity in the Plane of Mirror 1 When Scraper Mirror is Removed (d = hole diameter of scraper mirror, d_o = beam diameter at mirror 2).

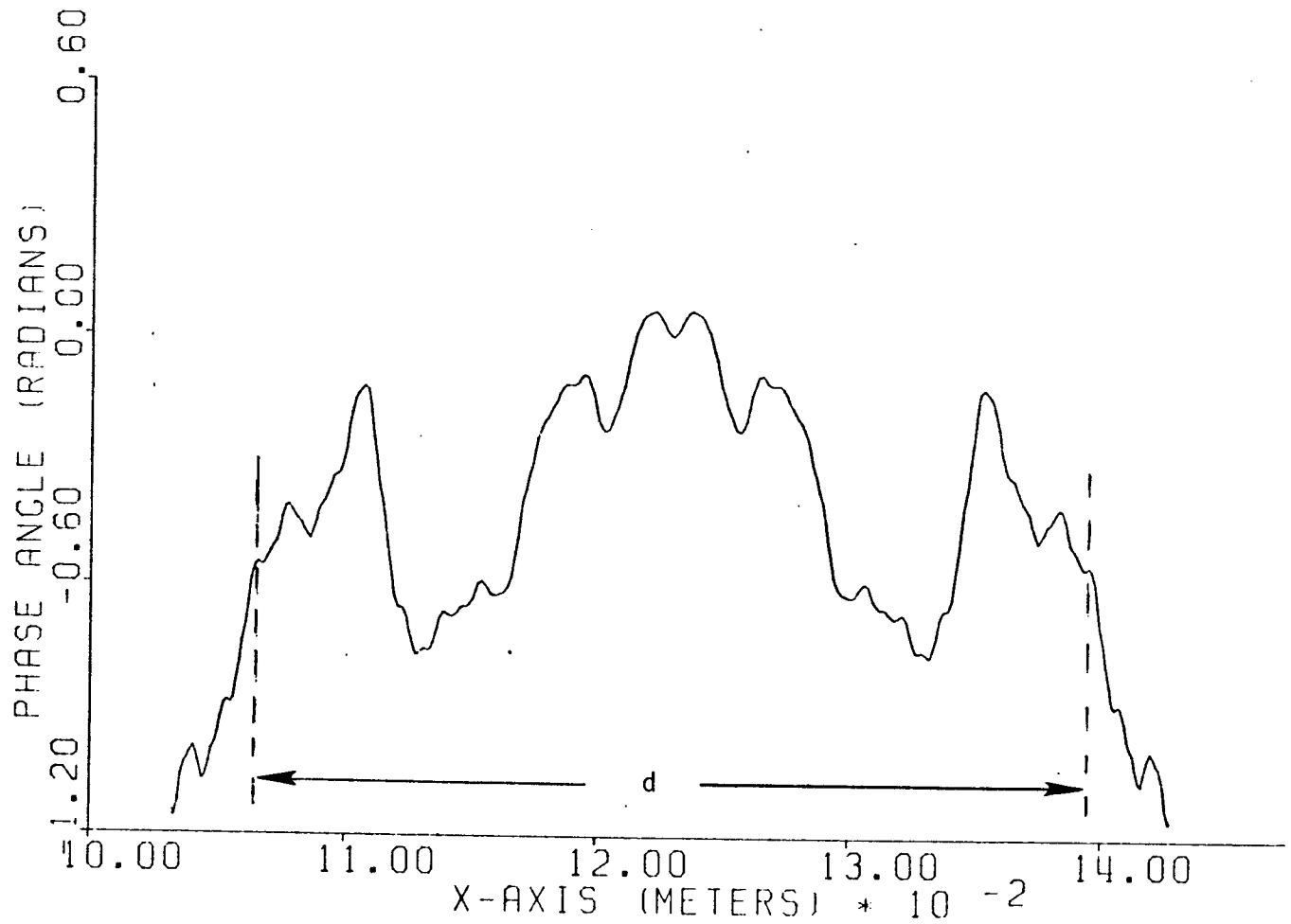

Figure 5. Near Field Phase Distribution of Passive Cavity in the Plane of Mirror 1 When Scraper Mirror is Removed (d = hole diameter of scraper mirror).

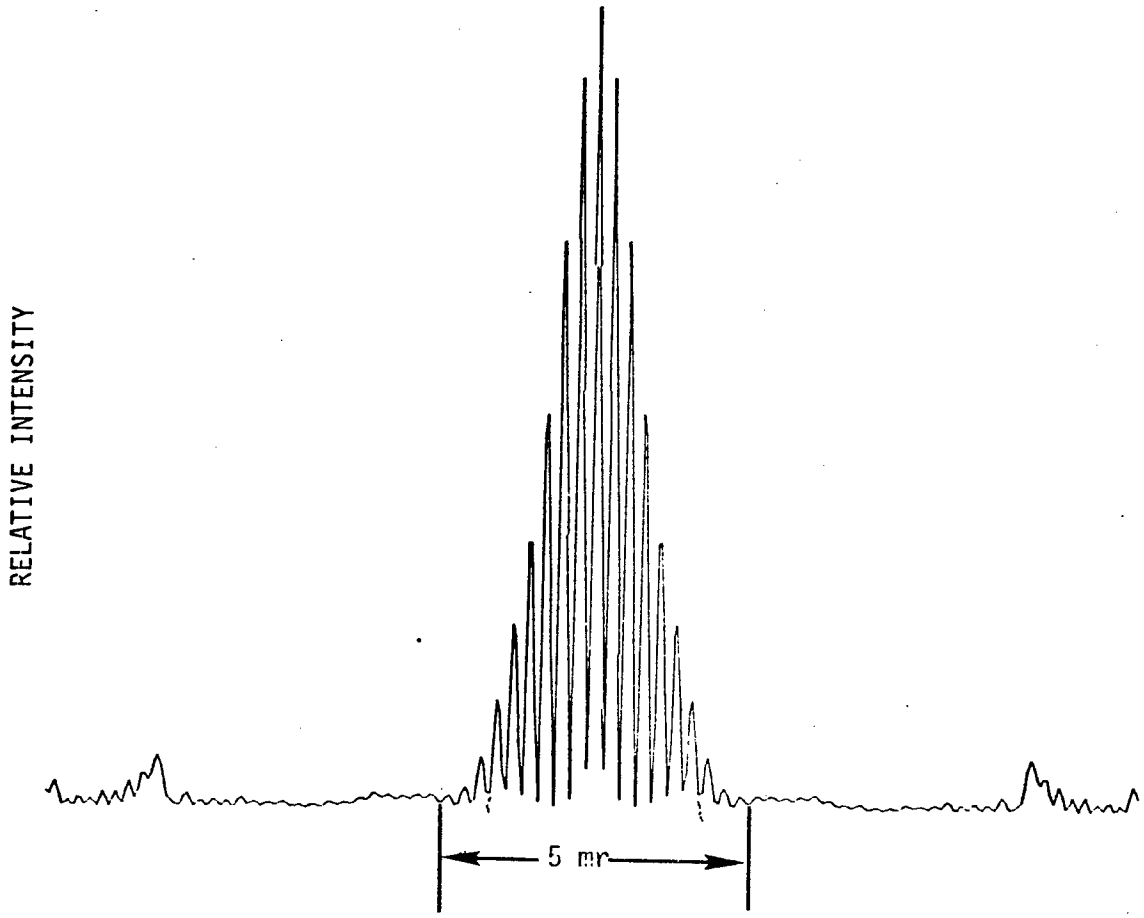

Figure 6. Far Field Intensity Distribution of Passive Cavity

tively, the internal intensity and phase distributions along a direction perpendicular to the cavity axis in the plane of mirror 1, when the scraper is removed. Unlike stable cavities, for which the dominant mode is Gaussian in amplitude and nearly constant in phase, the dominant mode of a typical unstable cavity has many fine structures (especially for large Fresnel number cavities). Since the field amplitude and phase distributions in the output annulus are not uniform, corresponding to the regions outside the dashed lines of Figures 4 and 5, the far-field pattern (Figure 6) is different from that of a uniform annulus of the same dimensions. For the far-field pattern of Figure 6, the lobe size is about 0.275 milliradians, which is about 1.13 λ/d_o. The far-field phase distribution (not shown) is found to be approximately uniform within the individual lobes, and the phase difference between adjacent lobes is about π, somewhat similar to that of a uniform annulus aperture distribution. The relative power within each ring structure is given in Table 1, with the central ring designated as ring 0. For heterodyne detection, it appears that optimum power can be achieved using a detector size of about 0.55 mr, just large enough to cover ring 1. This is so because the phase difference is about π between adjacent rings.

2. Effects of Focus and Tilt Errors

Figures 7 through 9 show the mode structure when the cavity length is decreased from 2.25 m to 2.09 m. That is, the focus of the large mirror is displaced 16 cm away from the confocal position, resulting in a focus error of about 1.5% (i.e., ratio of displacement to focal length). As can be seen from the figures, the effects of this focus error value on the mode structure are relatively small.

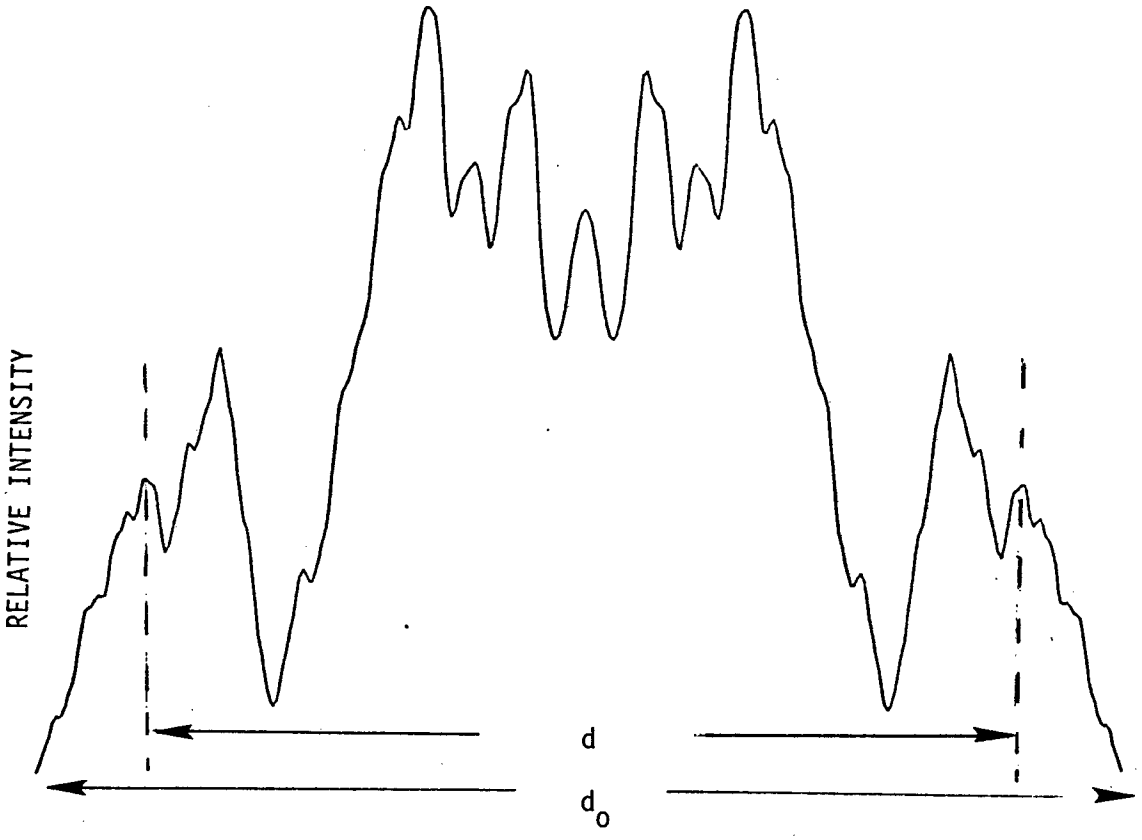

Figure 7. Near Field Intensity Distribution (with 1.5% Focus Error) in the Plane of Mirror 1 When Scraper Mirror is Removed (d = hole diameter of scraper mirror, d_o = beam diameter at mirror 2).

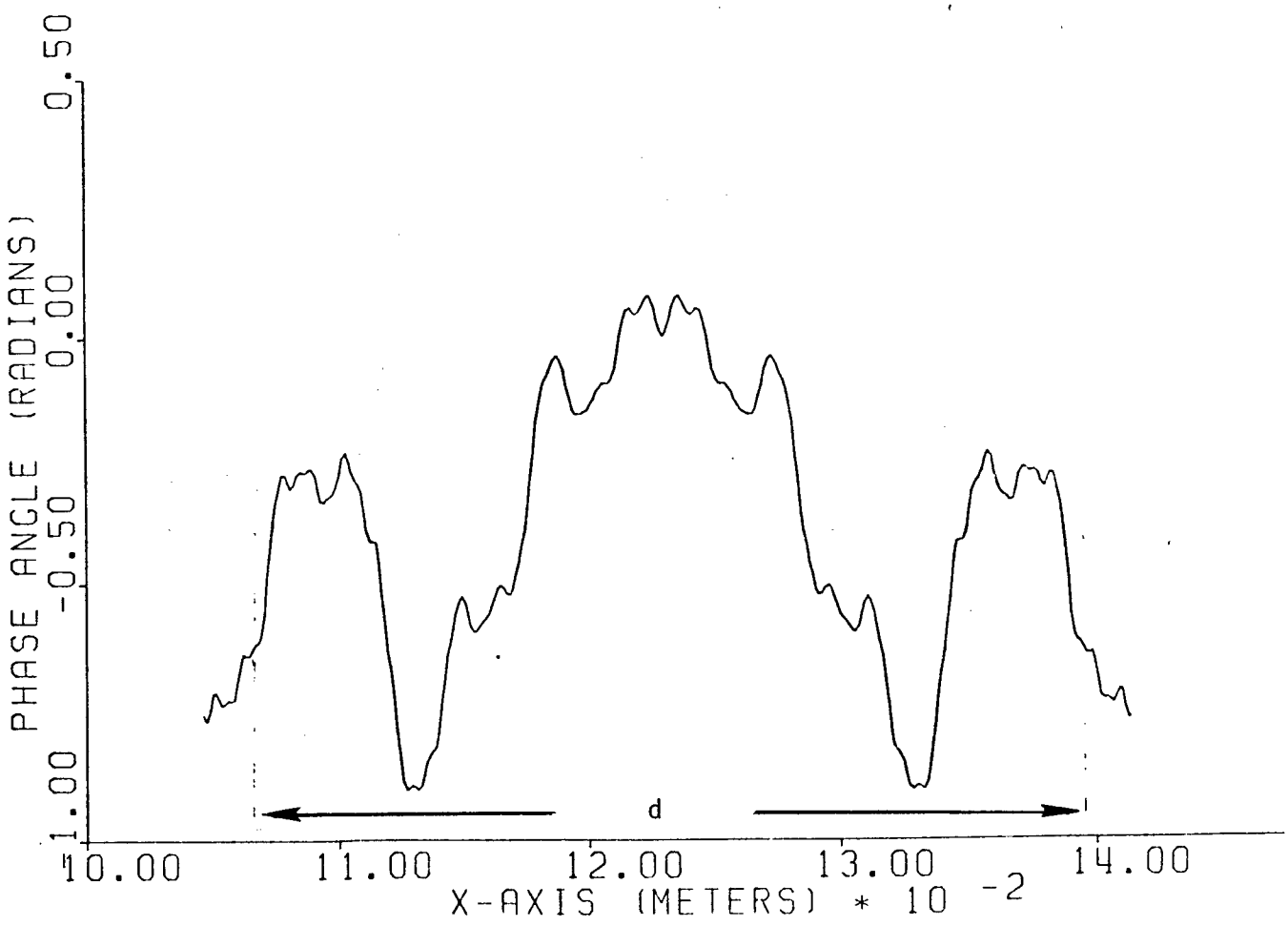

Figure 8. Near Field Phase Distribution (with 1.5% Focus Error) in the Plane of Mirror 1 When Scraper Mirror is Removed (d = hole diameter of scraper mirror)

05/02/78
PL120SF

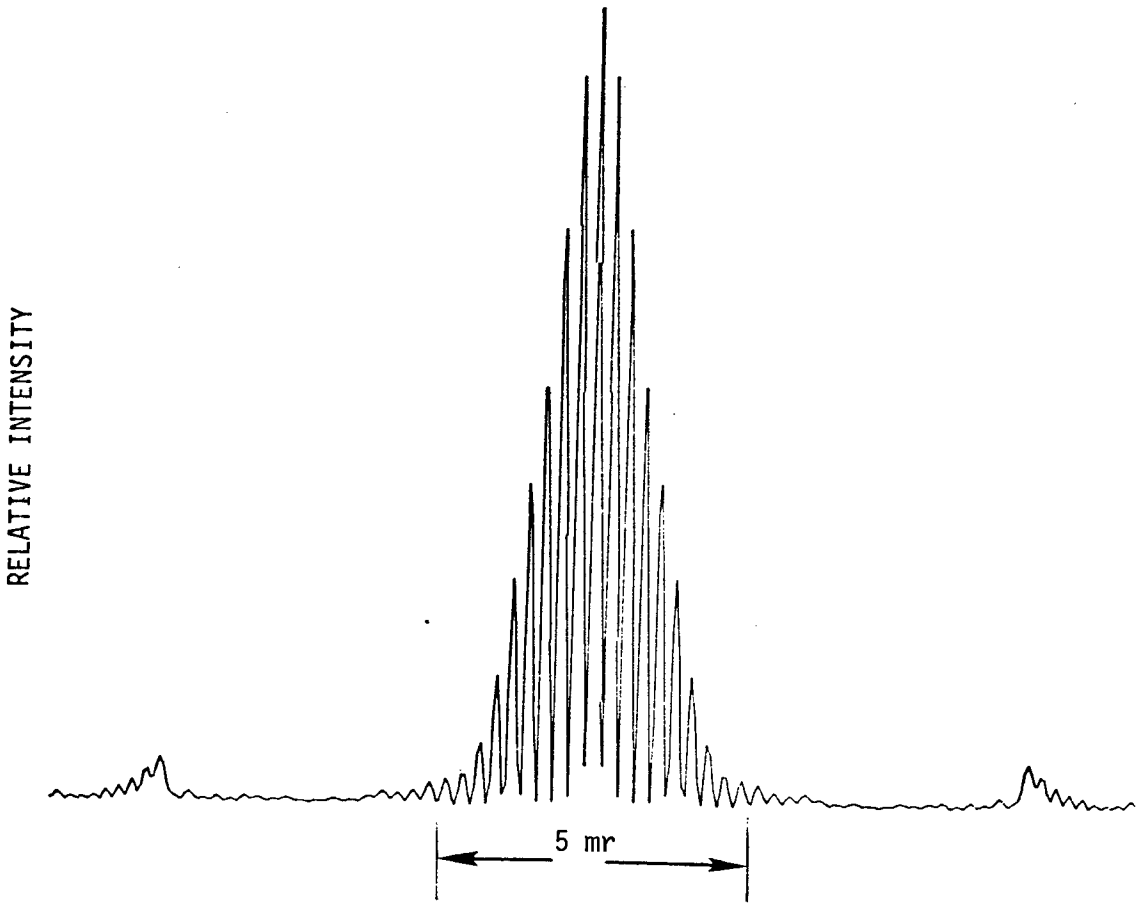

Figure 9. Far Field Intensity Distribution (with 1.5% Focus Error)

Table 1

Percentage of Total Power in Each Ring

Ring	% of Power
0	1.6
1	11.8
2	16.4
3	17.6
4	16.4
5	14.3
6	10.5
7	6.2
8	2.9
9	2.1

The effects of both tilt and focus errors are shown in Figures 10 through 12. Here the large mirror is tilted by an angle equal to $\lambda/4d_o$, with the focus error remaining at 1.5% as before. As can be seen from Figures 10 and 11, the tilt effect on the near field structure is rather significant. In particular, the output beam is tilted, which is indicative of the phase distribution shown in Figure 11. Because of the combined effects, the far-field pattern is shifted from the center of view, in addition to being defocused.

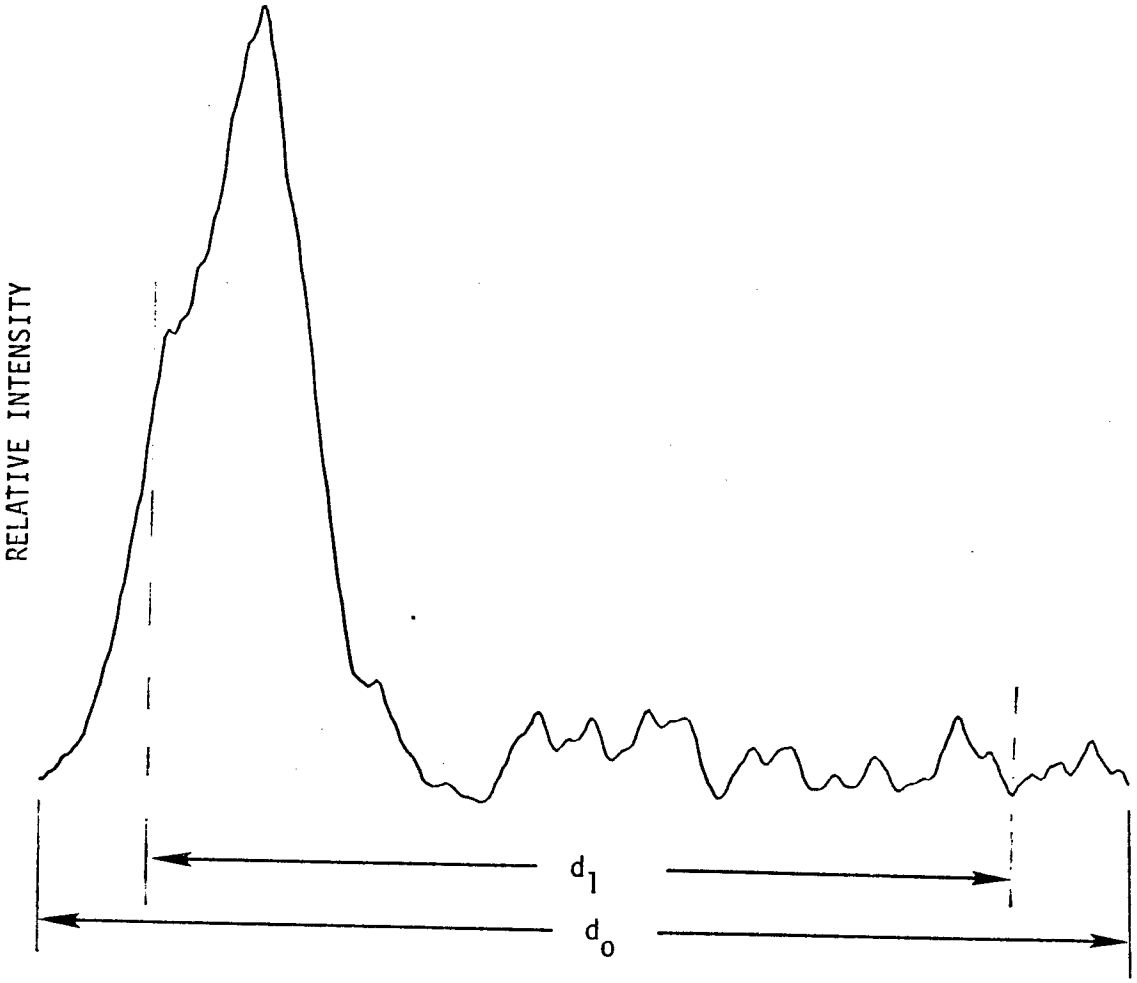

Figure 10. Near Field Intensity Distribution (Focus Error ~ 1.5%; Tilt Angle of Large Mirror = $\lambda/4d_o$)

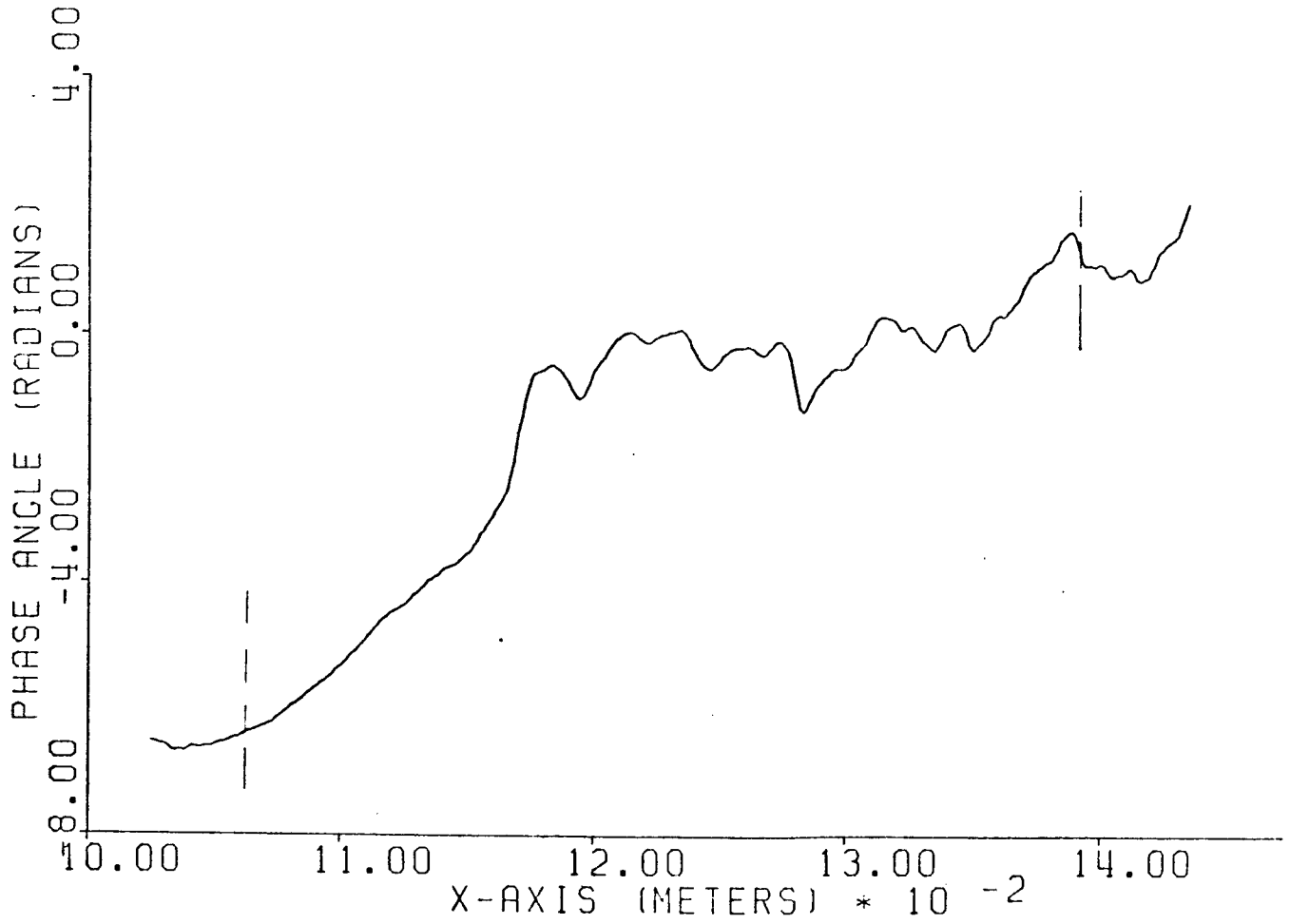

Figure 11. Near Field Phase Distribution (Focus Error ~ 1.5%; Tilt Angle of Large Mirror = $\lambda/4d_o$)

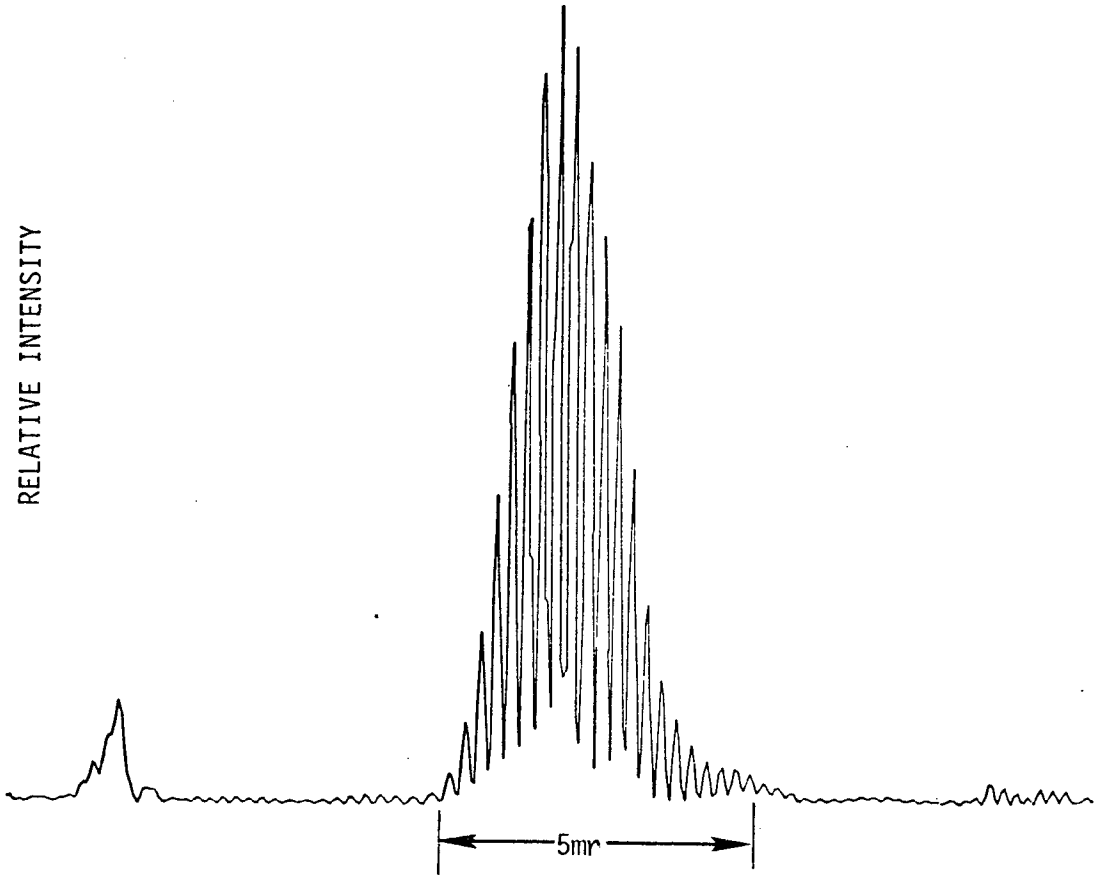

Figure 12. Far Field Intensity Distribution (Focus Error ~ 1.5%; Tilt Angle of Large Mirror = $\lambda/4d_o$)

C. Concluding Remarks

It appears that, for this type of cavity, both the field amplitude and phase of the output portion vary approximately linearly across the width of the output annular aperture. Consequently, the corresponding far-field pattern is deviated from that of a uniform annular aperture. For the tilt and focus error values considered, the effects on the far-field pattern are noticeable, but not serious. The results suggest that cavity-length perturbation, as required for phase locking, should have no adverse effect on the mode structure, provided that angular alignment properties are maintained.

III. LOW POWER UNSTABLE RESONATOR PHASE LOCKING EXPERIMENTS

A. Unstable Resonator Design

Based upon the results of the modeling, as described in the previous section, two unstable resonator lasers were designed and fabricated for use in low power phase lock experiments. The design had some unique features, in that it permitted both sealed off and flowing gas modes of operation. The rationale for this approach was the unknown effect of a flowing gas system upon the frequency stability of the system. This was quickly shown to be a very conservative approach as the initial tests indicated no deleterious effects were present. Consequently, sealed off phase locking tests were not conducted.

One of the two unstable resonator lasers is shown in Figure 13. The laser tube assembly consists of a 34 mm ID pyrex tube with a coaxial cooling jacket. The active plasma is approximately 120 cm long, terminated by a cylindrical copper cathode and a platinum anode offset perpendicular to the tube axis. Figures 14 and 15 show some closeup detail of the cathode/anode configuration, ZnSe Brewster windows, the piezoelectric cavity length tuning assembly, and the scraper mirror installation.

Since our test program was directed towards phase lock operation of the unstable resonator with an appropriate reference, minimization of frequency excursions were carefully considered. As shown in Figure 13, the cavity mirrors are mounted on four (4) Invar rods for longitudinal stability. Each Invar rod is supported by seven (7) crossmembers with unequal spacings between the uprights to reduce the possibility of low-frequency mechanical resonances. In addition, each rod is isolated from the frame by an acoustic absorber to damp out induced vibrations.

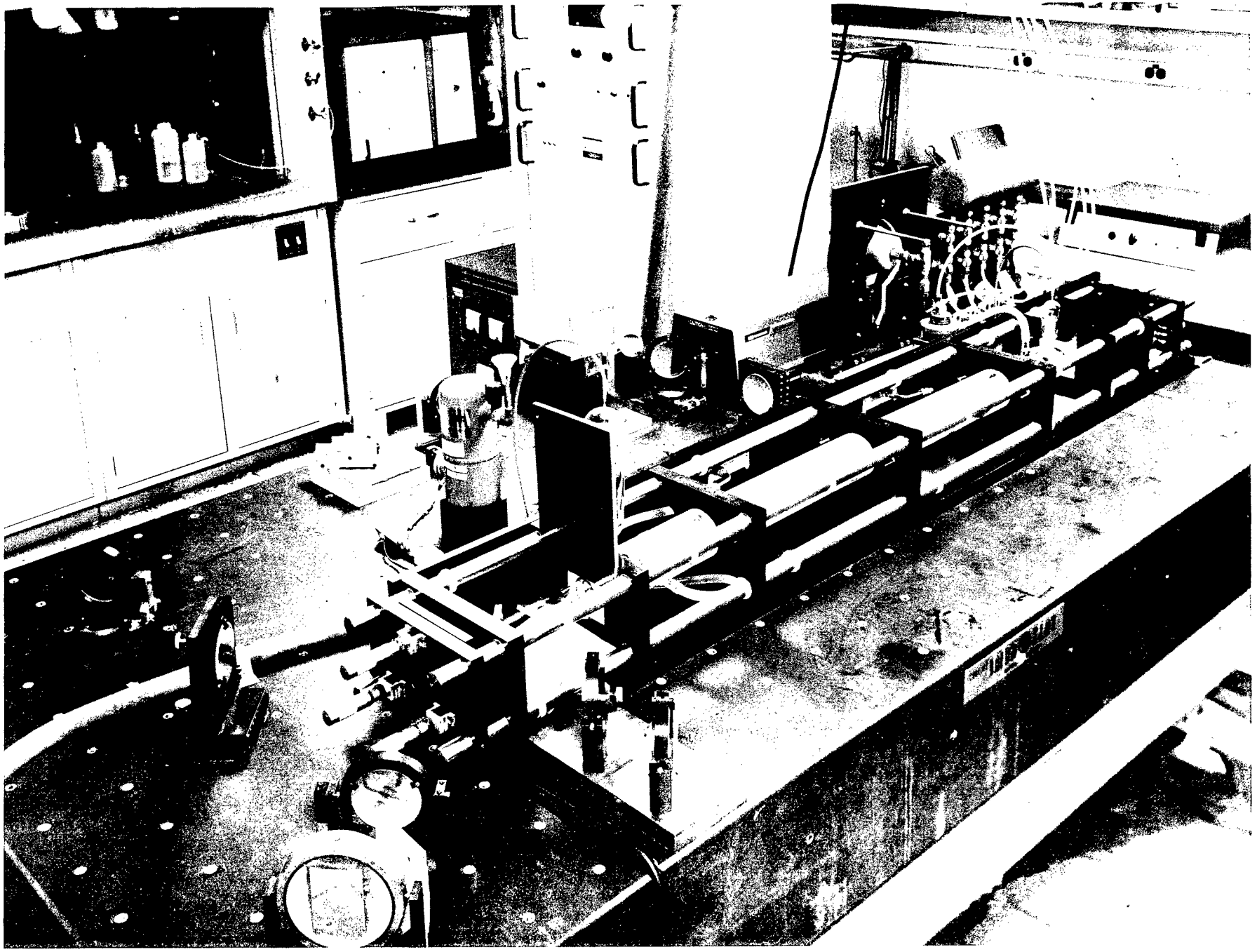

Figure 13. Unstable Resonator for Low Pressure Phase Lock Tests

For adjustment of cavity length as part of the phase lock control, the piezo-driven mirror (concave) of Figure 14 was implemented. The three PZT stacks located symmetrically around the center of the mirror were used to provide the necessary length control, as well as a "fine" adjustment for angular alignment. Interferometer tests prior to assembly within the resonator, showed no appreciable angular misalignment over the ± 5 μm movement required.

In this configuration, power is coupled out of the unstable resonator by the "scraper" mirror shown in Figure 15. This arrangement is more practical, experimentally, than extraction of power around the smaller resonator mirror. As shown, the reflecting surface is flat and is mounted at 45° to the tube axis with a carefully machined hole coaxial with the resonator axis. The diameter of the hole and the distance to the convex resonator mirror effectively determine the Fresnel number of the system. Thus, several mirrors of varying curvature were fabricated to investigate operation as a function of this parameter.

Basic alignment of the cavity was achieved by mounting the resonator mirrors on adjustable mounts with a triad of differential screw micrometers. With the adjusting mechanism under constant compression forces of approximately 60 lbs., a repeatable angular resolution of less than 5 μradians was realized.

Provision was made for varying the flow rate and gas mixtures through a metered manifold. An appropriate mixture of CO_2, He and N_2 flowed into the tube at the anode and was extracted at the cathode end.

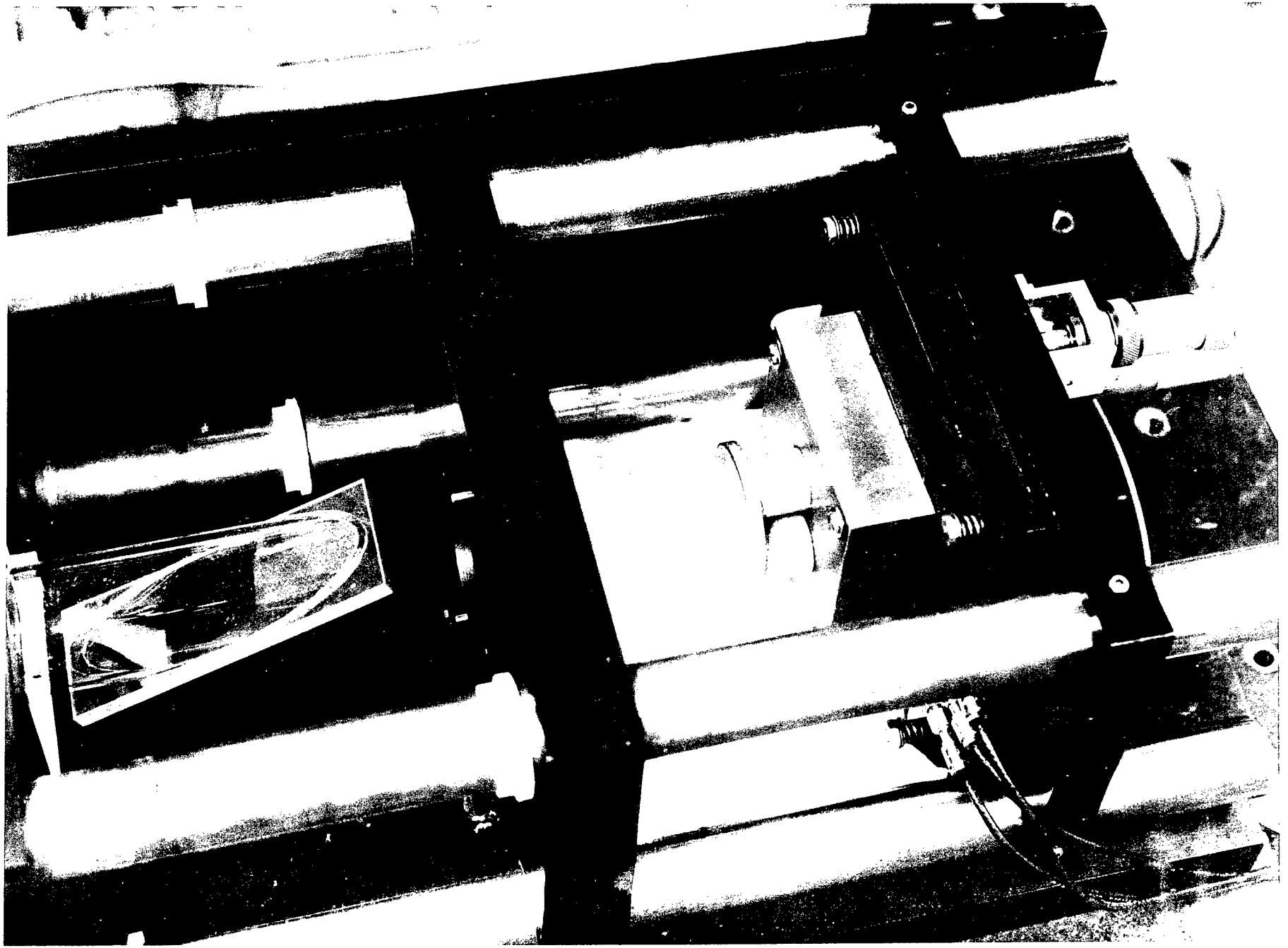

Figure 14. Length Tuning Assembly for Unstable Laser Resonator

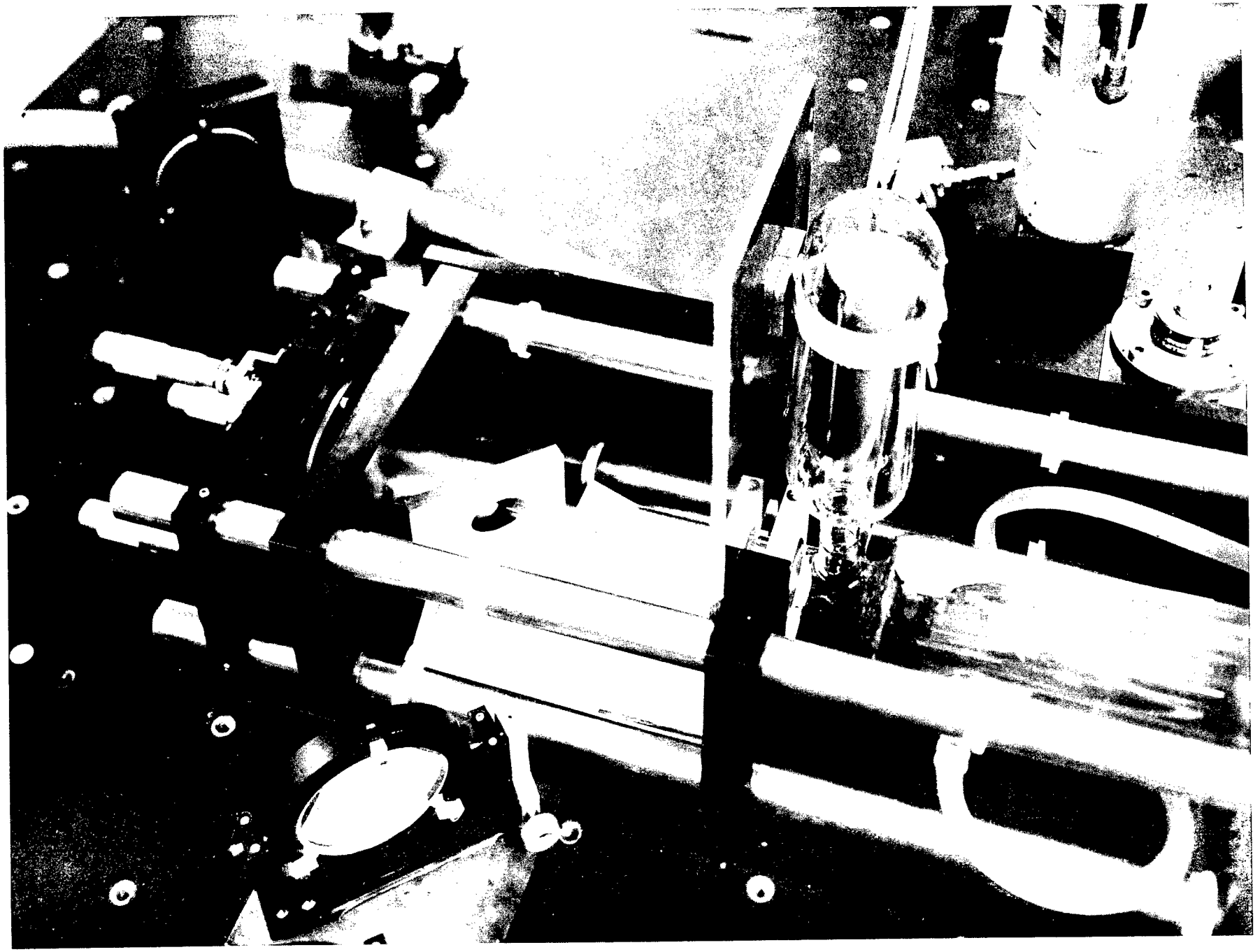

Figure 15. Scraper Mirror Assembly for Unstable Resonator

B. Experimental Measurements

The test apparatus used to measure the gain as a function of radial position, while operating as an amplifier, is illustrated in Figure 16. (Gain is defined as the ratio of the power detected with the amplifier discharge ON to the power detected with the discharge OFF.) A stabilized oscillator with grating control to restrict operation to the P(20) transition was used to generate a probe beam to excite the amplifier. After expansion and collimation, the beam was focused at the center of the gain region by long focal length optics. Beam width of the entrance and exit beams (FWHM) was designed to be 2.5 mm.

Synchronous translation stages were mechanized by using the same driving electronics for both stepper motor units. By mounting a detector on one unit and a mirror on the first stage, as shown in Figure 16, the probe beam was tracked as it traversed the tube diameter. To evaluate the probe beam, the input stage was held stationary with the beam centered in the tube. With a 0.1 mm slit mounted on the detector, a translational scan of the output stage yielded the intensity profile of the beam as it propagated through the system. A plot of this probe beam profile is shown in Figure 17.

During the small signal gain measurements, the intensity of the probe beam was kept below 100 mw. This yields an average power density of approximately 2 watts/cm^2. This is well below the saturation parameter of about 50 w/cm^2.

Figures 18 and 19 are representative gain profile curves for the sealed off and flowing gas modes of operation. Figure 20 shows one plot of tube power vs pressure for flowing and sealed off systems at various excitation currents.

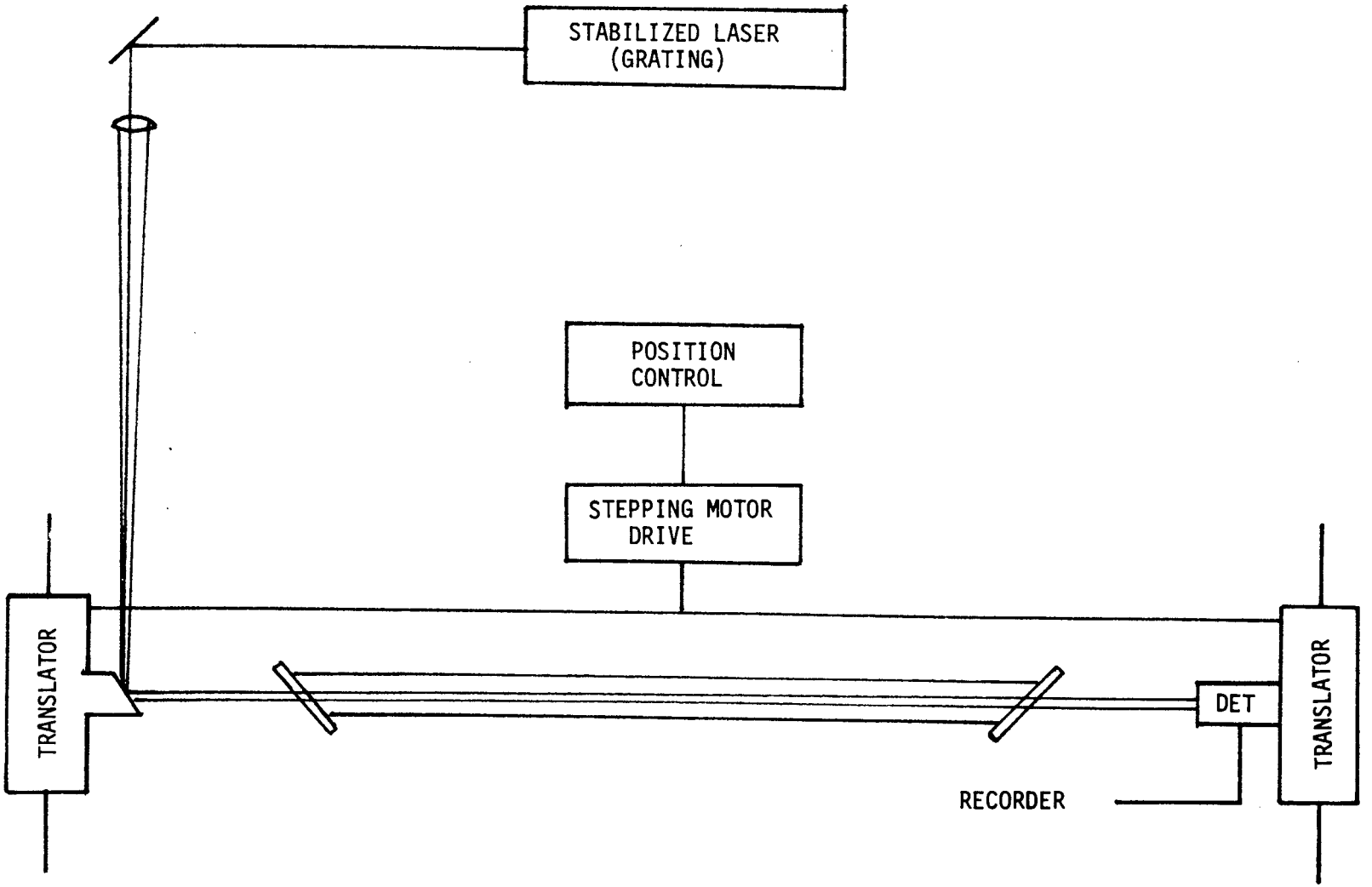

Figure 16. Apparatus for Measuring Radial Gain Profile

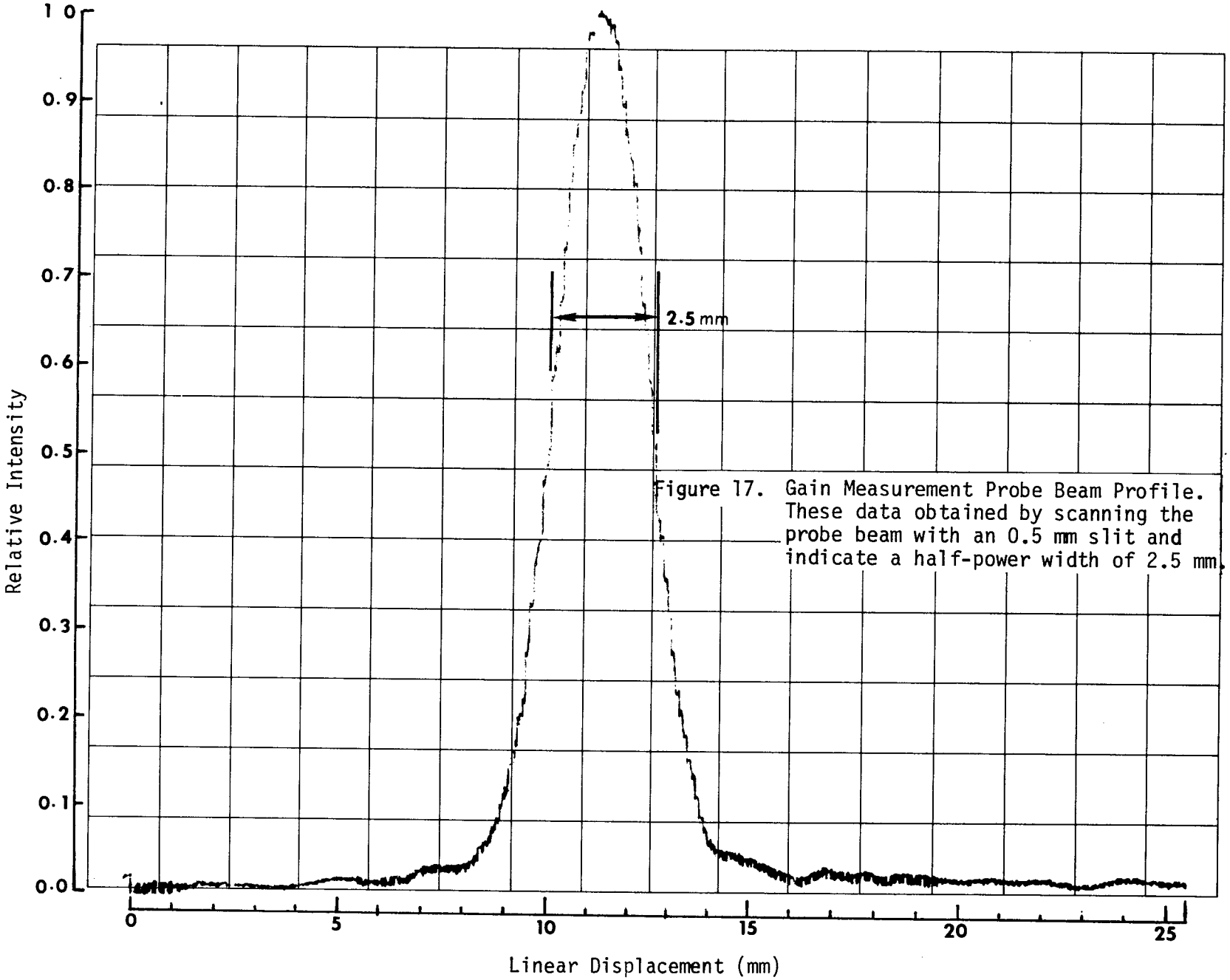

Figure 17. Gain Measurement Probe Beam Profile. These data obtained by scanning the probe beam with an 0.5 mm slit and indicate a half-power width of 2.5 mm.

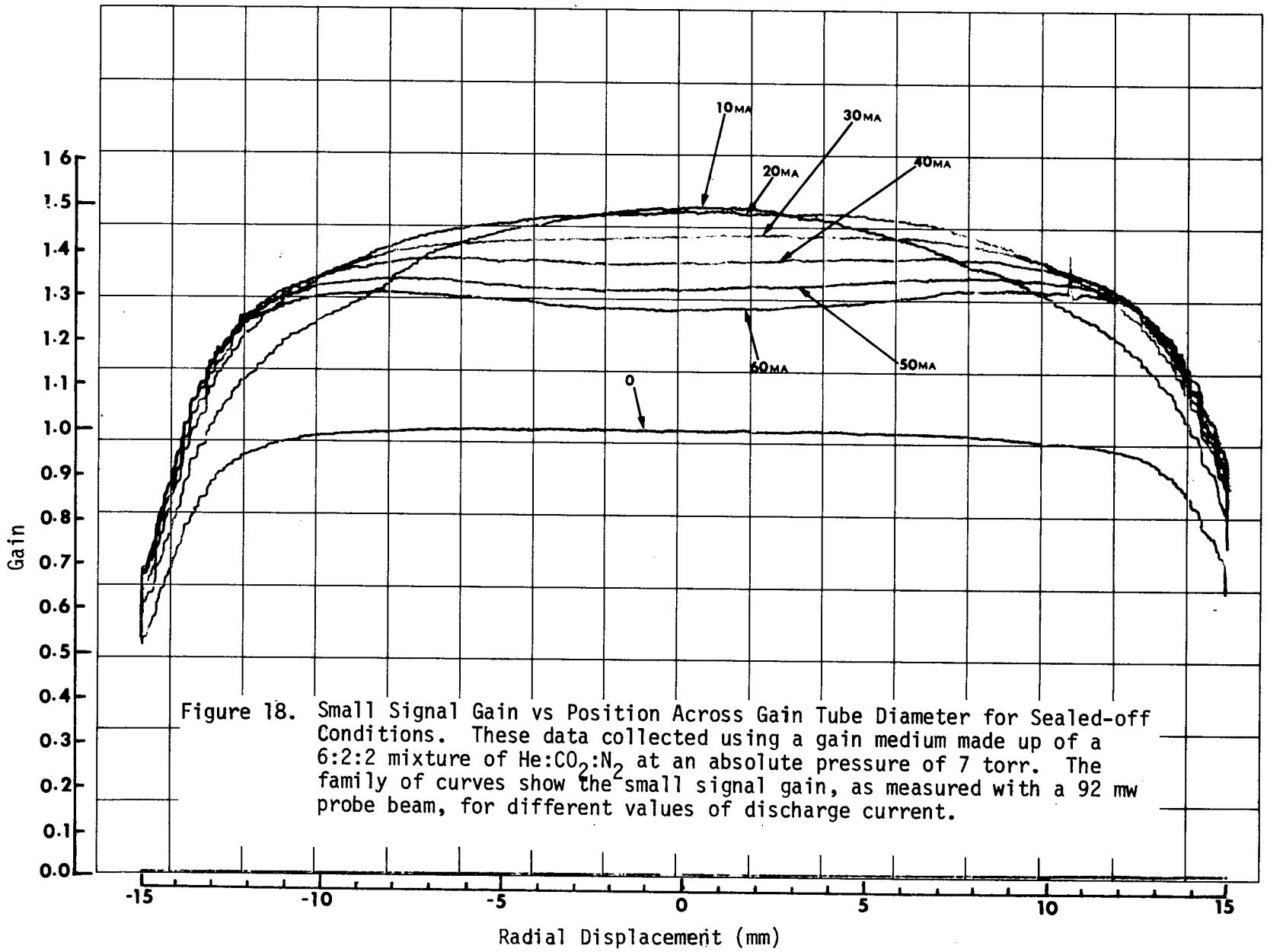

Figure 18. Small Signal Gain vs Position Across Gain Tube Diameter for Sealed-off Conditions. These data collected using a gain medium made up of a 6:2:2 mixture of $He:CO_2:N_2$ at an absolute pressure of 7 torr. The family of curves show the small signal gain, as measured with a 92 mw probe beam, for different values of discharge current.

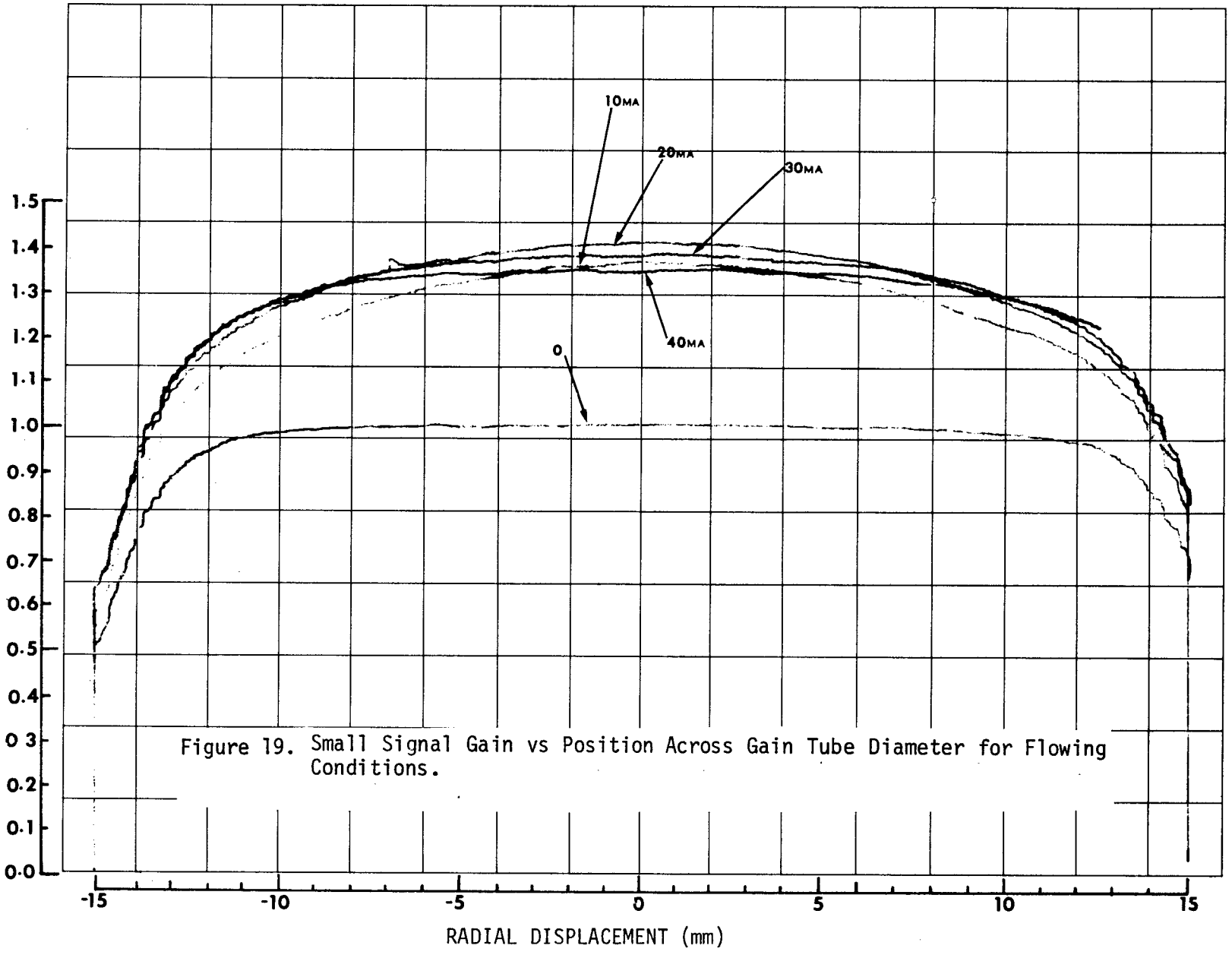

Figure 19. Small Signal Gain vs Position Across Gain Tube Diameter for Flowing Conditions.

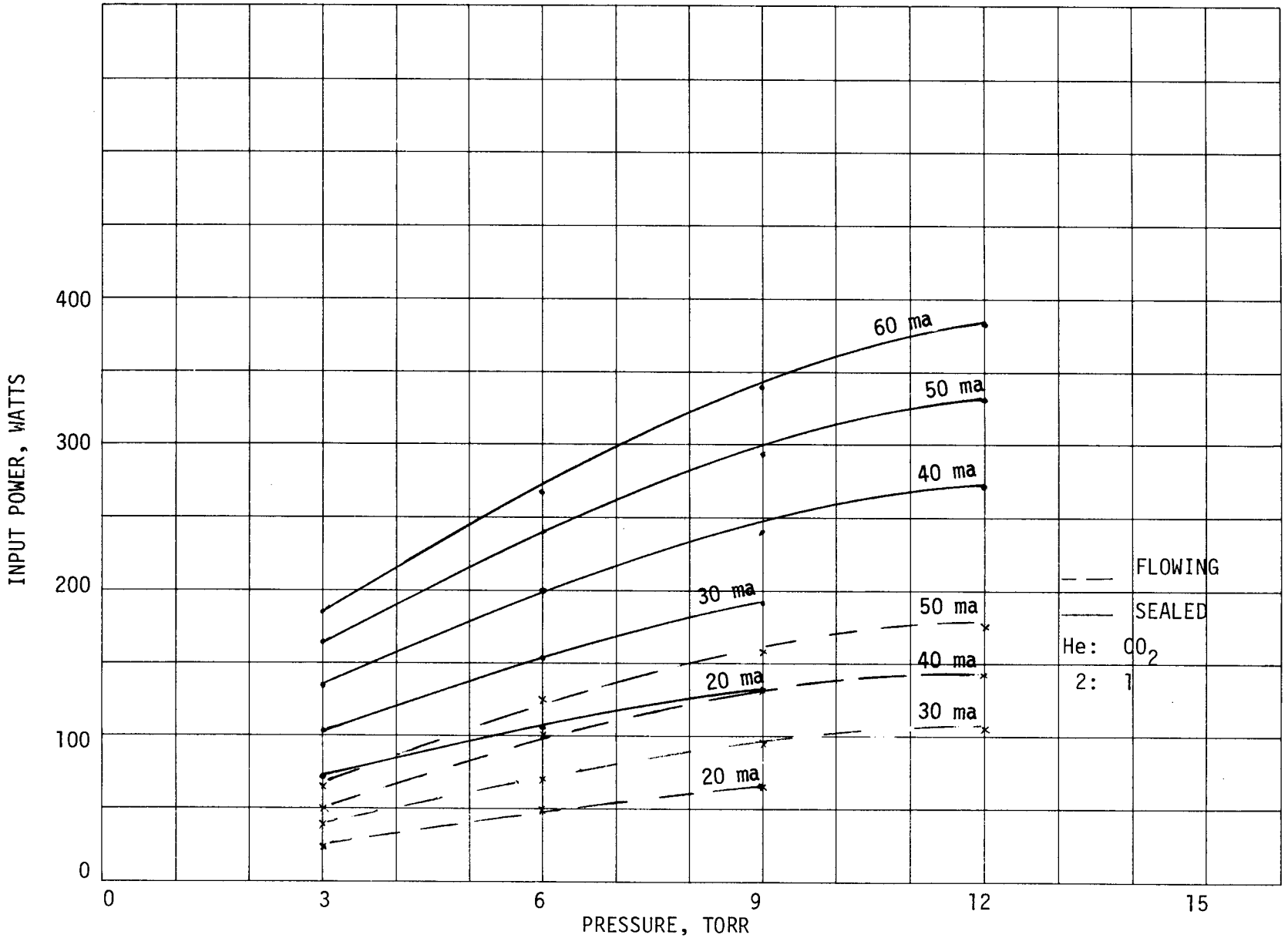

Figure 20. Pressure/Power Dependance for Flowing and Sealed-Off Operation

When aligned, typical output intensity distributions represented by Figure 21 were observed in the near field of the aperture. Some nonuniformity is present, but does not degrade the system performance when used in the phase lock system illustrated in Figure 22. For processing purposes, a low power, stable resonator, laser was used as a reference oscillator. The output was frequency shifted by the acousto-optic (A-O) modulator prior to mixing with the unstable resonator output. The combination signal, when focused on the detector, provides an offset frequency at the detector output for analysis. The spectrum of this signal is shown in Figure 23 for both short and long-term evaluation of relative frequency stability. As indicated, the short term effect is about 200 KHz in 50 msec and, typically, represents the control rate which the processor must provide to obtain phase lock control. The long-term stability ($\approx$ 1.5 MHz/sec) sets a design goal for the dynamic range of frequency adjustment which must be provided.

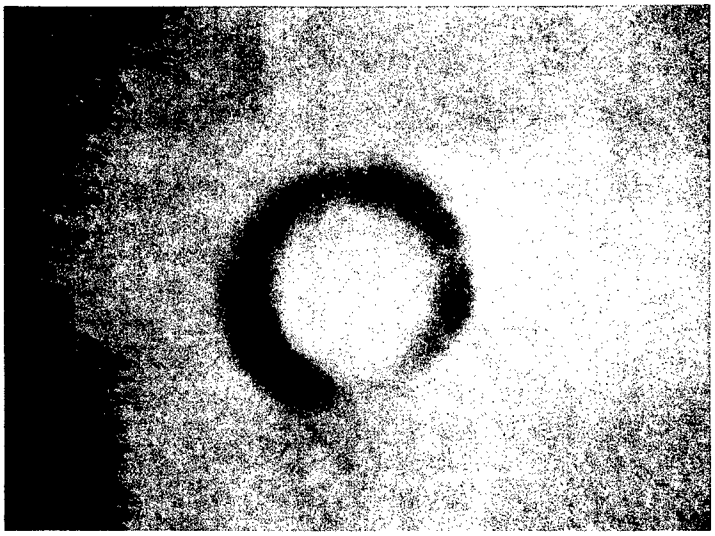

Figure 21. Intensity Distribution as Viewed in the Near Field of the Aperture

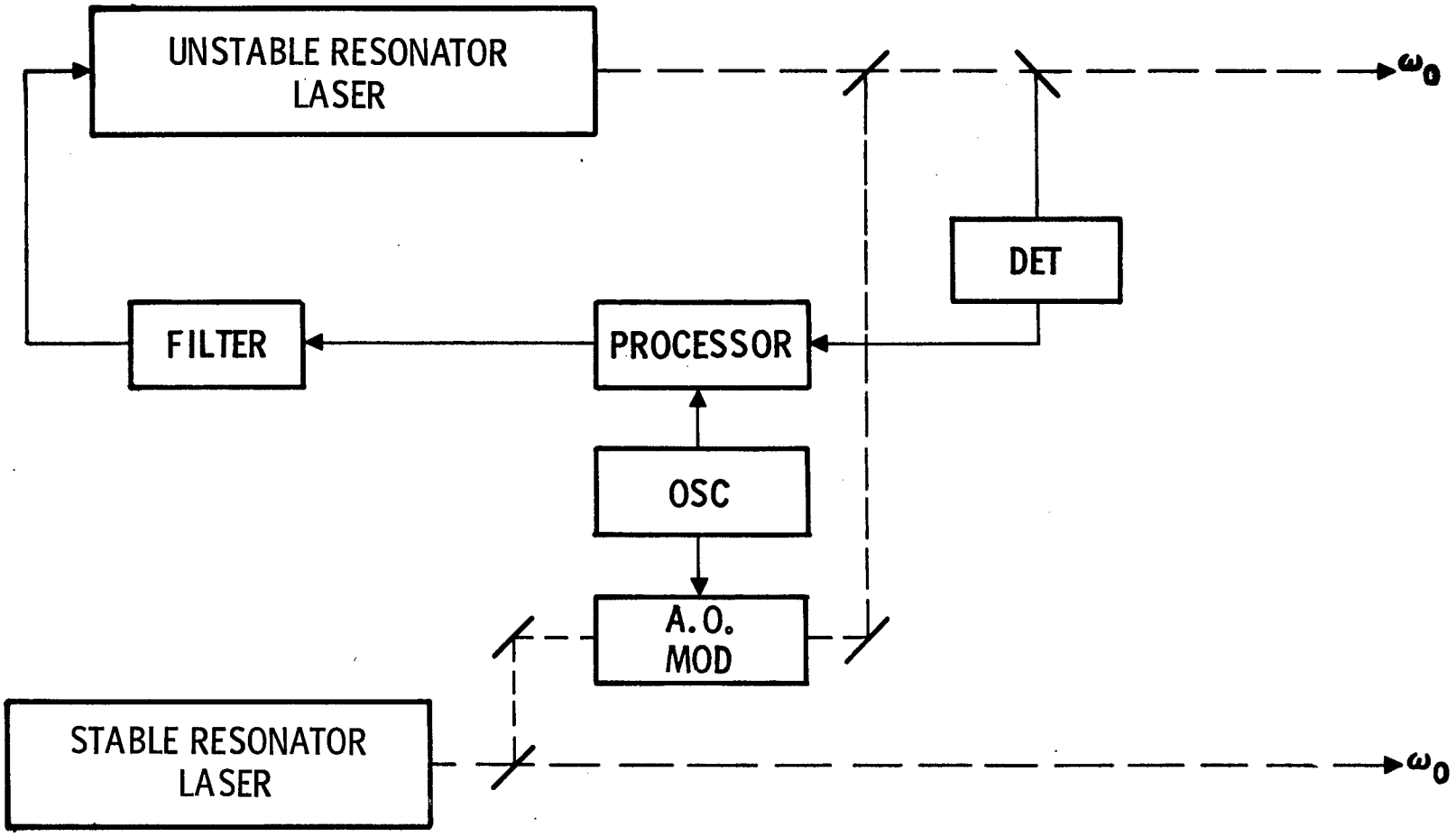

Figure 22. Functional Block Diagram of Unstable Resonator Laser Phase Locking Demonstrator

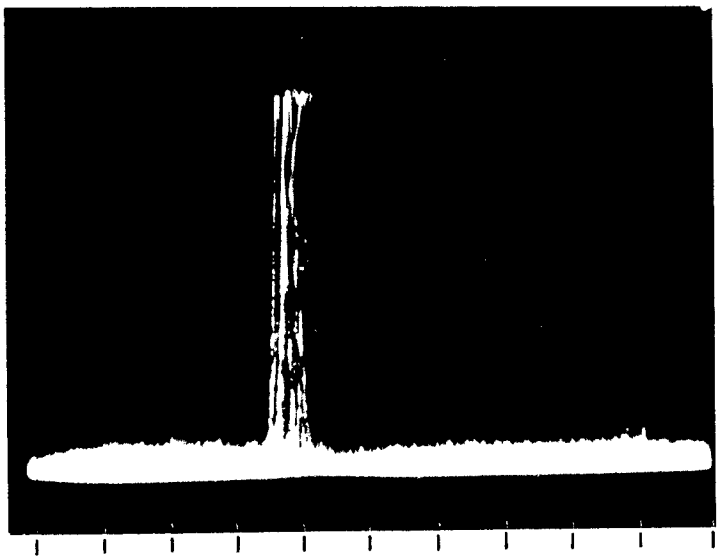

SHORT TERM STABILITY
200 kHz/DIV
50 MSEC

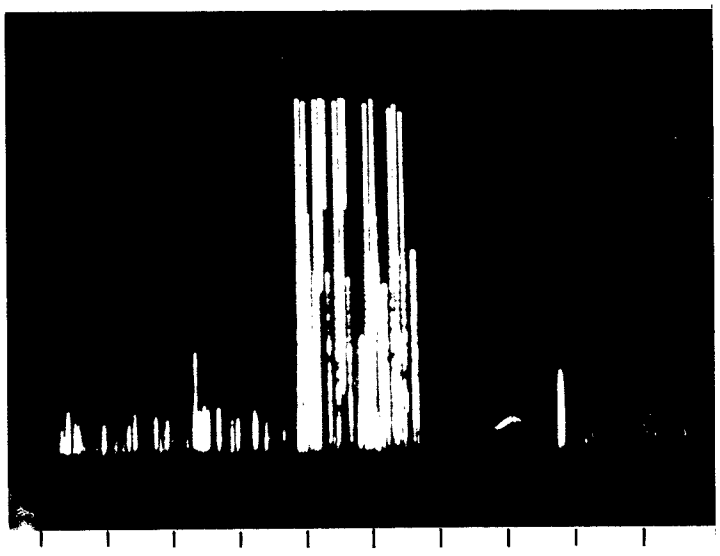

LONG TERM STABILITY
500 kHz/DIV
1 SEC

Figure 23. Spectrum of Heterodyne Signal to Evaluate Frequency Instability of System

Based on these data, the control loop (detector, processor, cavity length control) was designed to implement the phase lock function. Figure 24 represents typical results. As shown, the realtive phase control between the heterodyne signal and reference oscillator is very good with an rms error of less than 5 degrees. That is, the outputs of each laser, operating at 10^{13} Hz, have been synchronized by active control of the unstable resonator cavity. The effect is one of being able to coherently add (temporally) the fields of each laser for power combination.

Previous tests were concerned only with stable resonators and the ability to temporally and spatially combine beams. In summary, this experiment established the feasibility of cavity control of an unstable resonator for phase lock control. With this background data, the next phase of the program was structured to evaluate the design factors associated with control of the high power device.

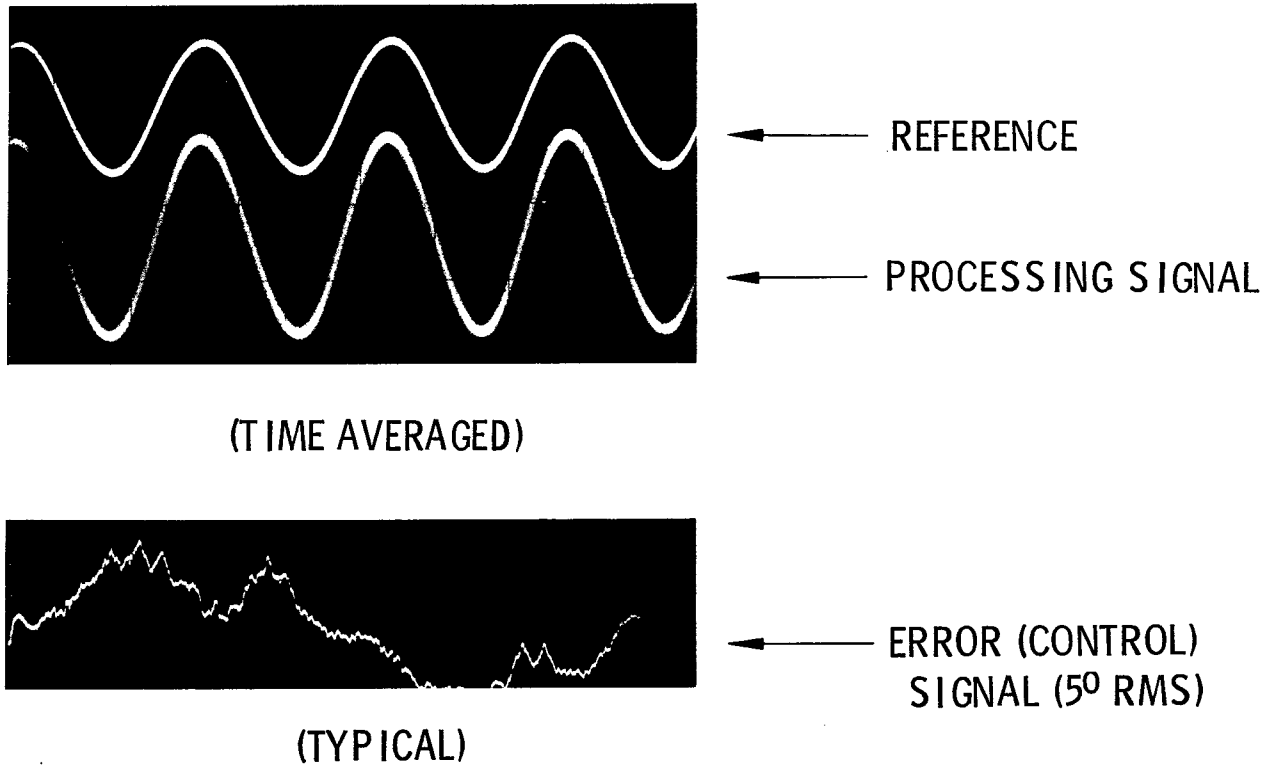

Figure 24. Phase Lock Processing Signals (Unstable Resonator)

IV. NASA LEWIS HIGH POWER LASER CHARACTERISTICS

A. Introduction

Having established the phase lock operation of unstable resonator cavities based upon the high power cavity parameters, the next issue in question centered around the operational characteristics of the high power device. Namely, does the operational environment of such a large scale machine and the inherent properties associated with the fast flow medium produce frequency instabilities beyond the control range of the servo system? A series of tests was structured to address these issues. The first investigation involved assessment of power fluctuations, line hopping properties, frequency stability, etc. Only a short period of time was available for this purpose, since other tests had been scheduled on the machine. However, the data collected, when analyzed, indicated further tests were warranted. Subsequently, a second series of characterization tests were conducted later in an attempt to pin-point and isolate various error sources. These tests and data are presented in this section and form the basis for the design of the high power cavity length controller for the servo control system.

All tests were conducted using the physical layout illustrated in Figure 25. The high power beam was directed to a closed room with appropriate safety interlocks. The power was measured using a calorimeter designed to accept the full power output. A small portion of the beam was directed into the shielded test room for detailed investigation.

The laser electrical discharge elements, anode and cathode, are, respectively, a conducting plate approximately 1 meter long by 15 cm wide, and a set of approximately 50 pins in each of 16 rows (see Figure 2). Cathode

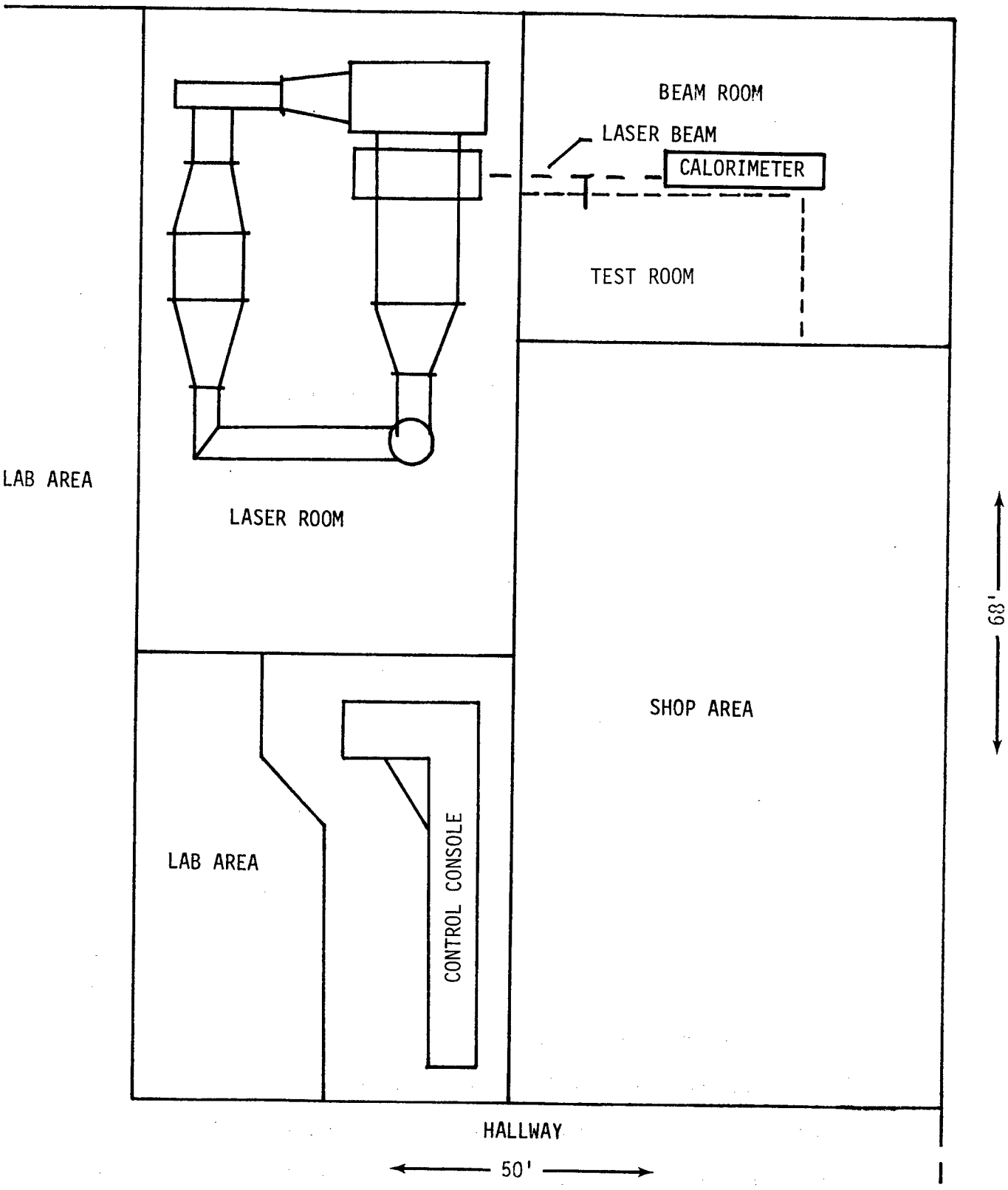

Figure 25. NASA-Lewis HEL Laser Facility

or "pin" currents are monitored via a 1 ohm resistor placed on the lower voltage side of the discharge with a resistor for each pin row. (Not all of the pin rows were operated during these tests.) Operators at the control console can assess operation with these data.

Each time the laser was operated, it was pumped out and recharged with a fresh fill of gas, to a total pressure of 140 Torr in the ratio of 20 He, 7 N_2 and 1 CO_2. Any exceptions to this are noted in the specific data. As the data were taken during a series of laser runs, the initial laser run of each day was designated as Run #1 and is so marked in the following discussion. (Data were taken at laser powers in the range of 1 to 5 KW, with a discharge current of 7 to 14 amps.)

B. Vibrational and Rotational Line Investigation

The first data recorded were observations of an IR optical spectrum analyzer to determine the operational wavelength. The optical layout for the test is shown in Figure 26. (The initial tests did not include the Pb-Sn-Te detector and optics.) The data recorded in these tests are strip chart records of the power meter output, the calorimeter output, and tabulated data taken from observation of the IR spectrum analyzer.

The first run of each day was primarily to check out and calibrate the test setup with no data recorded. From first observations, Runs 2 and 3, it was noted that the laser operated predominately in the P20 line upper vibrational branch (10.59 μm), but after a period of several minutes of operation or upon operating at elevated pin current (11 to 12 amps, as opposed to 9 to 10 amps), the laser output became erratic, shifting to the lower vibrational branch and hopping between P16 and P18 in that branch.

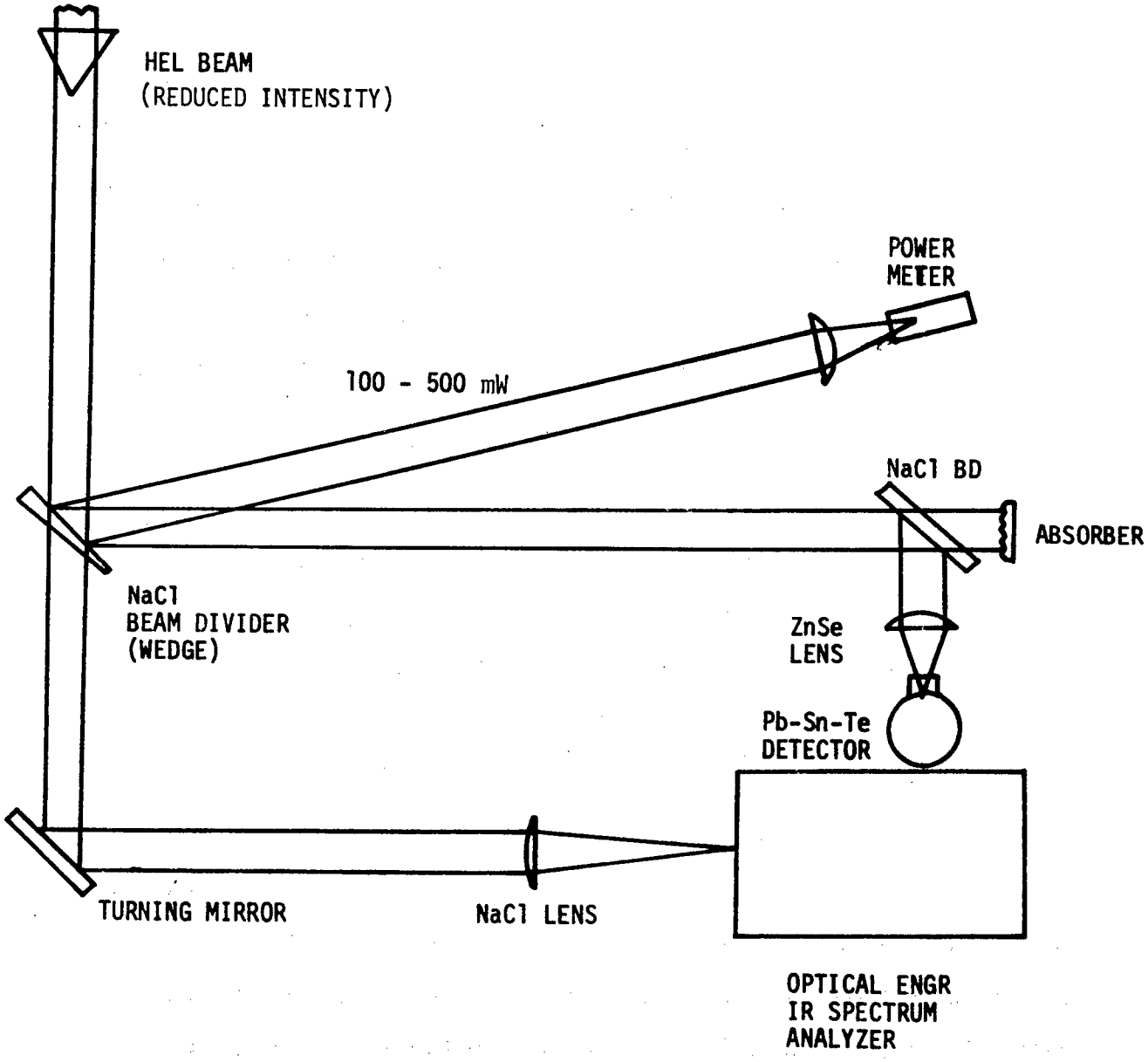

Figure 26. Test Room Optical Schematic

On Runs 4 and 5 (Figure 27), we introduced a chart record of the power meter output. Here, the erratic behavior of the laser is evident as a result of either sustained operation at low pin current or as a result of increasing the pin current to the 11 to 12 amp region.

On Run 6, a record of the calorimeter output for comparison to that of the power meter, and a record of the pin current (Row 13), was included in an attempt to find a correlation to the erratic behavior of the laser at elevated current levels. These are shown in Figure 28. The pin current, at least on Row 13, does not appear to be the cause of the erratic behavior. Since the power meter (Thermopile) response was unknown, an instrumentation change was made for the next series of data. The Pb-Sn-Te detector, as shown in Figure 26 was used. The response of this device is known to be in excess of 10 MHz.

For the second day of tests, the data recording was expanded in an increased effort to determine the cause of the previously observed erratic laser behavior. Figures 29 and 30 are again strip chart recordings of pin current, calorimeter output, power meter output, and the Pb-Sn-Te, true rms meter output. Figure 31 is a series of oscillograms of the output of the Pb-Sn-Te detector. A 30 Hz tone is apparent in the detector output, along with a significant high frequency noise accompanying it.

In a further effort to identify the nature of the "noise," the fast detector was mounted upon the IR spectrum analyzer, such that it viewed only the radiation of the P20 line position (10.59 μm). Oscillograms taken during Run #3 are shown in Figure 32. The upper trace is the direct output of the detector; the lower trace is the low frequency spectrum analyzer response. The noteworthy aspect of the comparison of this record and that of the oscillograms in Figure 31 are that the high frequency noise is absent.

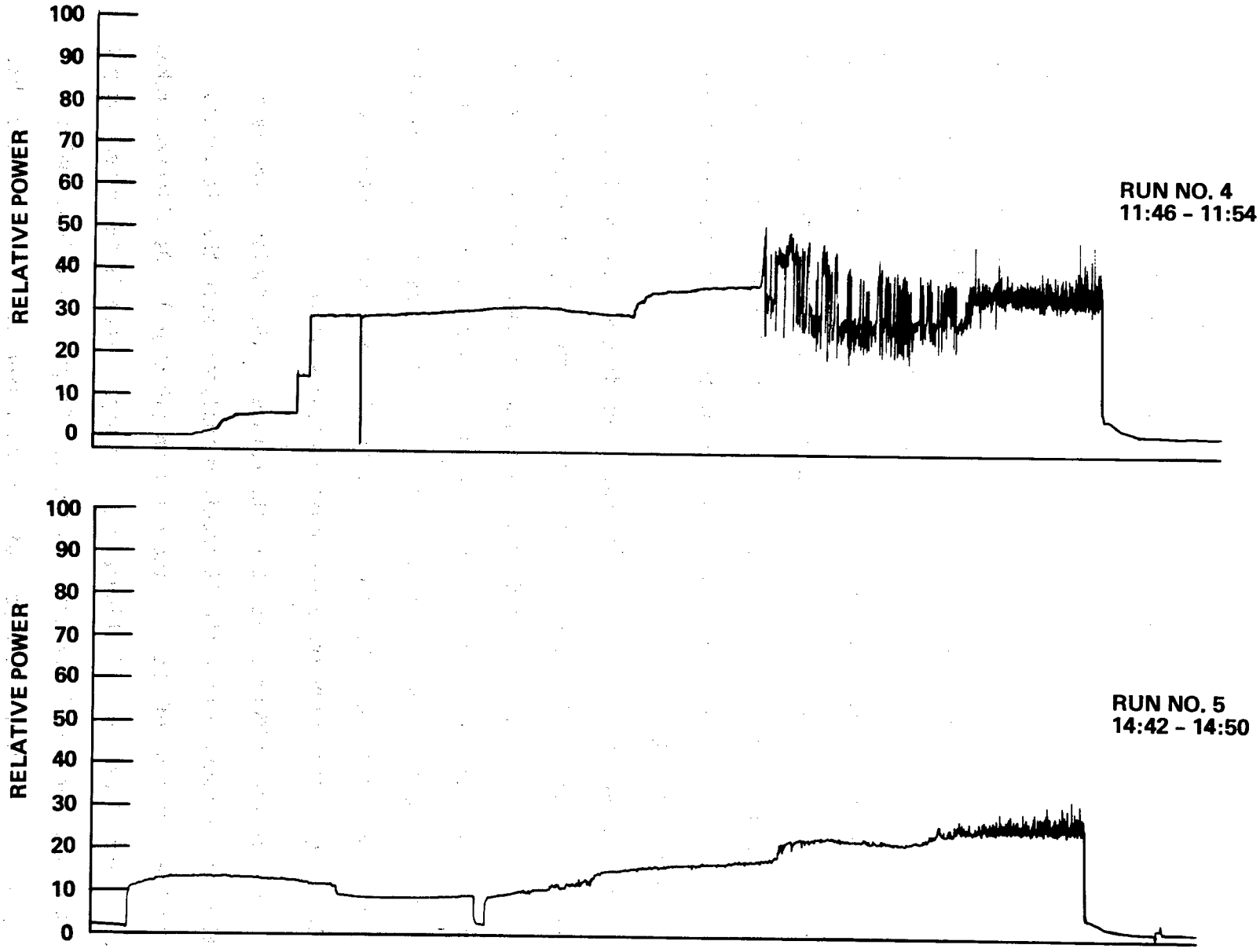

Figure 27. Power Meter Output for Runs #4 and #5, 3/24/77 (Chart Speed: 1" = 40 sec)

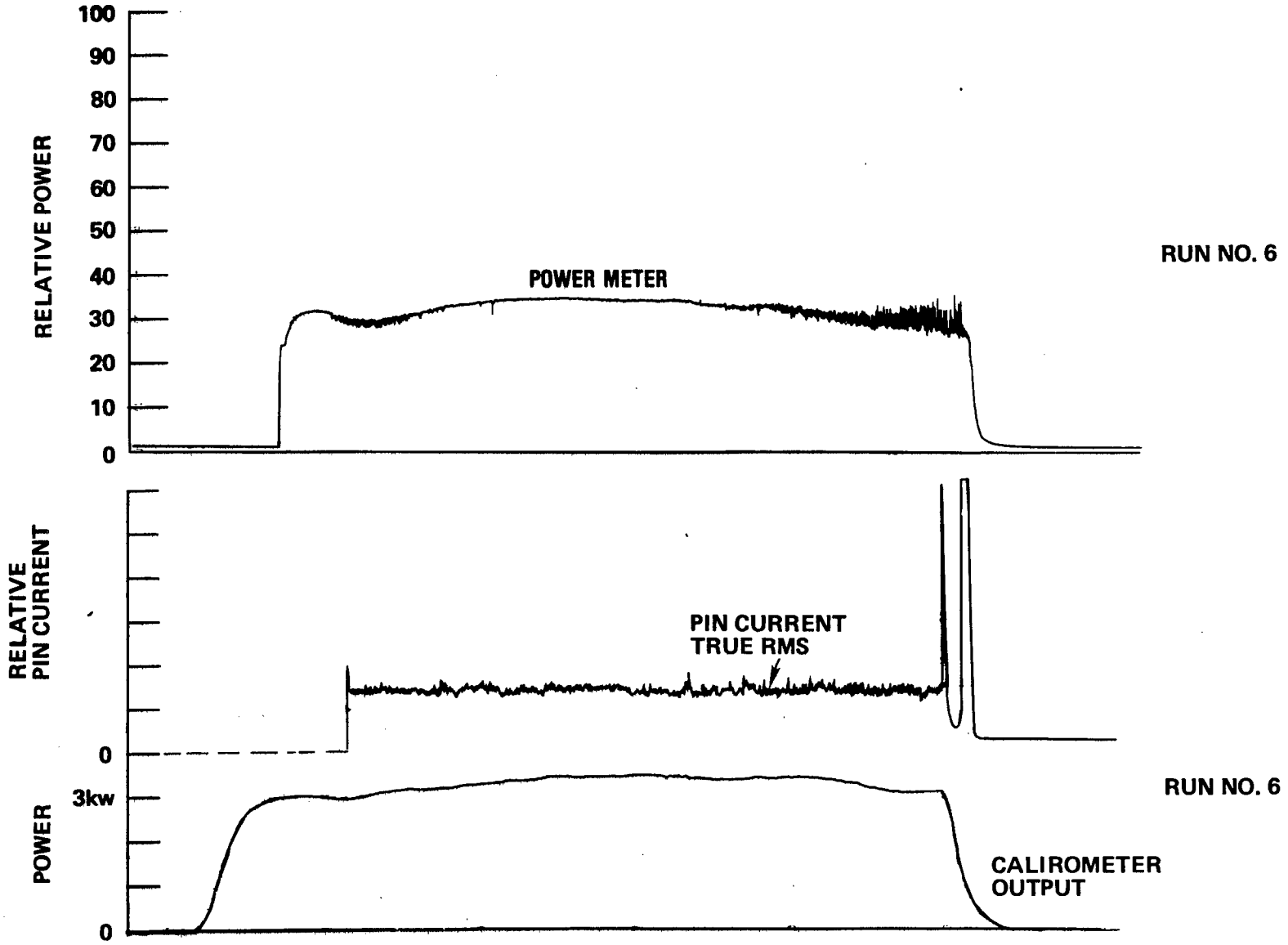

Figure 28. Power Meter, Pin Current, and Calorimeter Output for Run #6

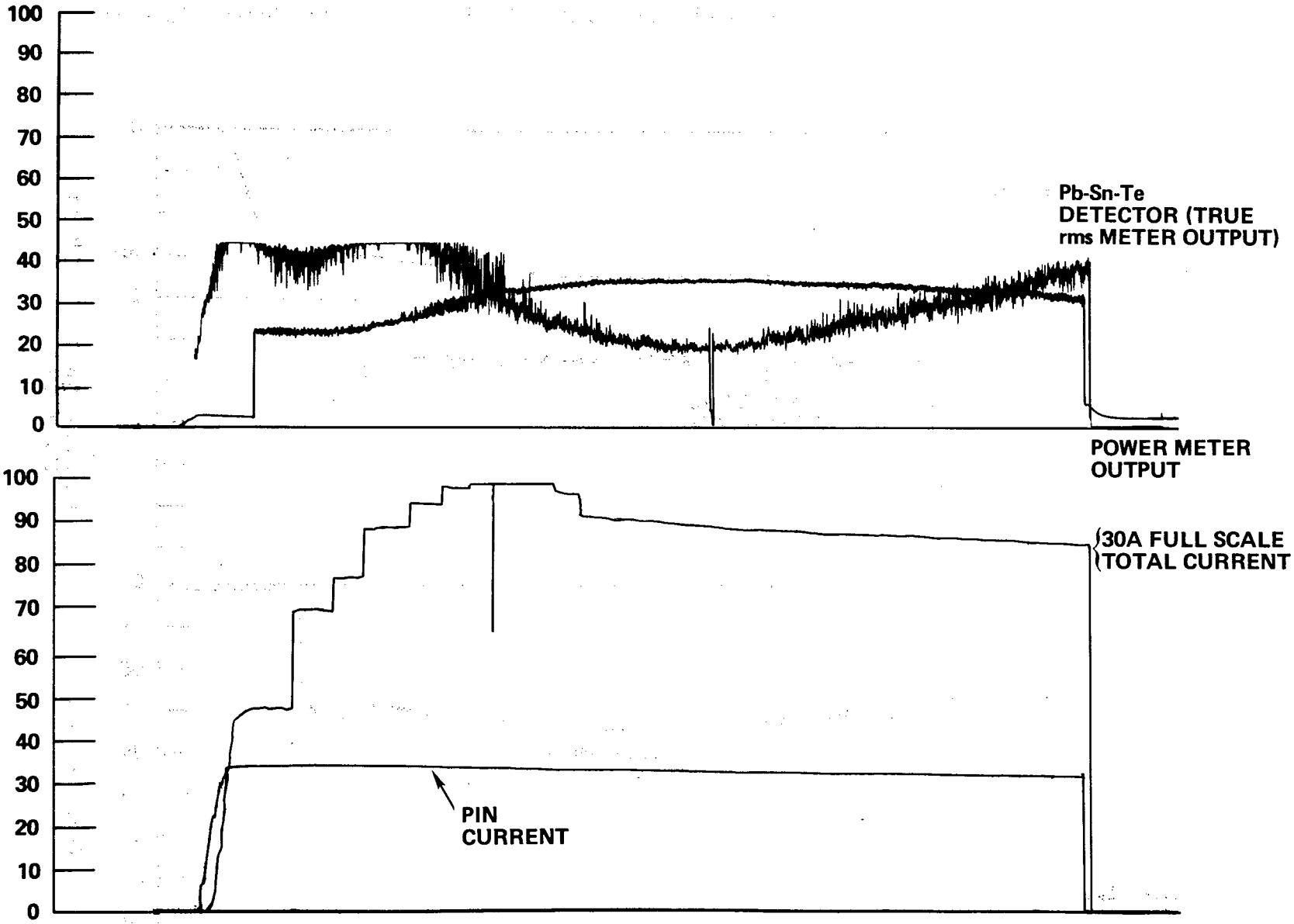

Figure 29. Chart Record of High Speed Detector, Power Meter, and Current Monitor
Chart Speed: 1" = 60 sec.

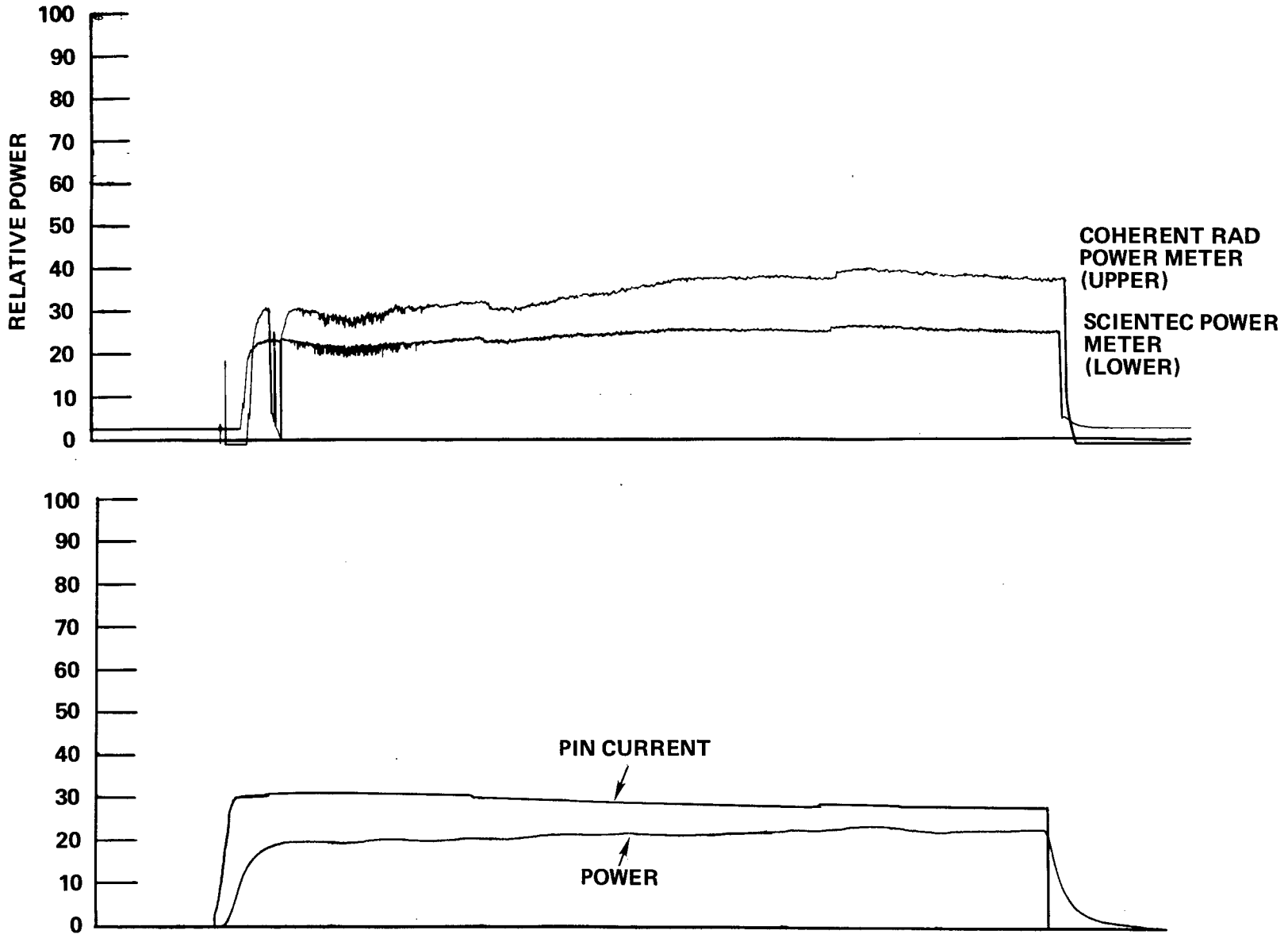

Figure 30. Chart Record of Power Meters and Pin Current Monitor
Chart Speed: 1" = 60 sec.

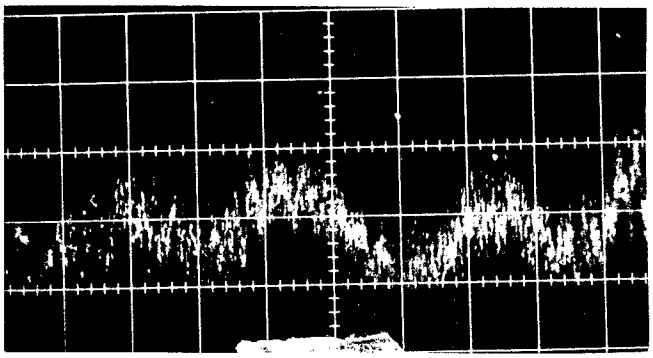

Time	Vert	Sweep
10:22	0.5 v/cm	10 ms/cm

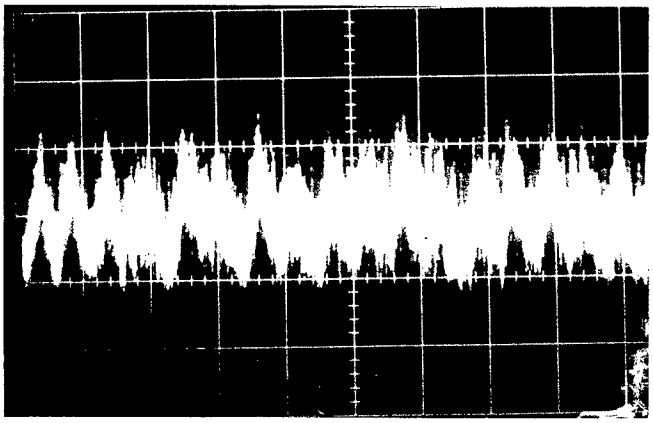

10:22 0.5 v/cm 50 ms/cm

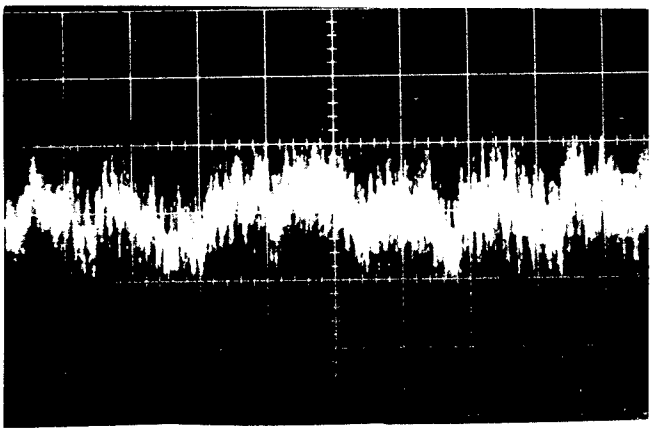

10:23 0.5 v/cm 10 ms/cm

Figure 31. Oscillograms of Pb-Sn-Te Detector Output During Run #1, 3/25/77

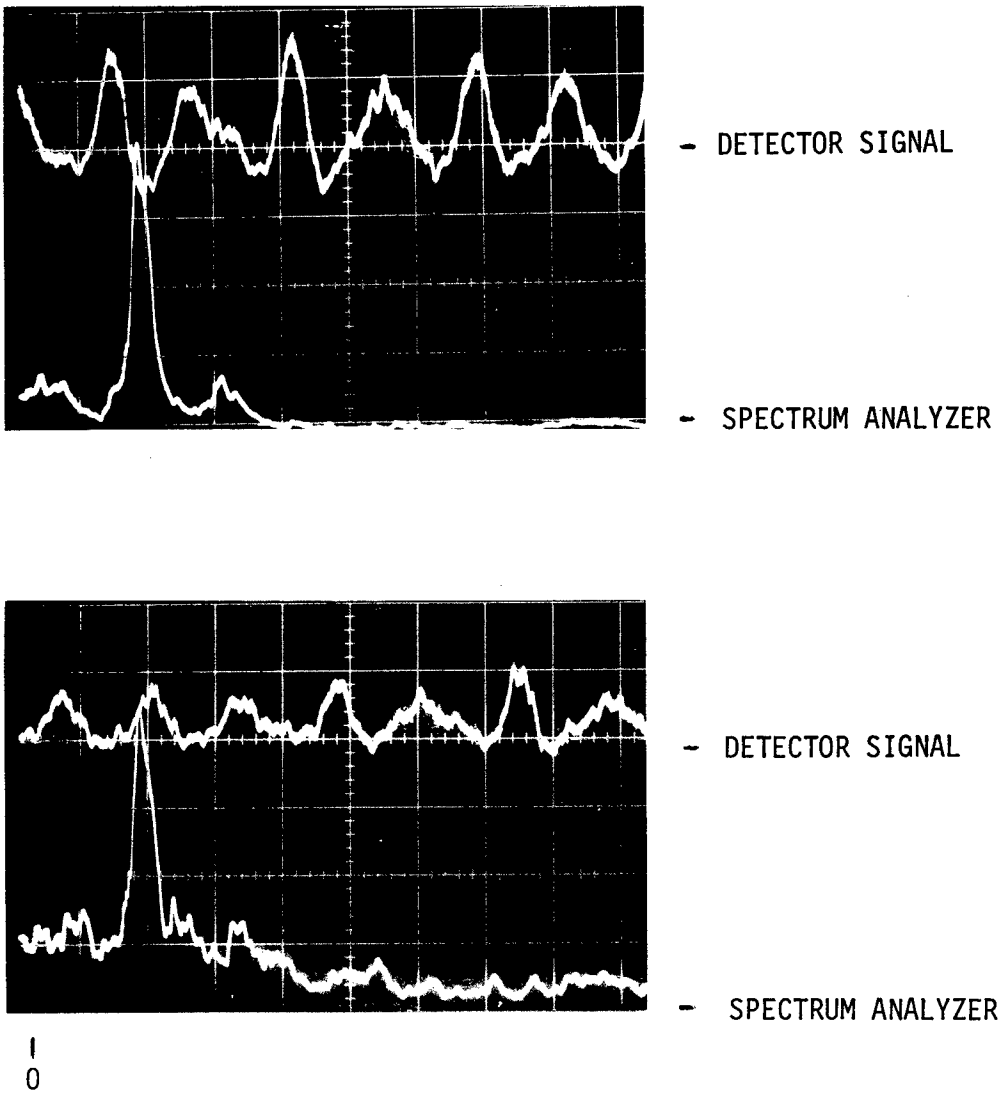

Figure 32. Oscillograms of the Fast Detector Monitoring the P20 Line
Upper Trace - 20 mv/cm, 20 ms/cm
Lower Trace - 10 Hz/div, 50/s Rate

Run #3, 3/25/77

As the testing progressed, one postulation was that the cause for the erratic behavior was a result of "poisoning" of the gas. This postulation could fit both observed conditions, i.e., high pin current level or long run time. Attempting to confirm this postulation on Run #4, 3/25/77, the pin current level was raised to force the erratic behavior and then lowered. As can be seen in Figure 33, after operating at a high enough pin current level to produce erratic behavior, when the current was lowered, the erratic behavior stopped, and, as can be seen in the upper trace (true rms meter output coupled with Pb-Sn-Te detector-amplifier) and the noise level continued to fall after the major erratic behavior stopped. This latter effect was more indicative of a thermal effect, rather than poisoning of the gas which would imply a permanent effect.

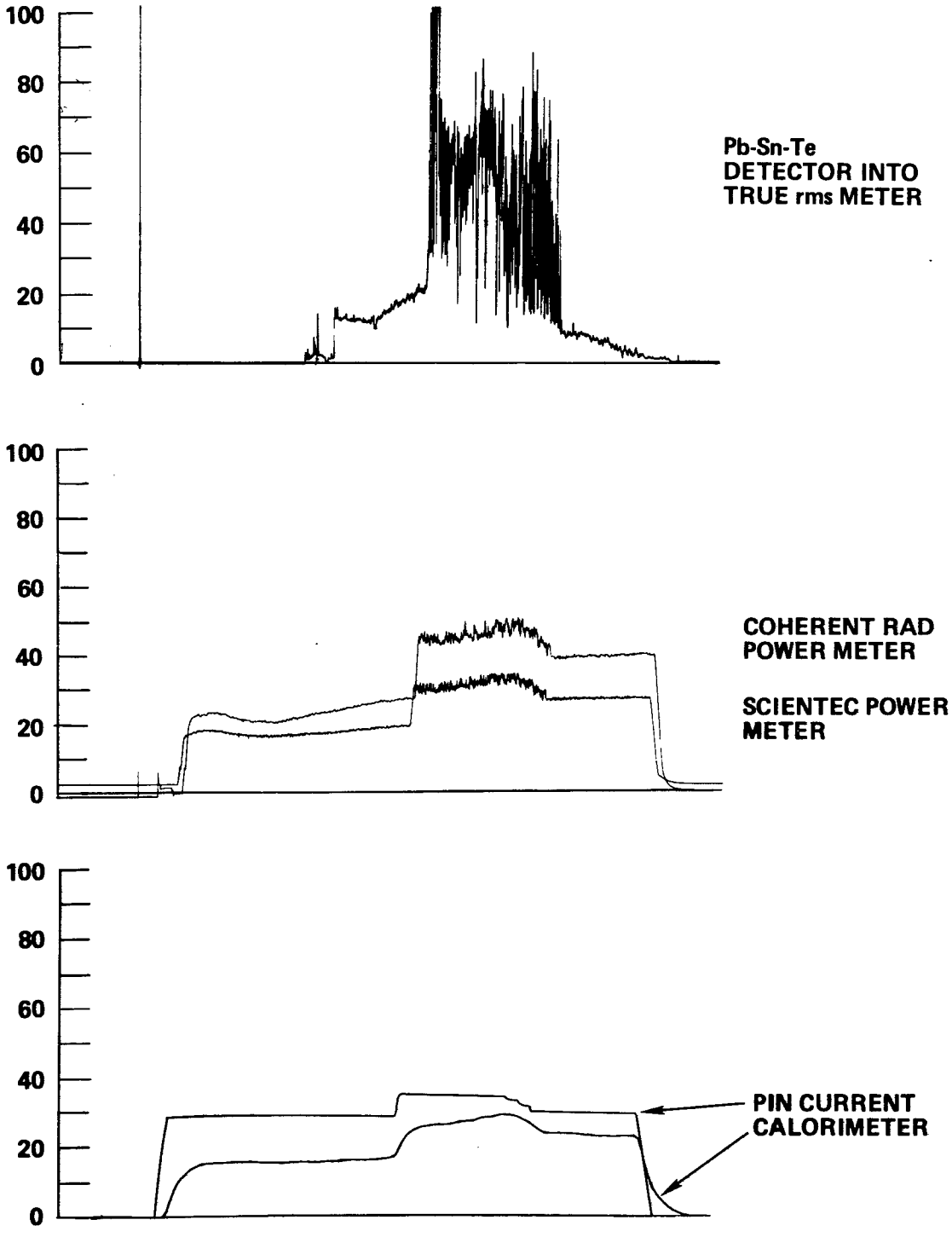

Figure 33. Chart Record of Detectors, Power Meters, and Pin Current Monitor. Chart Speed: 1" = 60 sec.

These data terminated the investigation of the vibrational-rotational line behavior. Although not all of the behavior was fully understood (or could be explained), it was agreed by both Rockwell and NASA Personnel to move on to the second area of investigation.

C. Heterodyne Tests

The second phase of this experimental program was dedicated to performing tests to ascertain the frequency stability of the laser. Given that the laser will operate in a single rotational line, a measurement of the relative frequency between two lasers is of interest. To do this, the laser was heterodyned with a known source and the beat note was observed. In this instance, the "known source" is a stabilized laser which is sealed off, has a stable resonator, and a grating for line control. The stability is given conservatively as

Short term ± 20 KHz at zero to 100 Hz

Long Term ± 5 MHz at zero to 0.1 Hz

Figure 34 shows an optical schematic of the test room. During the initial beat note tests, the fast power monitor was not utilized. Realizing the poor response of the thermopile power monitor could allow significant short time transient effects to occur undetected, the fast power monitor was added.

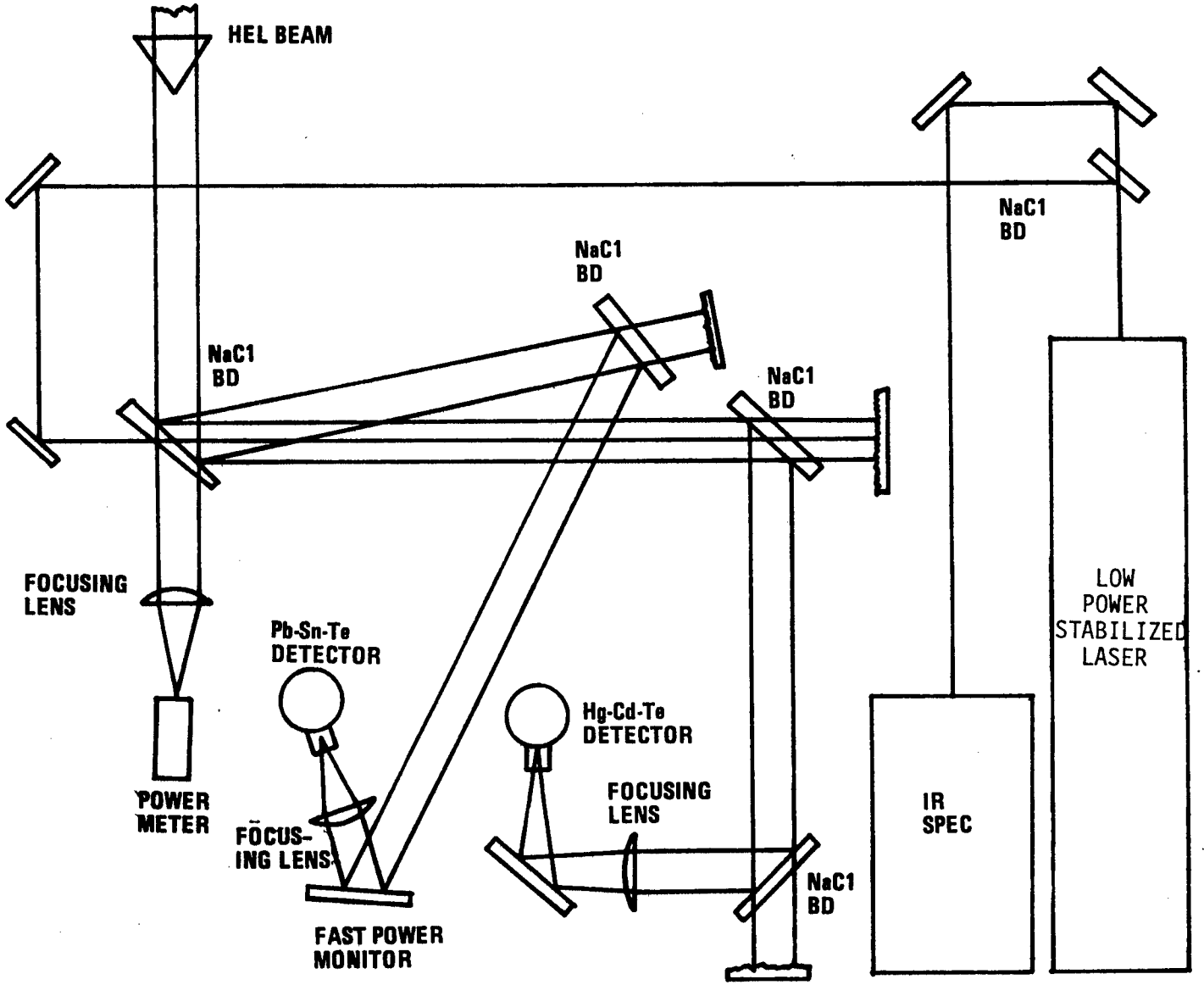

Figure 34. Test Room Optical Schematic (Tests 3/28/77 - 3/30/77)

The output of the Hg-Cd-Te detector was coupled to a fast oscilloscope, Tektronix Model 7904 (DC - 500 MHz) and one of two electronic spectrum analyzers: HP Model 141T, 0.1 to 110 MHz, or Tektronix plug-in, 0.1 to 1800 MHz. Both of these units have a minimum dispersion of less than 100 Hz per division. A dispersion of 100 KHz was the least dispersion at which data were recorded.

The anticipated line width of the HEL (operating pressure = 140 Torr) is of the order of 450 MHz (HWHM). Consequently, if this laser is operating to one side of line center, the beat frequency could be as great as 500 MHz (the low power laser has a line width of 75 MHz HWHM). Therefore, to monitor the beat note we selected the Hg-Cd-Te detector, BW > 500 MHz and employed a bias circuit and amplifier combination resulting in an overall bandwidth of 500 MHz. Figure 35 shows schematically the circuit employed with the Hg-Cd-Te detector.

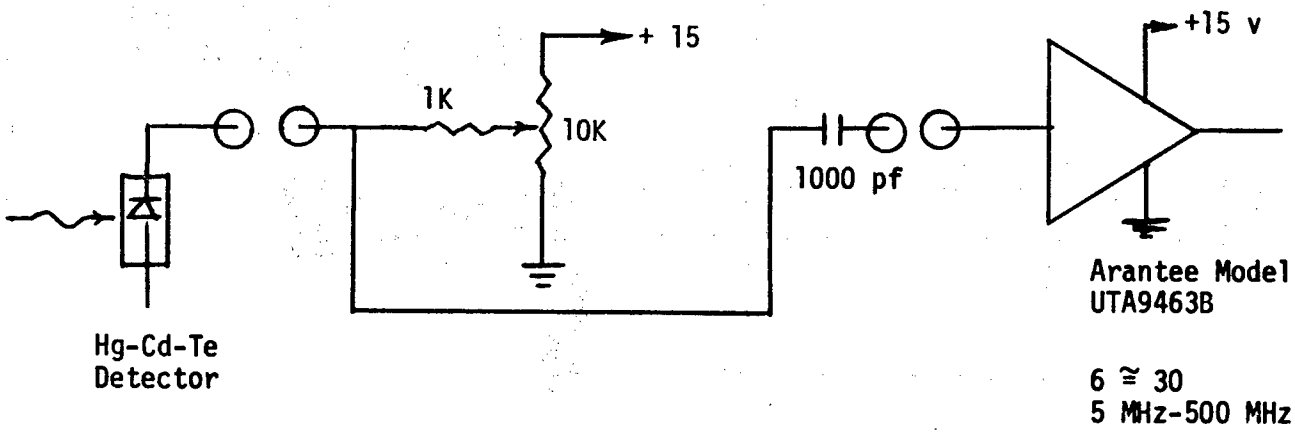

Figure 35. Beat Detector Amplifier and Bias Circuit

The first four runs of the laser were used in completing alignment of the system to verify detector operation. On the fourth run, a beat was observed and data recorded. Figure 36 shows the chart record of the calorimeter and pin current (the calibration on these charts was unchanged), in addition to an oscillogram of the beat signal. The beat note was in the range of 25 to 40 MHz with considerable FMing of the signal. The appearance of the beat signal appears sporadic. In Figures 37 and 38 are oscillograms, a spectrum analyzer trace and chart records of the fifth and sixth runs. It is evident that considerable FMing of the signal is present in the oscillogram. The spectrum analyzer does not show the FMing due to a very high sweep rate (1 ms/div). The frequency of the beat is $\sim$ 30 MHz.

After introducing the fast power monitor (i.e., the Pb-Sn-Te detector), the data shown in Figure 39 were recorded. With this change in instrumentation, oscillograms of the beat note and fast power monitor were made (see Figure 40), in addition to spectrum analyzer traces of the beat signal, as seen in Figure 41.

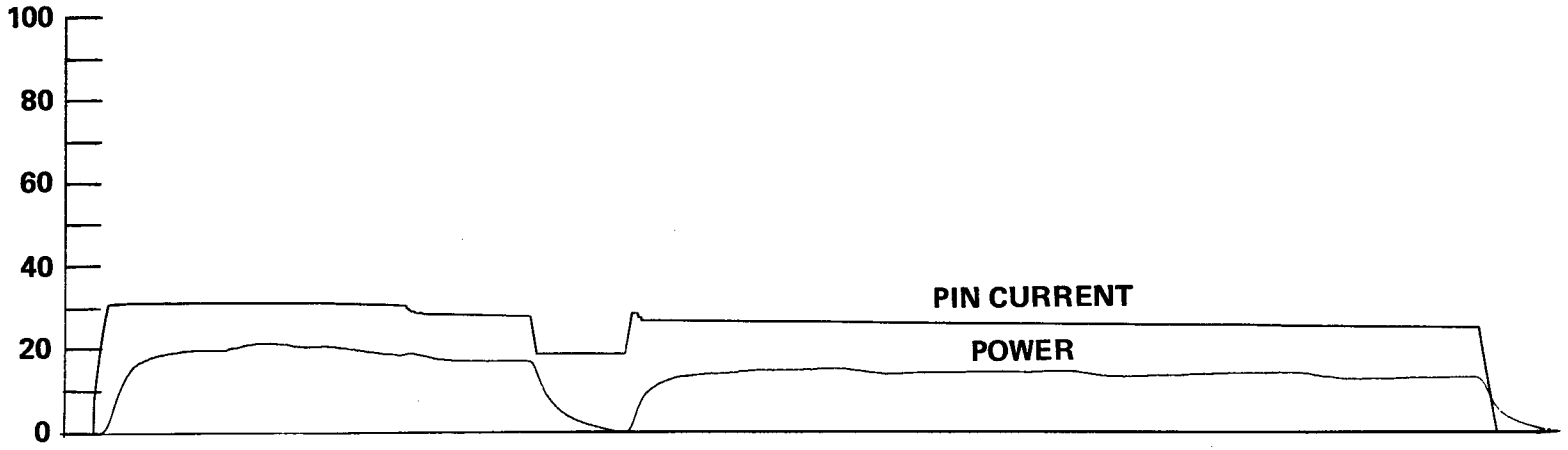

Figure 36(a). Chart Record of Calorimeter and Pin Current (3/28/77, Chart Speed 1" = 60 sec)

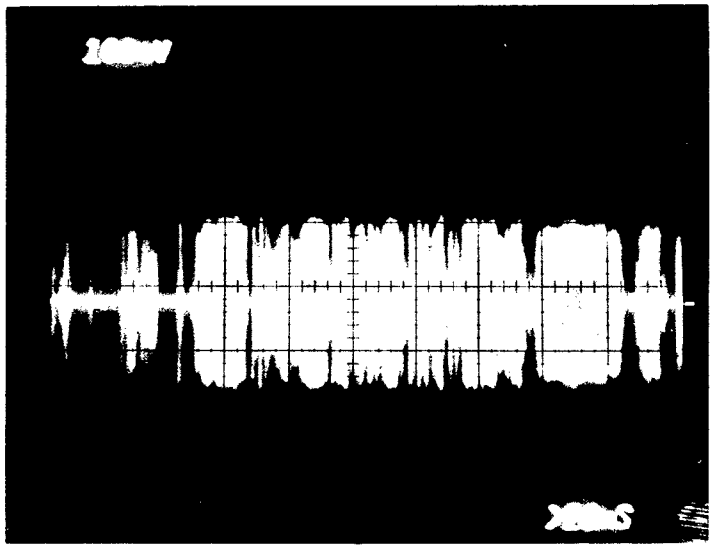

RUN NO. 4, 3/28/77

Figure 36(b). Oscillogram of the Beat Signal. Time 14:14 - 14:33

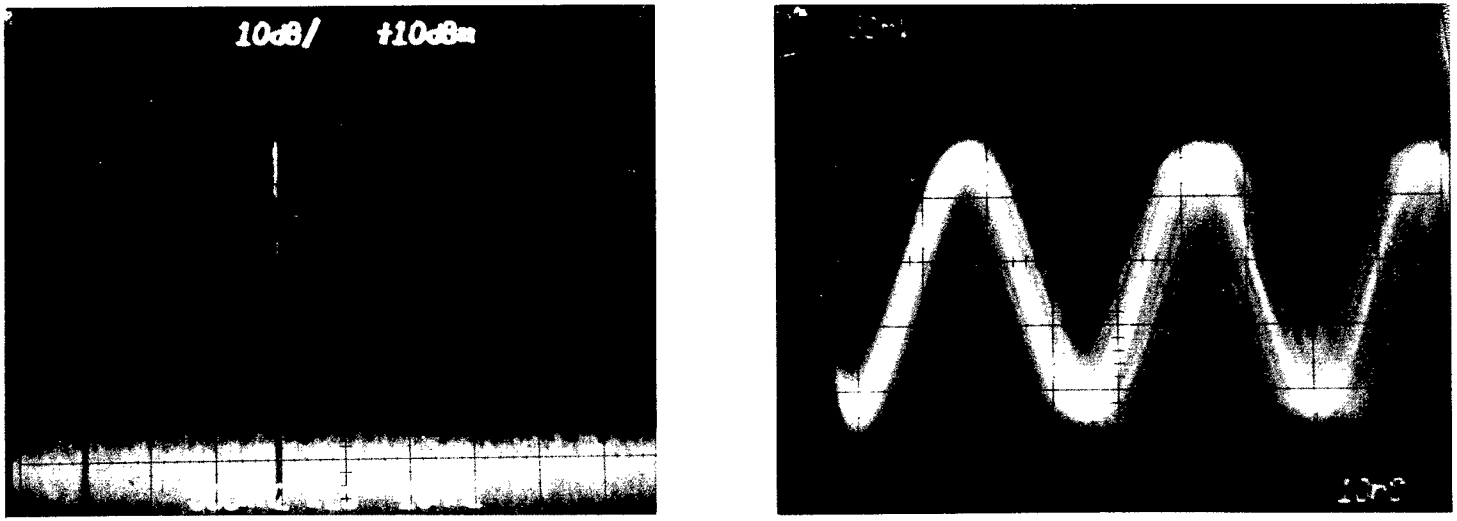

0

Figure 37. Spectrum Analyzer Trace and Oscillogram of Beat Note Between HEL Laser and Low Power Laser Taken During Run #6, 3/28/77

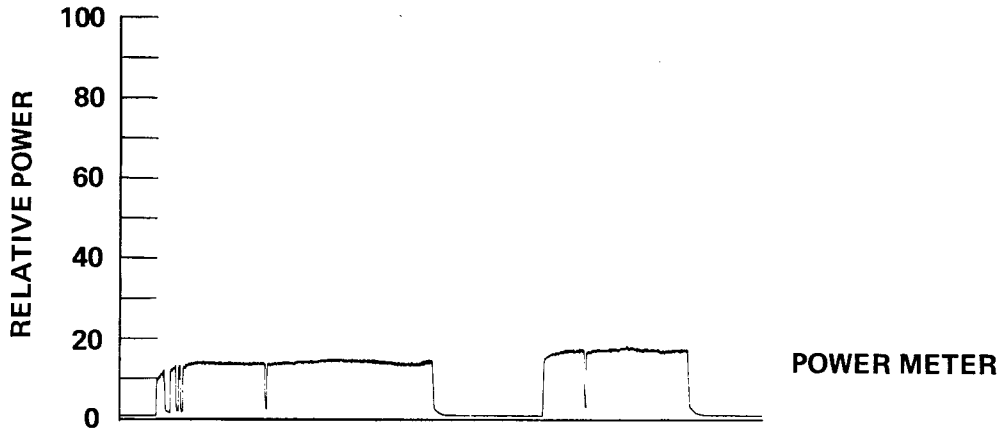

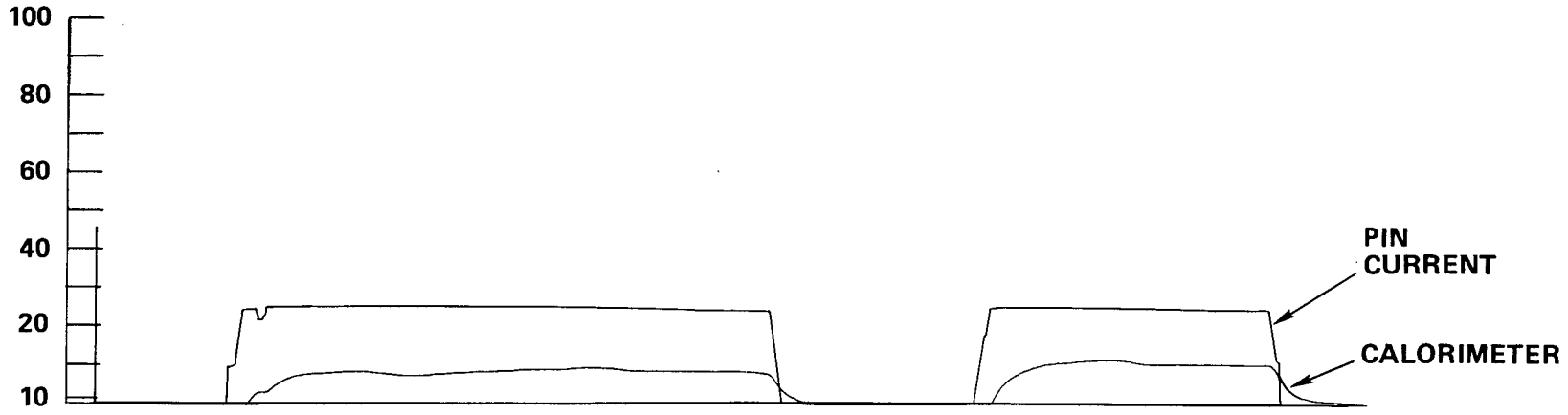

Figure 38. Runs #5 and #6, 3/28/77, Chart Records of Calorimeter and Pin Current (Chart Speed 1" = 60 sec) and Power Meter (Chart Speed 1" = 120 sec)

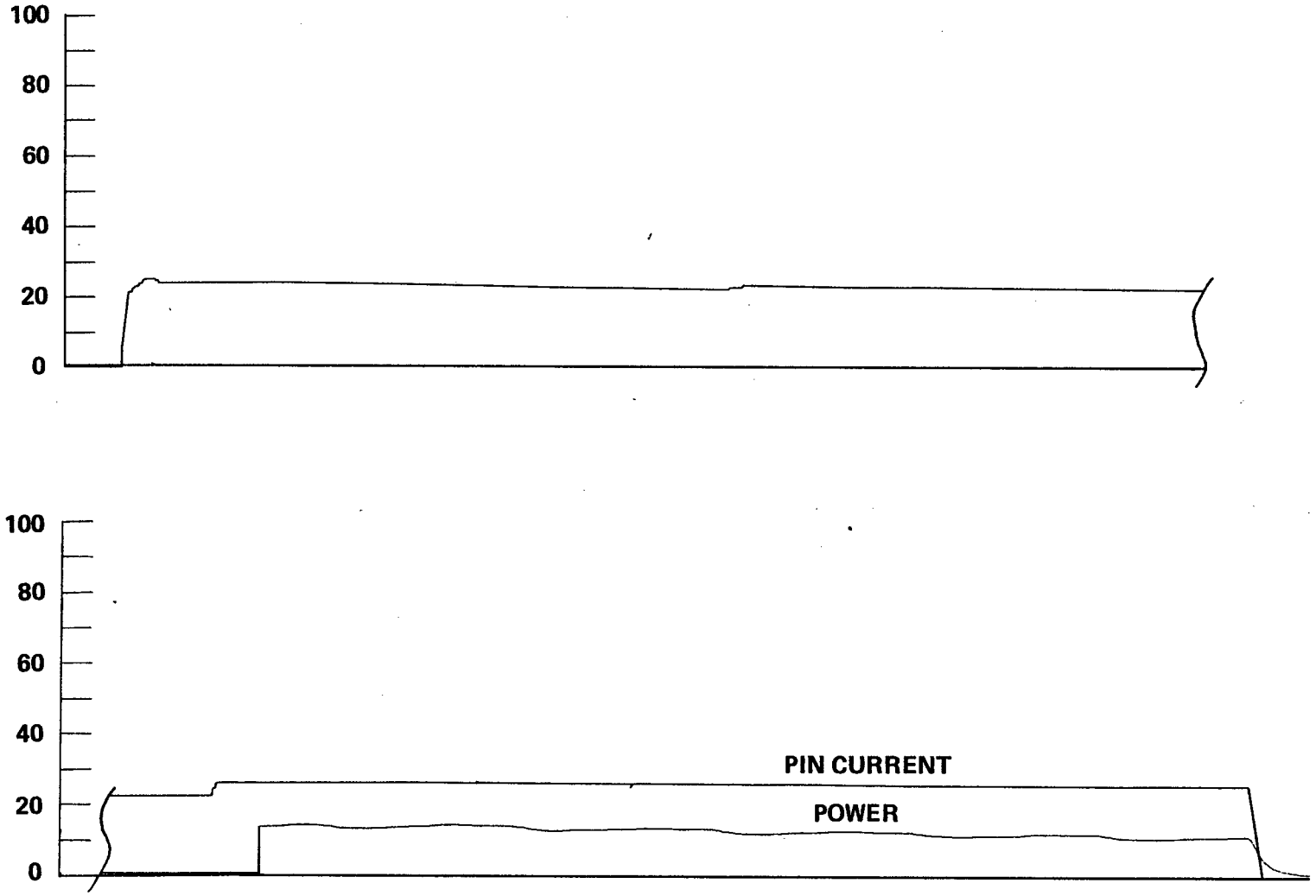

Figure 39. Chart Record of the Calorimeter and Pin Current for Run #1, 3/29/77, Time 10:05 - 10:40.

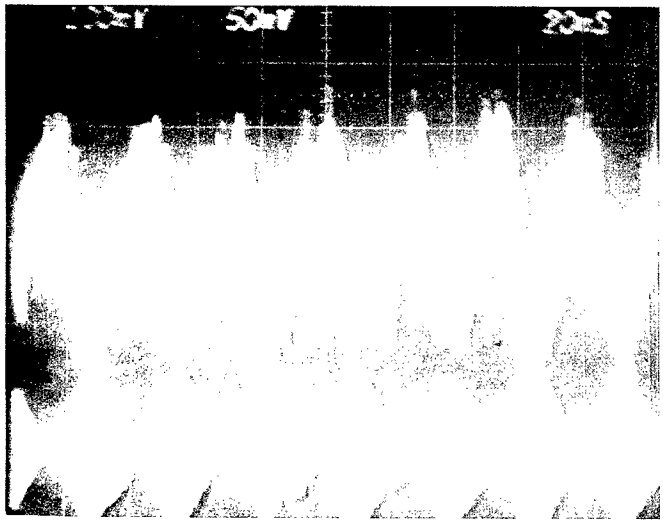

Time
10:23

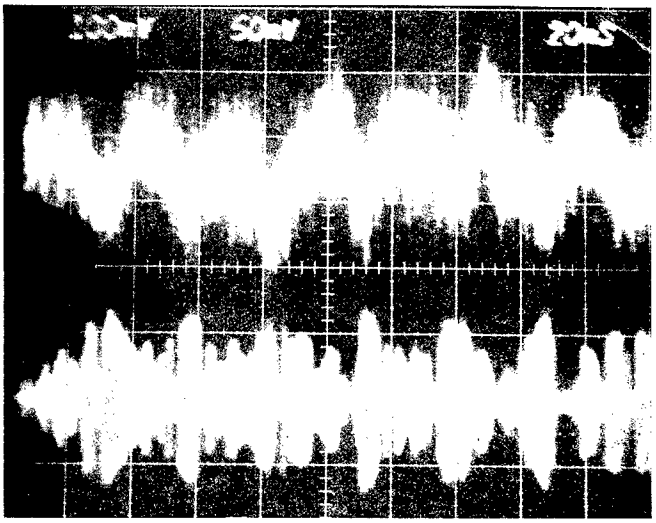

Time
10:27

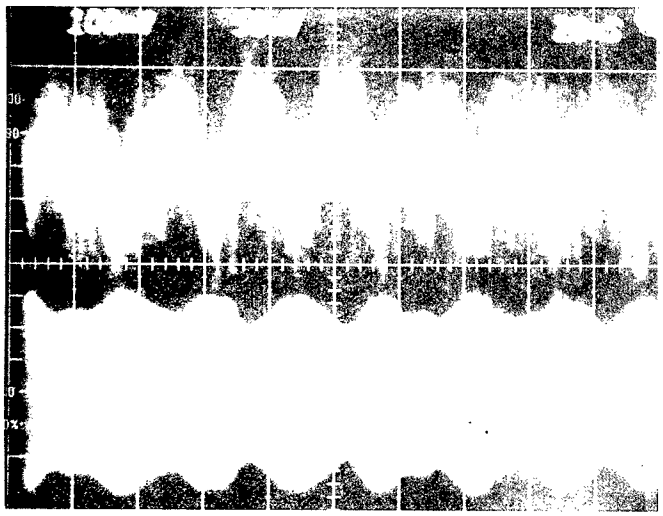

Time
10:30

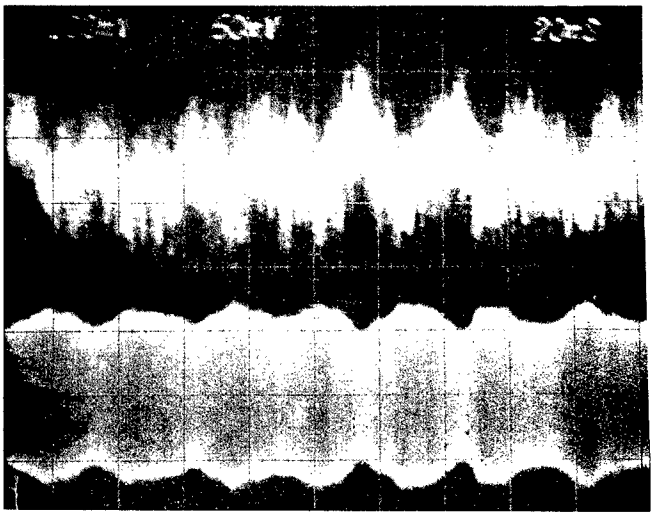

Time
10:31

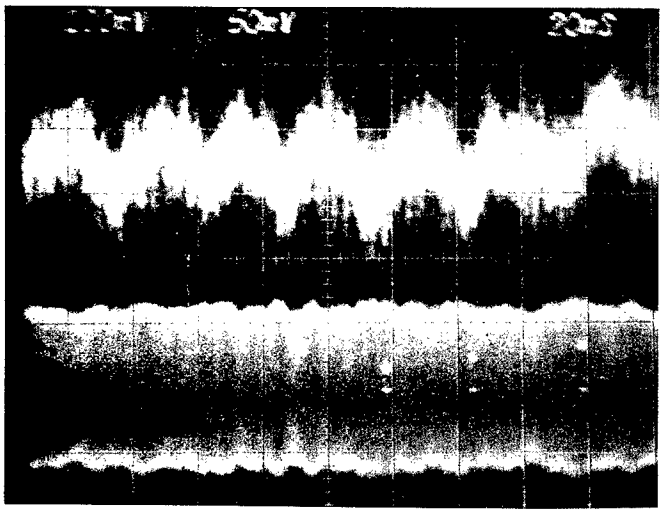

Time
10:32

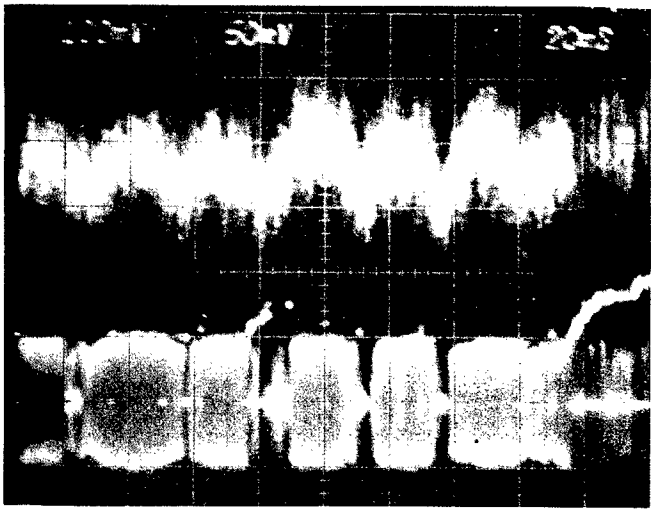

Time
10:38

Figure 40. Oscillograms of Fast Power Monitor (Upper) and Beat Signal (Lower), Run #1, 3/29/77

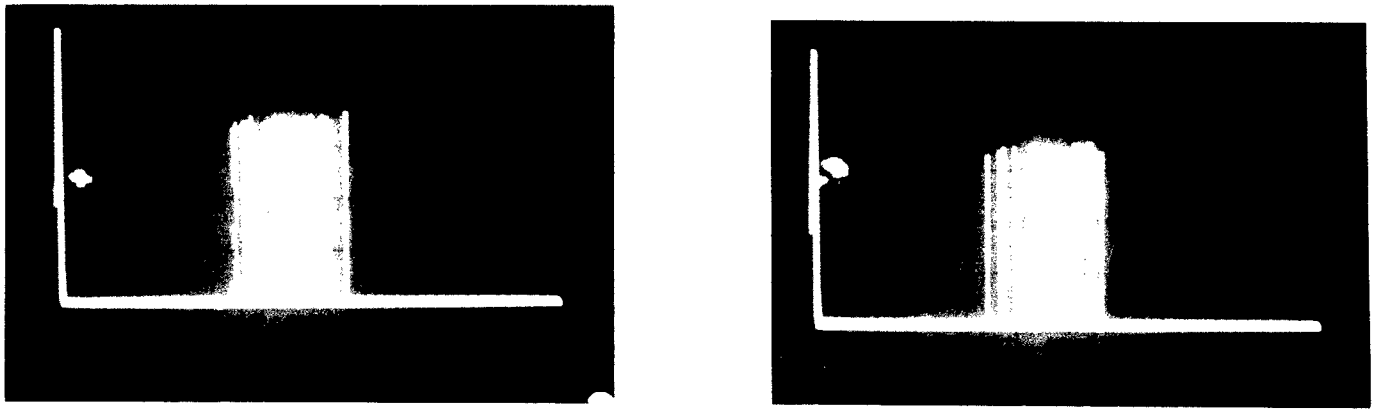

Figure 41. Spectrum Analyzer Traces of the Beat Signal - Sweep 20 ms/div, Dispersion 2 MHz/div, Run #1, 3/29/77

From analysis of these data, it appears that the FM had two driving functions; one about 6 Hz, the other was spread over the band 200-500 Hz. The 200-500 Hz rate produced a frequency deviation 2 MHz wide, while the 6 Hz appeared to be spread over $\sim$ 3.5 MHz. The result of many spectrum analyzer sweeps therefore produced a 5.5 MHz spread. Attempts to correlate the 200-500 Hz FM rate to power fluctuations (360 Hz) were inconclusive. The cause of this FM remains unknown.

D. Summary and Conclusions

The performance of the LeRC HEL laser was examined to determine (1) if a high energy unstable resonator laser will operate in a single rotational line, and (2) the degree of stability of that line.

The initial tests demonstrated that indeed the laser operated in a single line (00°1 - 10°0, P20 - 10.59 μm), but only at lower discharge current values (below 10 amperes), and when operating above 10 amperes, the laser became unstable after several minutes of operation. The laser instability was marked in two ways: (1) the output power fluctuated erratically, and (2) there was a shift in the operating line from 00°1 - 10°1, P20 to 00°1 - 02°0 (9.3 μm), where it hopped between the P16 and P18 lines.

In other tests the laser was unstable at the beginning of an operating run and then stabilized without any discharge current adjustments. The postulation that the instability was due to poisoning of the gas at high operating currents was refuted by raising the current to cause the instability, then lowering it, whereupon the laser again became stable.

By using a Mach-Zender interferometer with one branch, including the plasma region to monitor optical path length changes of the resonator cavity, it was concluded that the instability observed was the result of

an alteration in the cavity alignment, primarily as a result of the discharge current. Upon making alignment adjustments to the cavity at the higher discharge current levels (11-13 amps), the laser operation was steady in the P20 (10.59 μm) line. The nature of the cause for the cavity misalignment, whether a direct effect of increased current in the gas or secondary thermal effect upon the cavity, is unknown.

Also, during the second test phase, the beat note between the HEL laser and a stable local oscillator laser was observed and analyzed. After making the necessary cavity mirror alignment adjustments to produce stable operation of the laser, the envelope of the beat signal was found to be constant. Analysis of the beat note spectra resulted in the following estimates regarding the frequency stability of the beat note:

1. 2 MHz of frequency deviation @ 200-500 Hz rate
2. 3.5 MHz of frequency deviation @ 6 Hz rate.

These data represent an assessment of cavity quality and operational stability of the high power system. The servo system to adjust cavity length must be capable of responding to these rates with sufficient mirror movement to accommodate the frequency deviations. As such, these results were used to design the cavity mirror element described in the following discussion.

V. HIGH POWER CAVITY LENGTH TUNER

A. Background

The results of the frequency stability measurements performed at NASA LeRC suggested that, in order to phase control the LeRC laser adequately, a specially designed cavity length tuner must be fabricated. Specifically, it must be capable of changing the cavity length by as much as 0.5 μm at KHz rates to satisfy the condition, $\frac{\Delta L}{\Delta t} = \frac{L}{f}\frac{\Delta f}{\Delta t}$, where L is the cavity length, f is the laser frequency, and $\frac{\Delta f}{\Delta t}$ is the inherent frequency instability of the laser. Rigidity and dynamic-range requirements suggested that such a cavity length tuner can best be realized by sandwiching a voltage-controlled piezoelectric disk between the smaller cavity mirror and a heavy backup plate. Such a cavity length tuner was designed, fabricated and successfully applied, although the task was by no means straightforward, since the rather heavy mirror ($\sim$ 0.5 lbs) must be cooled during operation. Details of this cavity length tuner are discussed below.

B. General Description

The photograph of Figure 42 shows the laser cavity control mechanism to which the cavity length tuner for phase locking is attached. The piezoelectric disk, which is sandwiched between the mirror and the two cascaded backup plates, changes the cavity length by displacing the mirror when a signal voltage is applied to its terminal leads. The two backup plates are much heavier than the mirror and are physically isolated from each other by rubber gaskets. This provides sufficient rigidity and tends to minimize resonant vibrations.

Figure 42 -- Photograph of Cavity Length Tuner

Since a significant amount of energy is absorbed by the mirror during laser operation, the mirror itself must be cooled in order to avoid deformation of the surface. Here, cooling is accomplished by flowing water to the interior of the mirror via the two metallic tubes shown in Figure 42. The details of the cooling mechanism can best be discussed with reference to both Figures 42 and 43. The interior of the mirror is illustrated in Figure 43, which consists of a spiral-channel structure designed for maximum cooling at minimum flow-rate. Two holes are drilled through the piezoelectric disk, allowing water to flow to and from the mirror interior via channels inside the front backup plate. Both holes are insulated to prevent water seeping into the piezoelectric material. The purpose of the spiral-channel is to maximize the area of contact with the cooling fluid.

C. Calculations

1. Absorbed Power

Power absorption results in heat which must be conducted away to prevent system performance degradation. For the LeRC cavity configuration, which is positive branch confocal, the average internal power, P_i, is approximately given by

$$P_i \simeq \frac{M^2}{M^2 - 1} P_o, \qquad (1)$$

where M is the cavity magnification and P_o is the average output power. For $P_o \simeq 10$ kw and M = 1.257, the internal power is calculated to be about 27 kw. The maximum intensity, I_{max}, incident upon the mirror surface is therefore approximately

$$I_{max} \simeq \frac{2}{\pi\, d^2/4} (P_i - P_o) \simeq 4 \text{ kw/cm}^2, \qquad (2)$$

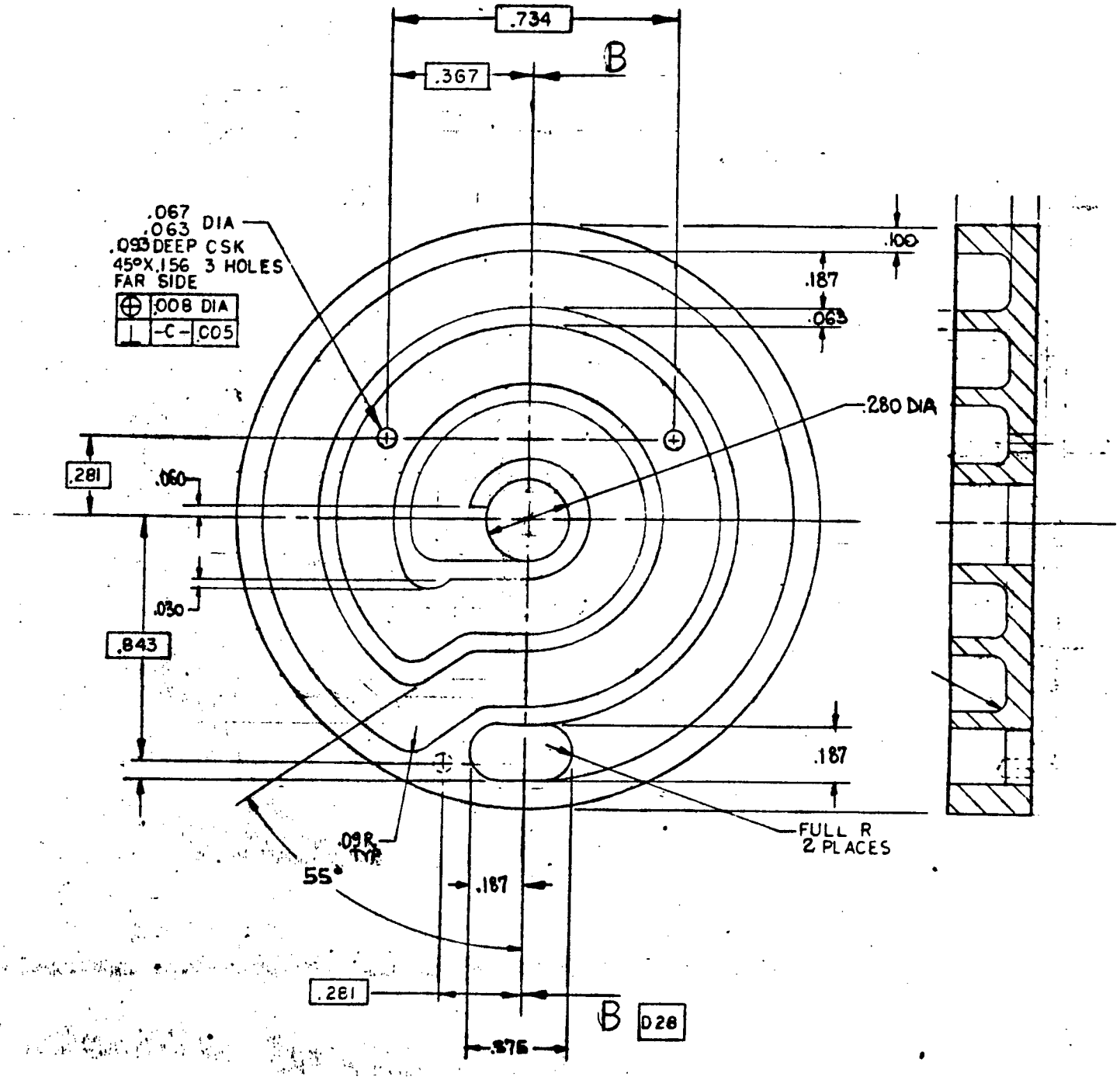

Figure 43. Two-View Drawing Showing Interior of Mirror

where $d \approx 3.28$ cm, the mirror diameter. The reflectivity of the copper mirror is close to 99%, and so the heat generated (or absorbed power) to be conducted away is about 350 watts.

2. Temperature Rise and Mirror Cooling

Since the beam profile is not uniform, absorption of the energy results in a non-uniform temperature distribution on the mirror surface. Such a temperature distribution induces surface distortion; therefore, the heat generated must be conducted away.

Cooling of the mirror may be discussed with reference to the following equation:

$$P_a = hA(T_M - T_F). \qquad (3)$$

In Eq. (3), P_a is the power absorbed (or the heat generated); T_M and T_F are, respectively, the temperature of the mirror and the cooling fluid; h is the coefficient of heat transfer, which varies between about 5,000 to 50,000 watts/M^2 °C, depending upon the flow rate and the surface roughness; A is the total area in direct contact with the flowing fluid.

The present configuration was designed to operate at a water temperature of 2°C and a flow rate of $1.26 \times 10^{-4} M^3$/sec. In particular, it was designed to limit the mirror temperature to no more than 2.5°C above its normal operating temperature, even for an absorbed power considerably greater than the 350 watts specified.

D. Experimental Tests

The cavity length tuner was experimentally tested for frequency response, as well as for stability as a function of flow rate. Two low power CO_2 lasers were used in the experiments; however, one of the lasers was modified in that its back mirror was replaced by the cavity length tuner. A photograph of the experimental setup is given in Figure 44.

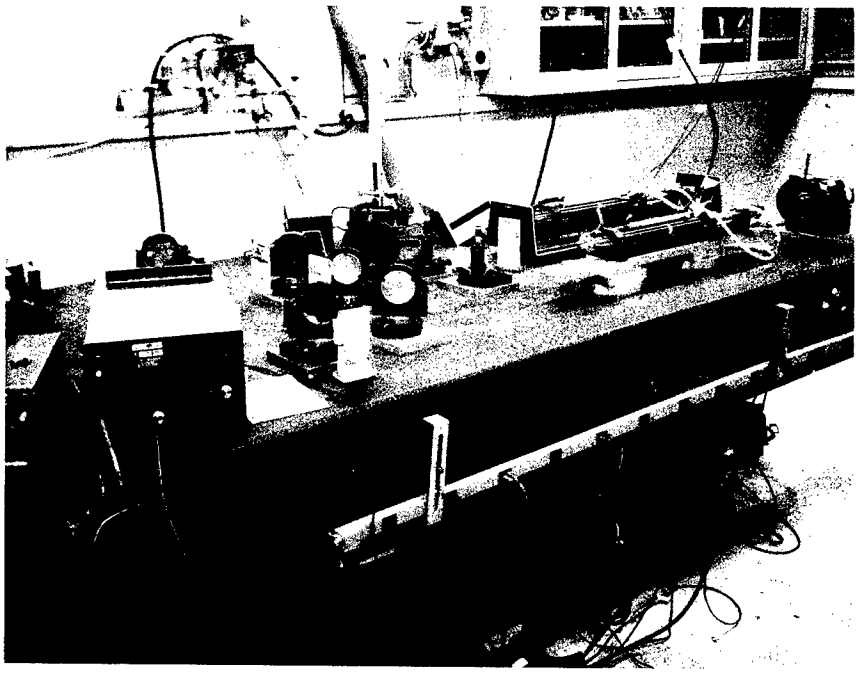

Figure 44. Experimental Setup for Evaluation of Cavity Length Tuner

The initial test was performed to evaluate the frequency response of the cavity length tuner. For this test, the tuner was driven by a sweep generator at constant output, resulting in frequency, or cavity length, tuning of the modified laser. The frequency response was determined from the frequency spread of the beat signal of the two lasers. Figure 45 shows the normalized frequency response as a function of the drive frequency. We see that the useful bandwidth is limited by the resonance at about 9 KHz. However, bandwidth improvement can usually be realized by more elaborate design, if required. For frequencies below about 9 KHz, the fractional cavity length change per unit drive voltage is about 10^{-9}/volt. For a cavity length of two meters, half a micron change would therefore require about 250 volts.

Since the cavity length tuner was designed to operate with a flow rate up to .126ℓ/sec, a test was undertaken to investigate the effect of water flow on the stability of the tuner under phase-locked condition.

Initially, the two lasers were phase-locked at zero flow rate (i.e., no water flowing). The flow rate was subsequently increased and varied up to .126ℓ/sec at increments of about .03 ℓ/sec. Noticeable phase jitters were present at rates exceeding about 0.1 ℓ/sec. In all cases, however, the lasers remained locked.

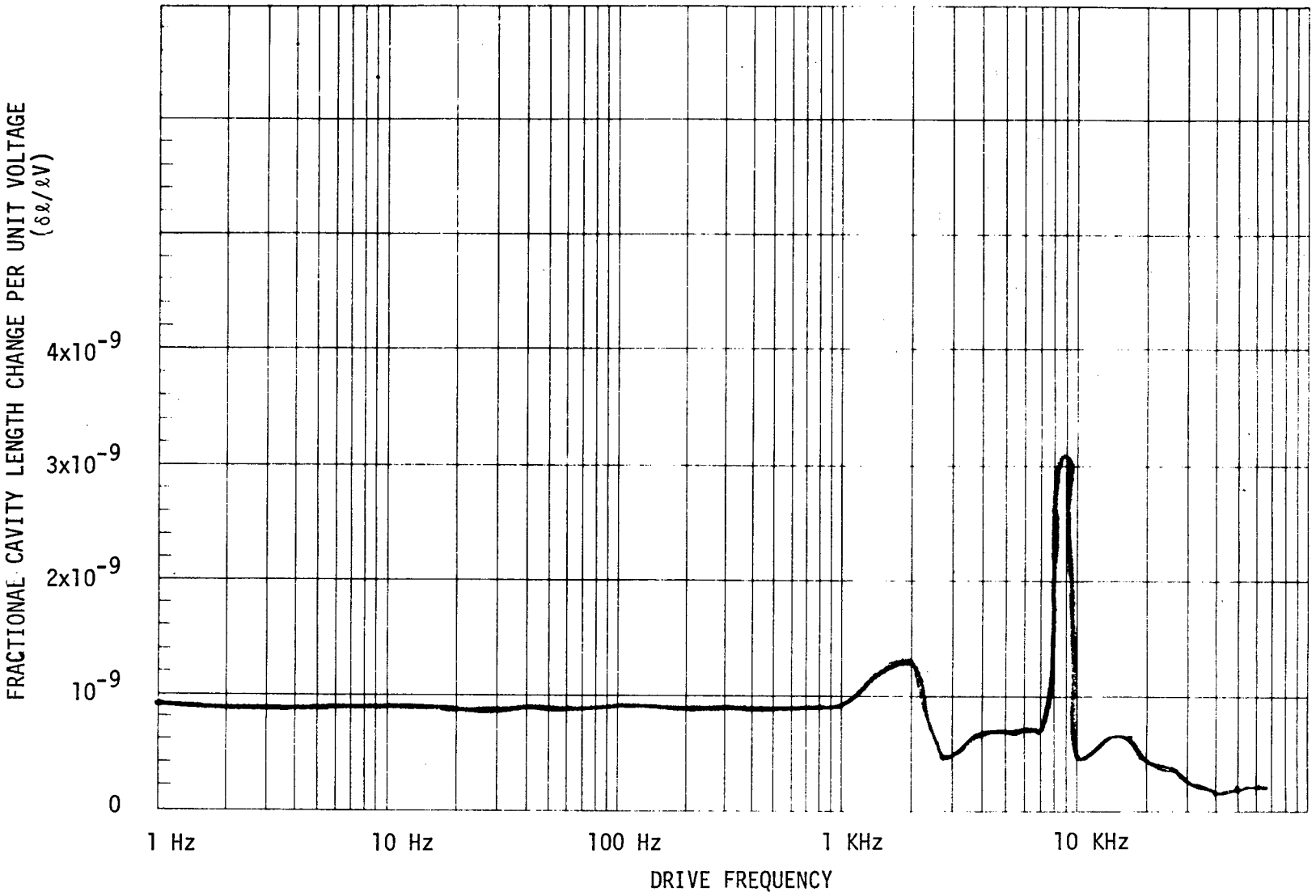

Figure 45. Frequency Response of Cavity Length Tuner

VI. NASA LEWIS HIGH POWER PHASE LOCK TESTS

A. Introduction

With the design and fabrication of the water-cooled mirror for cavity length control, the next phase of the program addressed the problems associated with phase lock control of the high power cavity. The mirror was installed and the laser operated at a high power level to ensure the operation was the same as with a fixed mirror. Having accomplished this goal, numerous tests were conducted over a cumulative three-week period of time. To ascertain the loop control requirements with the control mirror in place, the first sequence of tests involved the phase lock of a low power cavity to the high power unstable resonator. The control signals represent a demodulation of all perturbation effects and identified new sources of error for the single channel tests performed.

The tests then proceeded to an evaluation of intercavity effects with two channels in operation. Among the parameters measured were: amplitude stability, frequency stability, and polarization effects. With these data as background, phase lock control of the high power cavity was attempted. To achieve the phase lock condition, it was necessary to augment the control process with a wide bandwidth control unit in the low power laser. However, phase lock was achieved and the results indicated the necessary improvements in the mirror design necessary for unaugmented operation.

The following discussion briefly addresses these areas. As in all research effort, numerous trials were made to establish the operational concept. Only the most important data are reported.

All tests were conducted with the optical configuration of Figure 46, where a small fraction of each HEL beam was directed to heterodyne instrumentation

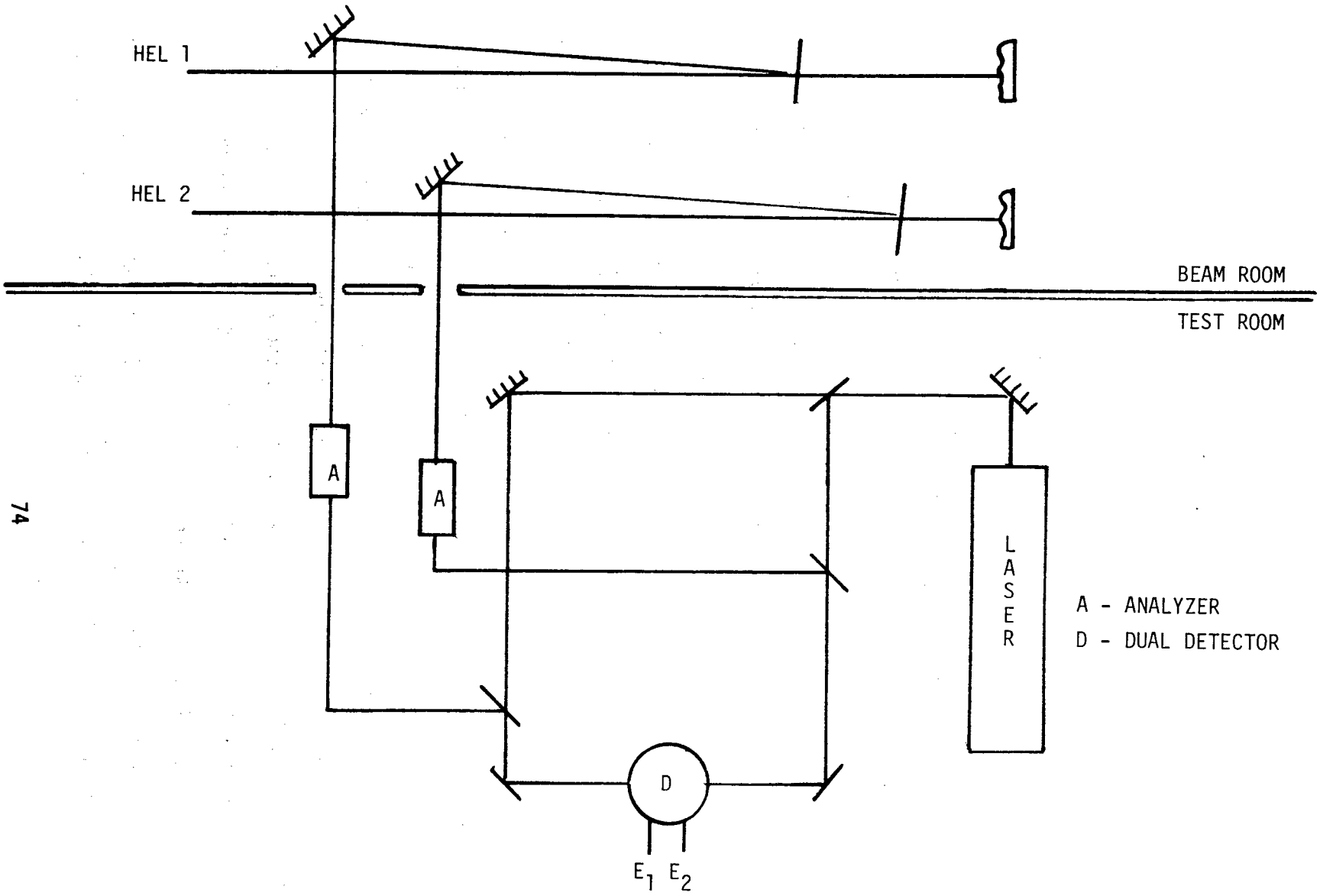

Figure 46. Heterodyne Phase Lock Test System (Simplified)

shown. Analyzers were necessary to determine the effects of polarization and are not required for phase lock operation. Processing signals E_1 and E_2 represent the information necessary for servo control.

B. Single Channel Phase Lock Tests

As mentioned previously, the first series of tests were conducted to establish the fact that the output of the high power device could be locked to a low power system, i.e., the frequency behavior of the device was such as to not preclude the possibility of phase lock control. The system for accomplishing this has been designated as a dual channel control configuration (Figure 47), based on a cross-over servo principle. A brief discussion of this instrumentation is necessary to explain the data to follow.

In this system, designed for a noisy environment, the "cross-over processing signal is divided into low-pass and high-pass channels. The low range of frequencies is filtered to drive a piezo-element having sufficient movement to tune the cavity through one free spectral range. Thus, correction is made for perturbations such as thermal drift which require a large dynamic range. The high-pass channel is processed and applied to an intracavity electro-optic phase modulator. Active phase control with response from DC to over 100 KHz is thus obtained.

To characterize operation from a control system anlaysis, consider the closed-loop of Figure 48.

F(s) and G(s) represent filter functions which condition the signal prior to application to $T_1(s)$ [piezo] and $T_2(s)$ [E-O Modulator]. For frequency (phase) control of a laser, the following relationship applies:

$$\phi_o(t) = +2\pi\int(\Delta\nu)\,dt = -2\pi\,\frac{\nu}{L}\int(\Delta L)\,dt,$$

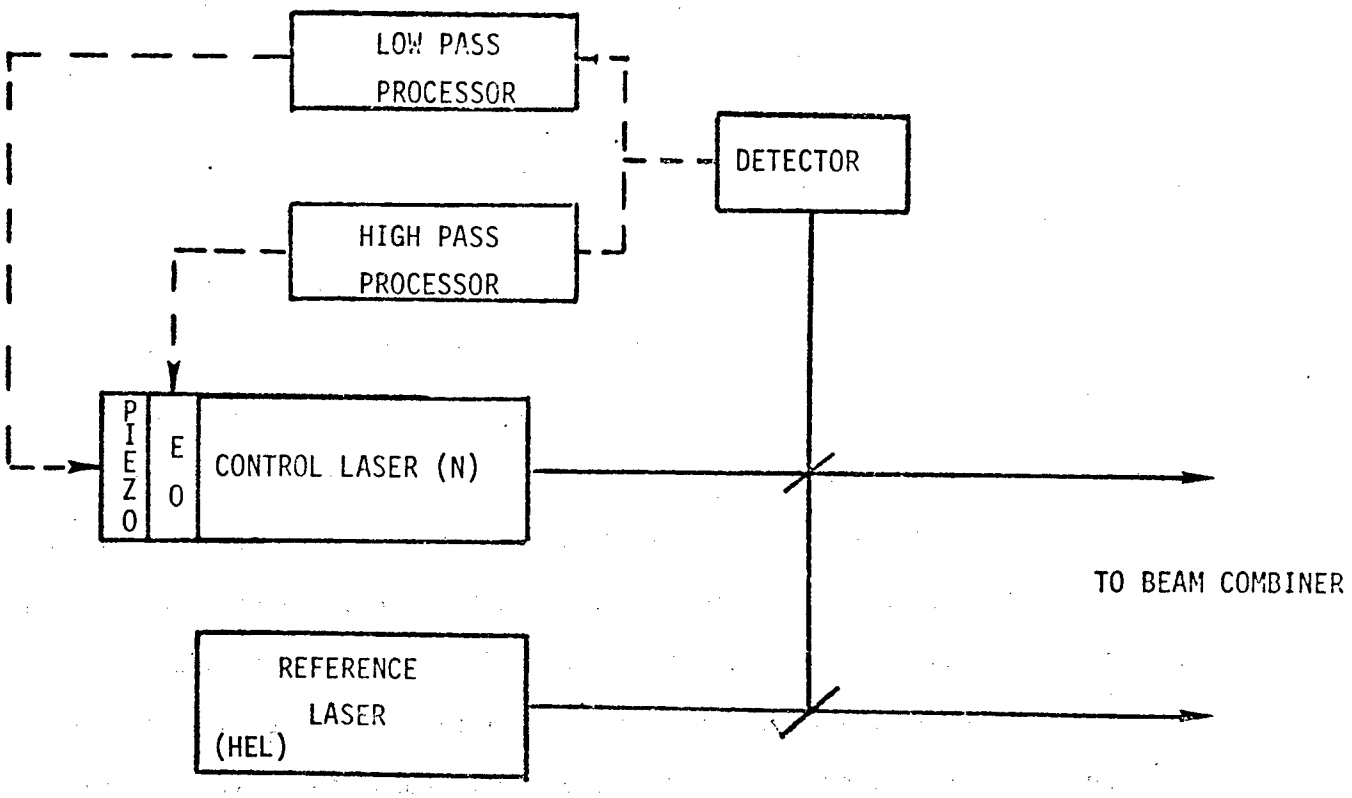

Figure 47. Dual Channel Control System

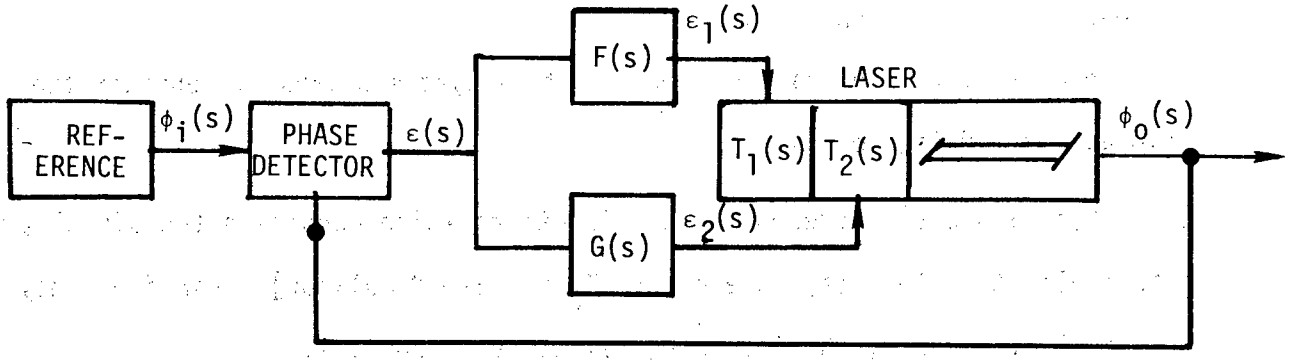

Figure 48. Closed-Loop System

where L = the cavity length

ν = laser frequency, and

ϕ_o = output phase variable.

In LaPlace notation,

$$\phi_o(s) = \frac{2\pi\nu}{L} \frac{\Delta L(s)}{S}, \text{ where S is the complex quantity } \sigma + i\omega.$$

Since the function we wish to reduce to zero is the difference in phase (ε) between the input and output:

$$\varepsilon = \phi_i(s) - \phi_o(s)$$

$$= \phi_i(s) - \frac{2\pi\nu}{L} \frac{\Delta L(s)}{S} = \phi_i(s) - K_1 \frac{\Delta L(s)}{S}$$

$$= \phi_i(s) - \frac{K_1}{S} [\varepsilon_1 T_1(s) + \varepsilon_2 T_2(s)]$$

$$= \phi_i(s) - \frac{K_1}{S} [\varepsilon F(s) T_1(s) + \varepsilon G(s) T_2(s)],$$

where K_1 is defined as $\frac{2\pi\nu}{L}$.

This becomes, then,

$$\varepsilon(s) = \frac{S \phi_i(s)}{S + K_1[F(s) T_1(s) + G(s) T_2(s)]}.$$

Since we desire the steady state phase error to approach zero, that is,

$$\lim_{t \to \infty} \varepsilon(t) \to 0$$

from the final value theorem

$$\lim_{S \to 0} S\varepsilon(s) = \lim_{S \to 0} \frac{S^2 \phi_i(s)}{S + K_1[F(s) T_1(s) + G(s) T_2(s)]} = 0.$$

Choosing the reference as an oscillator of frequency ω_o,

$$\phi_i(s) = \frac{\omega_o}{S^2}$$

and

$$\lim_{S \to 0} \frac{\omega_o}{S + K_1[F(s)\ T_1(s) + G(s)\ T_2(s)]} = 0.$$

The necessary form of the filter/transfer function to achieve a steady state error of zero can be specified as

$$F(s)\ T_1(s) + G(s)\ T_2(s) = \frac{(S + a)(S + b)\ - - - -}{S(S + c)(S + d)\ - - -}$$

Circuitwise (for no noise perturbations), the overall control network is, then,

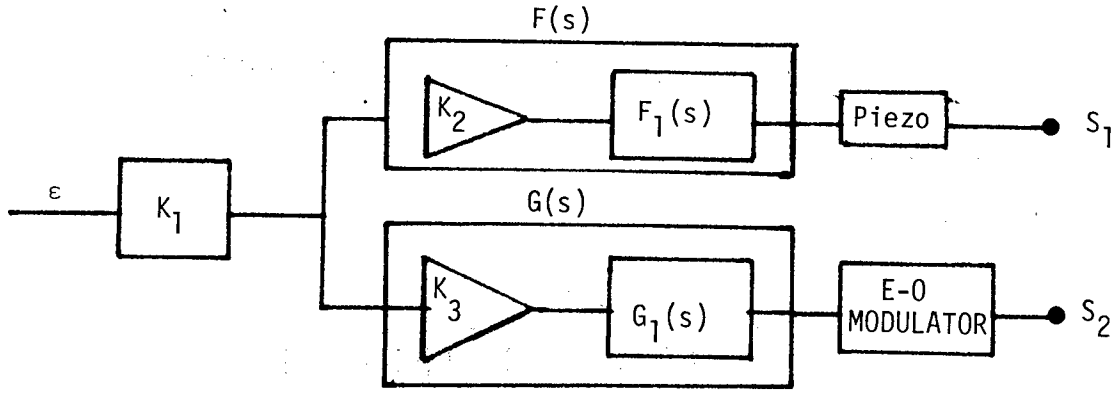

Figure 49. Cross-Over Network for Phase Lock Control

where K_1, K_2 and K_3 are adjustable gain functions and $F_1(s)$ and $G_1(s)$ represent the appropriate response function. S_1 and S_2 are signals which represent demodulated outputs of each channel and are the means for evaluating the system under test.

Using this approach with the processing signal developed by heterodyning HEL 1 with the low power device, the first test sequence resulted in phase lock operation, as illustrated by the data of Figure 50(a). The control signal, when compared to the reference signal, shows very little phase instability indicating a high quality lock. The piezo control (S_1) and E-O modulator (S_2) signals indicate sharing in the control function. Of note is the low frequency content of the signals. No high frequency perturbations are indicated. This corresponds to a "well-behaved" heterodyne beat of Figure 50(b) having a spread of about 5 MHz at the corresponding perturbation rates.

Prior to the second sequence of tests, the prime power supply to the HEL experienced a catastrophic failure. When brought back on line, the demodulated signal spectrum (rate of FM-ing) exhibited the characteristics shown in Figure 51(a). As indicated, a large frequency content corresponding to 120 Hz is evident with some frequency content extending to 500 Hz (no higher frequencies existed).

Since a 120 Hz signal is normally indicative of power supply ripple, a high voltage probe was convected to the anode of the plasma region. Figure 51(b) indicates about 50 v_{p-p} of ripple is present. The spectrum of this signal (51(c)) shows the fundamental and third harmonic content. When compared to the spectrum of the demodulated heterodyne signal used for processing, it is evident that the 120 Hz has a major effect upon the laser

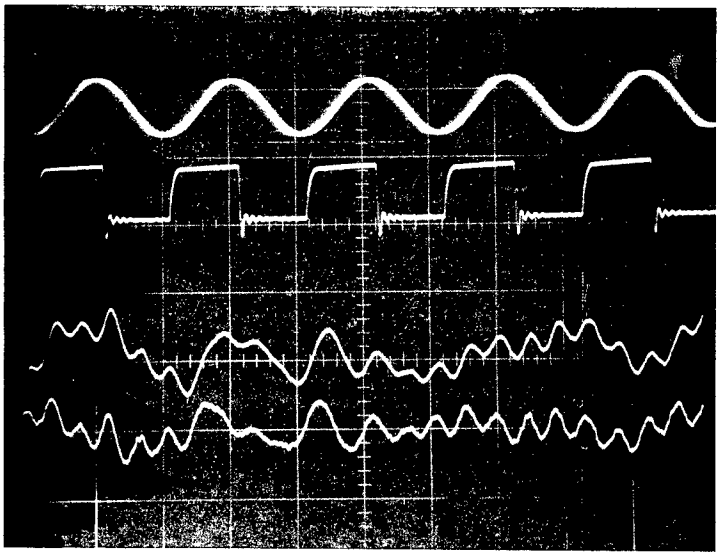

REFERENCE SIGNAL

0.5 μSEC/CM

HETERODYNE SIGNAL

S_1 - PIEZO CONTROL SIGNAL

S_2 - E-O CONTROL SIGNAL

5 mSEC/DIV

(a)

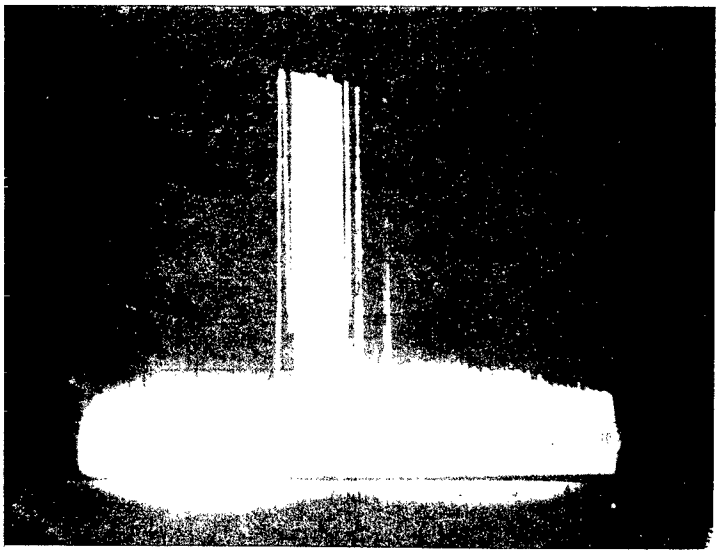

HETERODYNE BEAT
(UNLOCKED)

2 MHz/DIV

CENTER FREQUENCY - 10 MHz

(b)

Figure 50. Phase Lock Control Signals

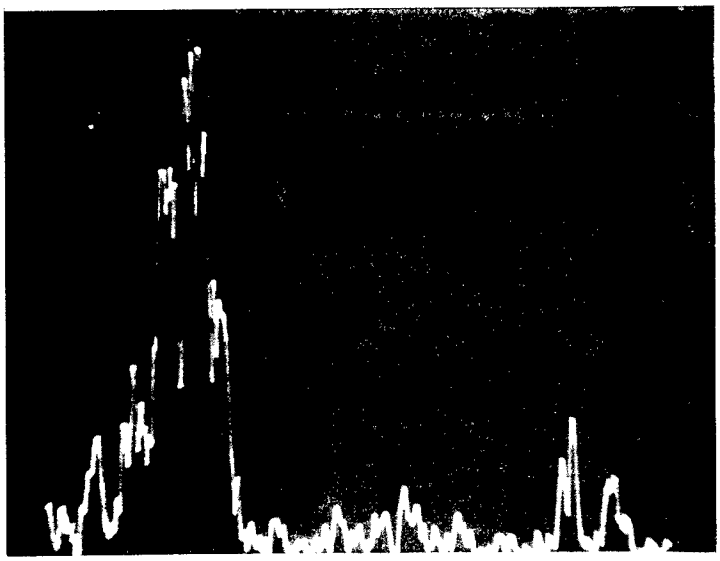

(a) SPECTRUM OF FREQUENCY DEMODULATED HETERODYNE PROCESSING SIGNAL

DISPERSION - 50 Hz/DIV
RESOLUTION - 10 Hz
LINEAR SCALE

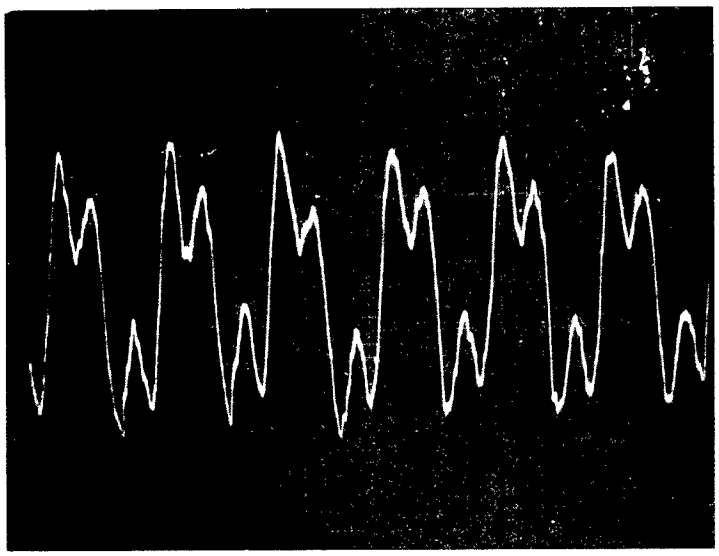

(b) POWER SUPPLY RIPPLE

10 V/DIV
5 MSEC/DIV

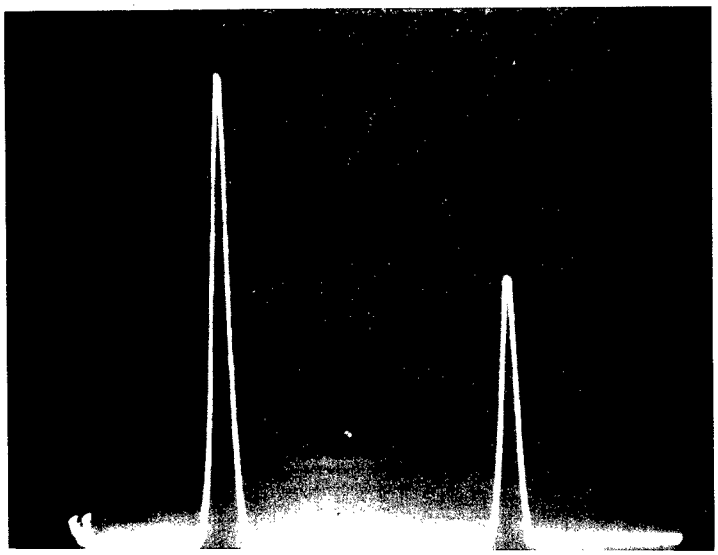

(c) SPECTRUM OF POWER SUPPLY RIPPLE

DISPERSION - 50 Hz/DIV
RESOLUTION - 10 Hz
LINEAR SCALE

Figure 51. Effect of Power Supply Ripple

characteristics. The induced frequency deviation at the 120 Hz rate was measured in excess of 10 MHz and exceeded the capture bandwidth of the phase lock electronics. Also to be noted is the absence of any induced modulation at the 360 Hz harmonic.

With these data available, the first series of tests were concluded. Successful locking of the low-power/high-power laser combination had been demonstrated. Extension of the experiments to control of the high power cavity was delayed until the ripple present on the power supply could be reduced.

C. Cavity Interaction Tests

Prior to the second series of phase lock tests, NASA personnel were successful in reducing the amount of ripple appearing at the anode of the discharge section. With the device lasing, the reduction was an order of magnitude, as shown in Figure 52. The spectrum of frequencies now shows not only the reduction in ripple, but illustrates the relative contribution of "noise" from sources other than the 120 Hz and 360 Hz residuals. In all likelihood, this "noise" can be attributed to current variations in the multiple pin discharge system. Of particular note is the low frequency content and the fact that all variations appear to be less than 500 Hz. (Demodulated lock signals seem to be correlated to this spectrum.)

Before attempting a multiple channel lock at this time, tests were conducted to determine: (1) the sensitivity of the output polarization to mirror alignment, and (2) intercavity effects from channel to adjacent channel. These experiments yielded several expected and unexpected results.

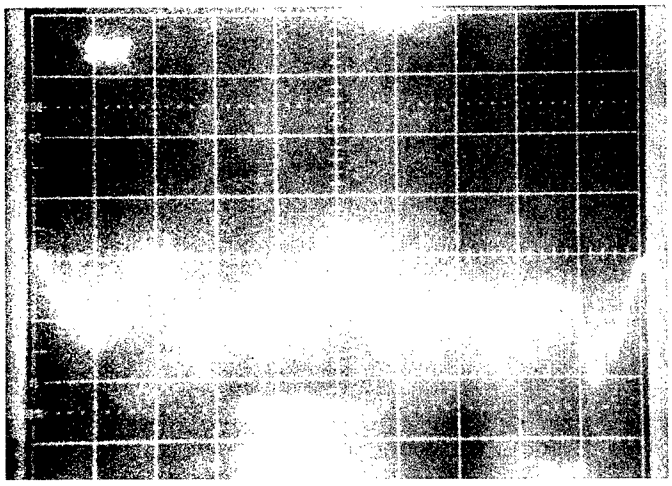

(a) POWER SUPPLY RIPPLE AT ANODE (X1000 PROBE)

5 V/DIV

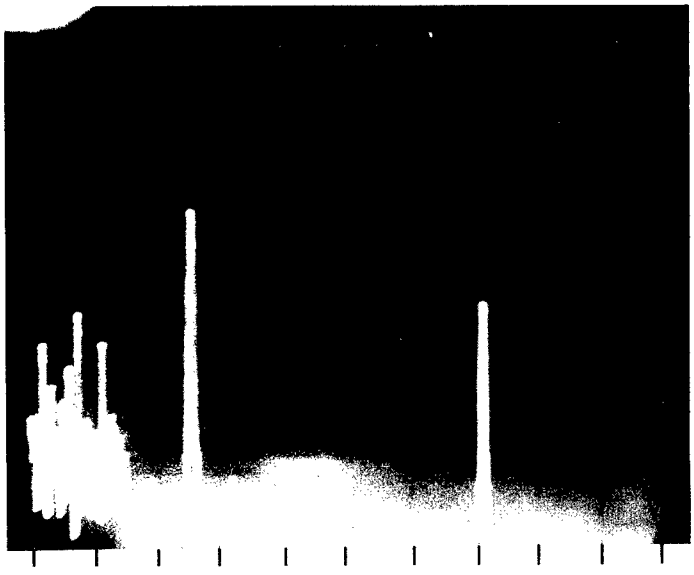

(b) SPECTRUM OF RIPPLE

DISPERSION – 50 Hz/DIV
RESOLUTION – 10 Hz
LINEAR SCALE

Fig. 52. Power Supply Ripple (Filtered)

As presently configured, the laser does not incorporate into the cavity an element to produce a preferred plane of polarization. The state of polarization is determined by various "defects" in the optics and mirror alignment conditions. Since the ability to phase lock lasers depends upon heterodyne processing, the polarization should remain constantly aligned with the local oscillator for the best results. To evaluate each channel, the planes of polarization for each channel were monitored as shown in Figure 53.

The Ge flat was oriented at Brewster's angle to effectively separate the output planes of polarization as seen by the detectors. Typical of the results are those shown in Figure 54. As indicated, the polarization is very critically dependent upon small alignment changes. Nearly a complete change in polarization from vertical to horizontal is shown. This result is not too surprising, in that the cavity is not designed with polarization elements. However, also shown is the periodic nature of the output power. With the reference level indicating no output, a 30 Hz pulse of 10 msec duration is indicated. This anomaly disappeared when the gas blower speed (30 rev/sec) was reduced to about 23 rev/sec and can only be attributed to a mechanical resonance in the cavity structure. Once discovered, subsequent tests were conducted at the reduced speed to ensure a continuous output.

To evaluate intercavity effects, the horizontal planes of polarization of two channels were then monitored. Figure 55 is typical of the results. Two features are significant. First, the output of Channel 1 is reasonably steady at the kilowatt level and does not fluctuate. Channel 2, which is located on the downstream side of Channel 1, exhibited a reduced output with significant fluctuations in power. Current excitation to this channel was

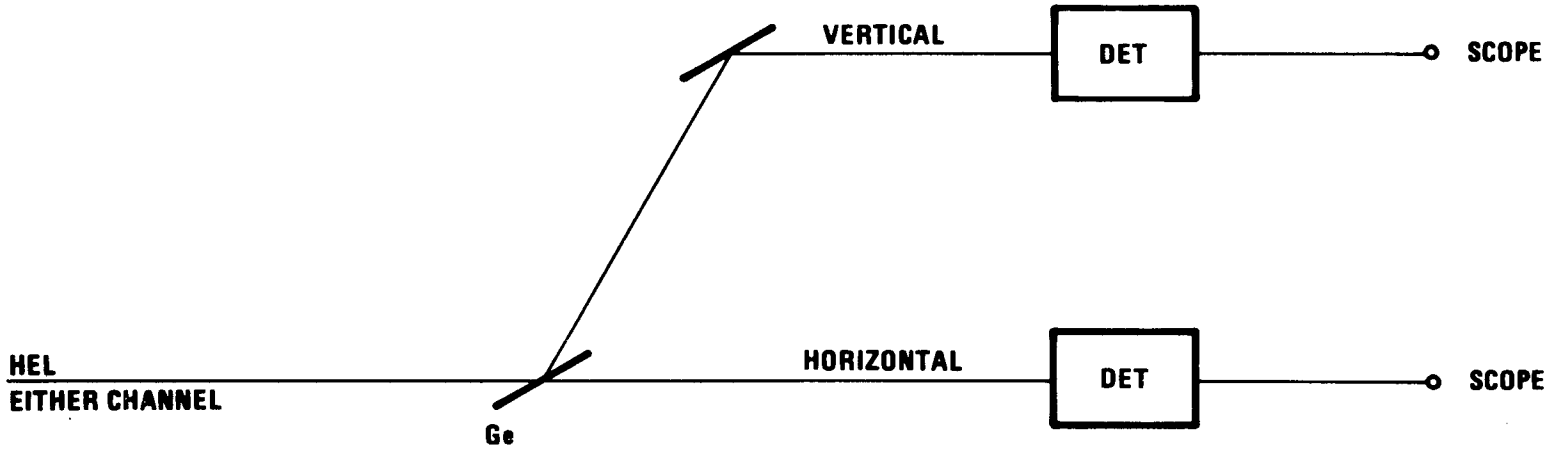

Figure 53. Polarization Instrumentation

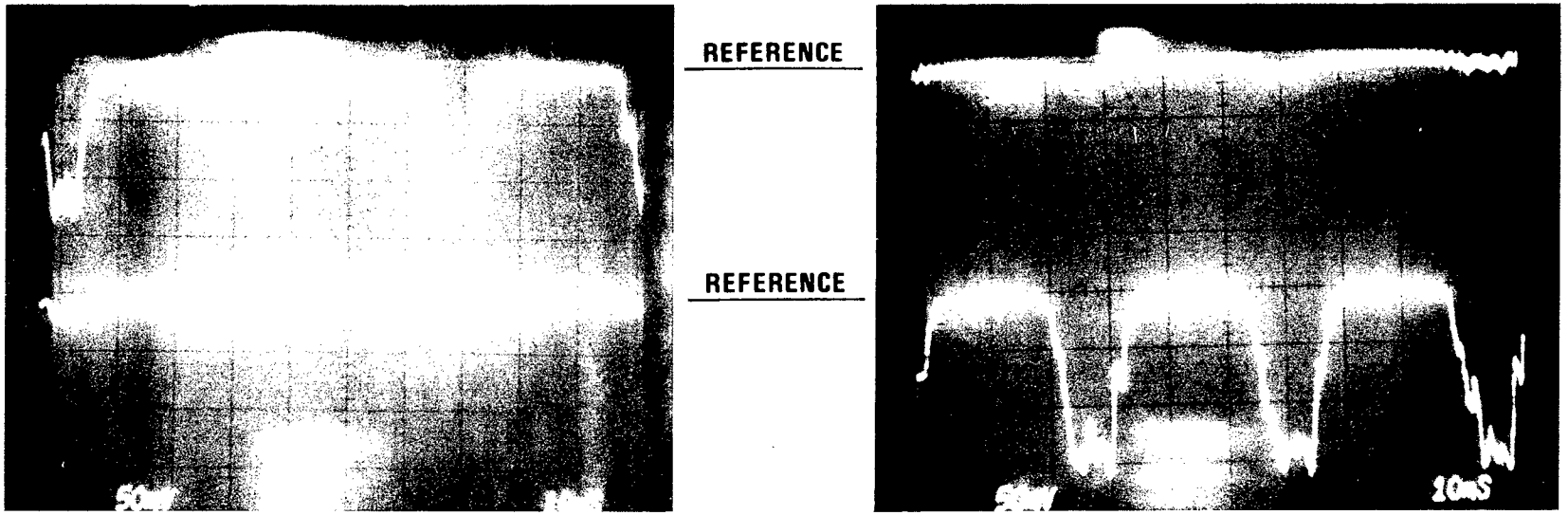

(a) CAVITY ALIGNED FOR VERTICAL POLARIZATION

(b) CAVITY ALIGNED FOR HORIZONTAL POLARIZATION

UPPER TRACES: VERTICAL
LOWER TRACES: HORIZONTAL

Figure 54. Polarization Tests - Channel 1

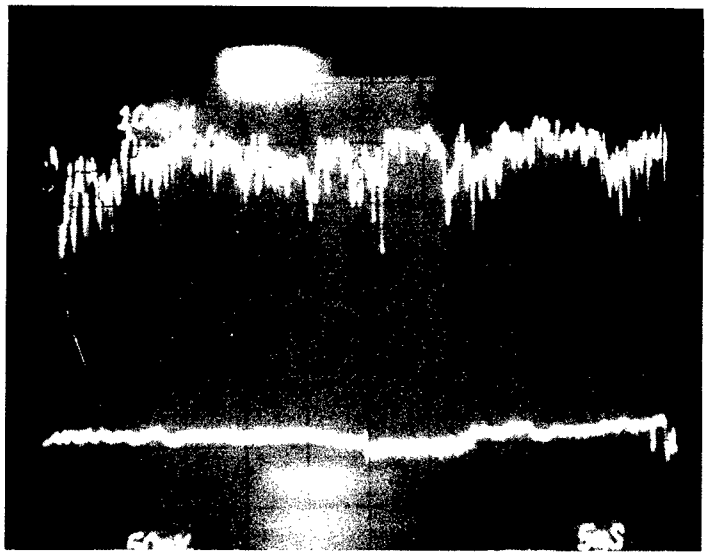

Figure 55. Polarization Tests Channel Interaction

approximately that applied to Channel 1. The reasons for the differences are a subject for design tradeoff and evaluation. The key issue here is that no discernible interaction from cavity to cavity could be detected. That is, it is reasonable to expect that each cavity in the common flow field functions independently of each other and frequency control of each cavity is possible with independent signal processors. Having established this fact, tests were then conducted to demonstrate phase lock control of Channel 1.

D. Multiple Channel Phase Lock Tests

The final test sequence was conducted to evaluate the cavity control which could be expected with the water cooled, piezo driven mirror. Figure 56 illustrates the basic optical/electronic system. With the necessary alignment for polarization, the offset heterodyne signal available at the detector was processed and applied to the control mirror. Due to the dynamic range and the perturbation rates present in the system, phase lock could not be established in this configuration. However, the control system had enough bandwidth to realize a "frequency" lock, as shown in Figure 57 Here, the processing signal has been narrowed from about a 10 MHz spread in the uncontrolled mode to about 1 MHz. This clearly established that the mirror system was functioning, but the errors introduced by the system exceeded control limits.

To assess the character of the inherent perturbations, the error signal spectrum was monitored (Figure 58). Several features are of note. First, there appears to be a strong perturbation source at 30 Hz. Based on previous data, a strong correlation to a component vibration (resonance) driven by the

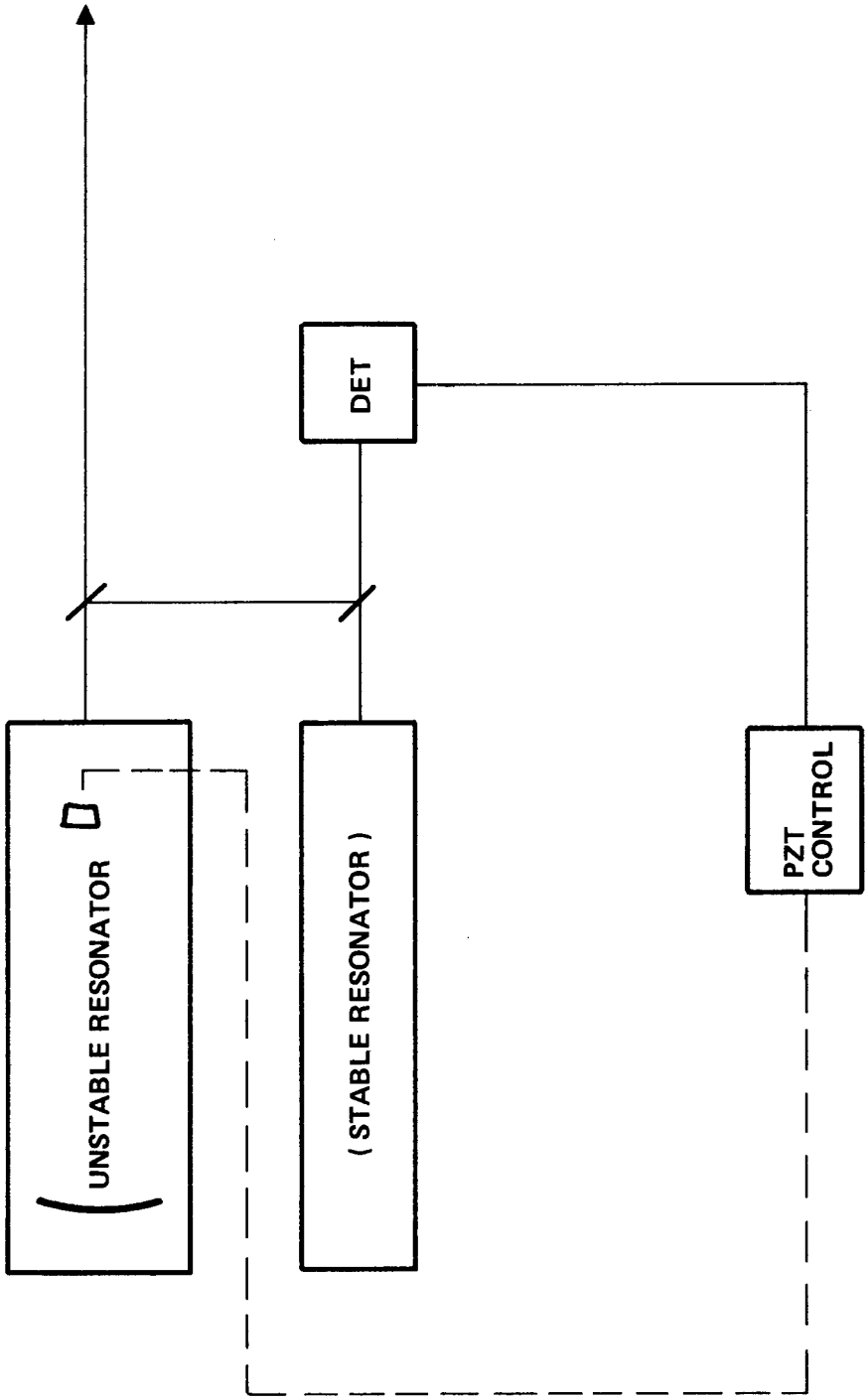

Figure 56. Phase Lock Tests HEL to Low Power Reference

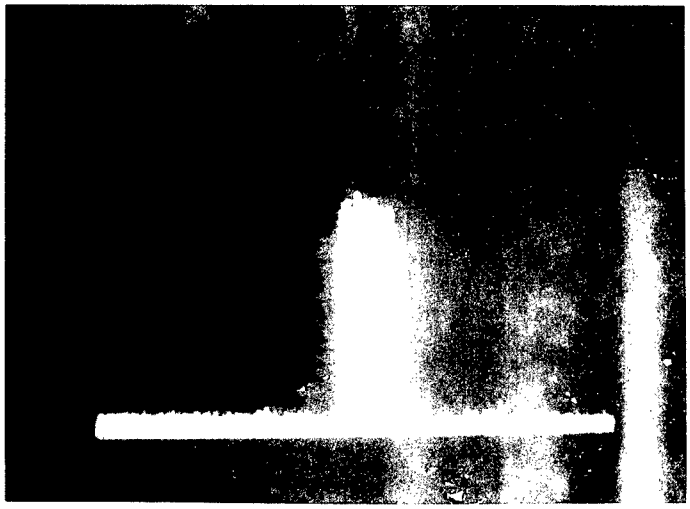

DISPERSION – 1 MHz/DIV
CENTER FREQUENCY – 10 MHz

Figure 57. Spectrum of HEL Heterodyne Lock Signal (Frequency Lock Condition)

DISPERSION – 50 Hz/DIV
RESOLUTION – 10 Hz
LINEAR SCALE

0

Fig. 58. Spectrum of HEL Mirror Control Signal in Frequency Lock Mode

blower at 30 cps is suspected. However, given the low frequency content and with the known mirror response, total compensation by the control loop is to be expected.

Second, the mirror appears to be responding out to about 450 Hz with a significant contribution apparent at 250 Hz. However, previous data again indicate that significant perturbations are present in the system at 450 Hz. Since phase lock operation requires a "total" compensation of all error sources, any deficiency in response causes the system to "slip" cycles. This appears to be the case in this instance; not enough control bandwidth.

To evaluate the amount of improvement required in the mirror response, the test system was modified to that shown in Figure 59. With this hybrid system technique, wide band response is furnished by the E-O modulator to maintain the relative frequency between lasers in lock with an external reference (part of the processor).

The test procedure, in this case, is to establish the system in a phase lock mode and monitor the error signals to each control element. With a known response factor for each part of the system, the relative contribution from each is readily calculable.

When brought up to operational power levels, the system performed as described. Complete phase lock was established, as shown by Figure 60. The heterodyne signal was limited by the digital processor and compared to the external reference. Very little phase jitter is present, as a result of the additional response provided by the E-O modulator. Comparison of the piezo and E-O control signals illustrates the high frequency content of the E-O signal necessary for the phase lock condition. The relative contribution can be ascertained from the independent spectra of both control

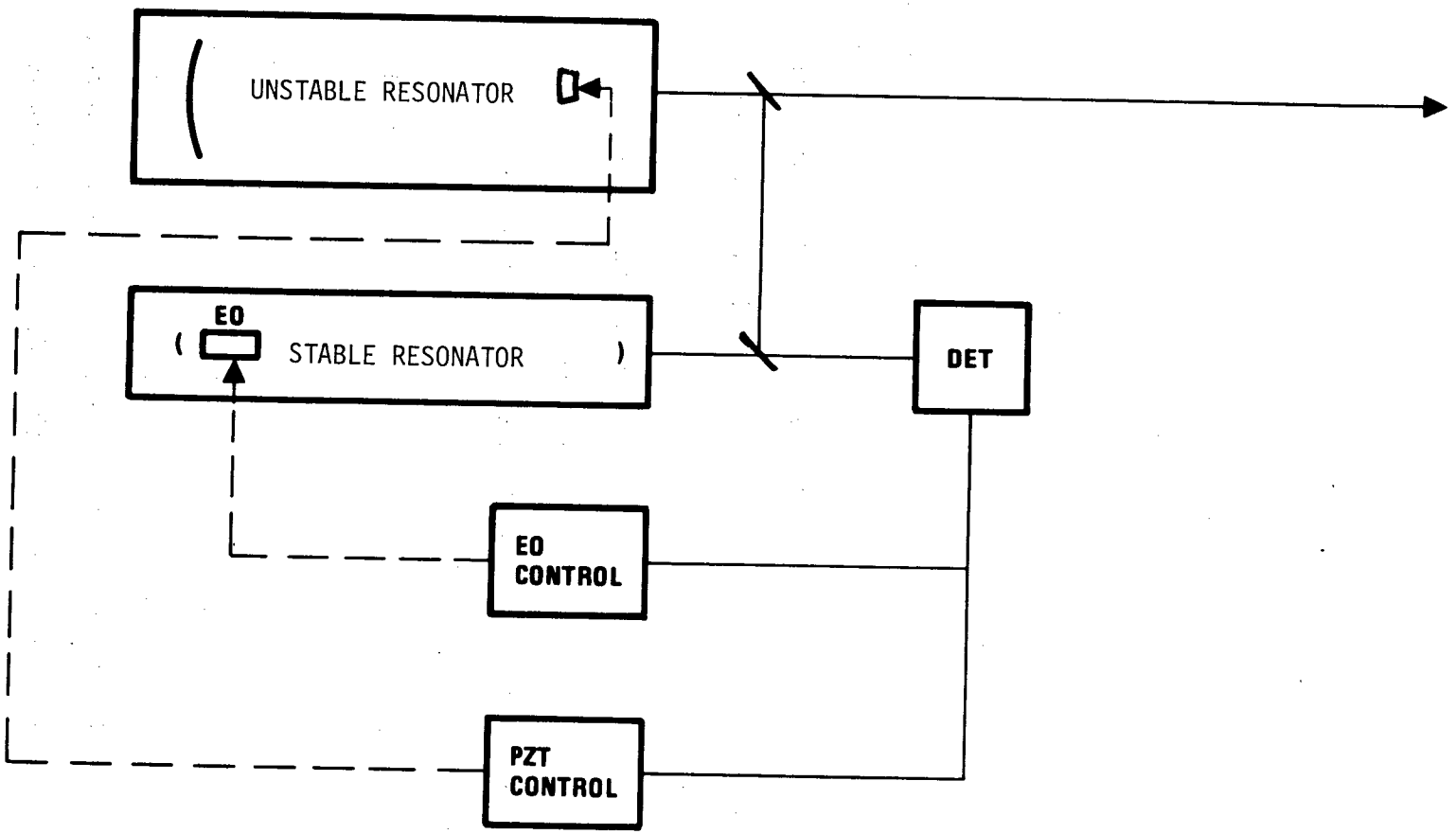

Figure 59. Phase Lock Tests HEL to Low Power Reference

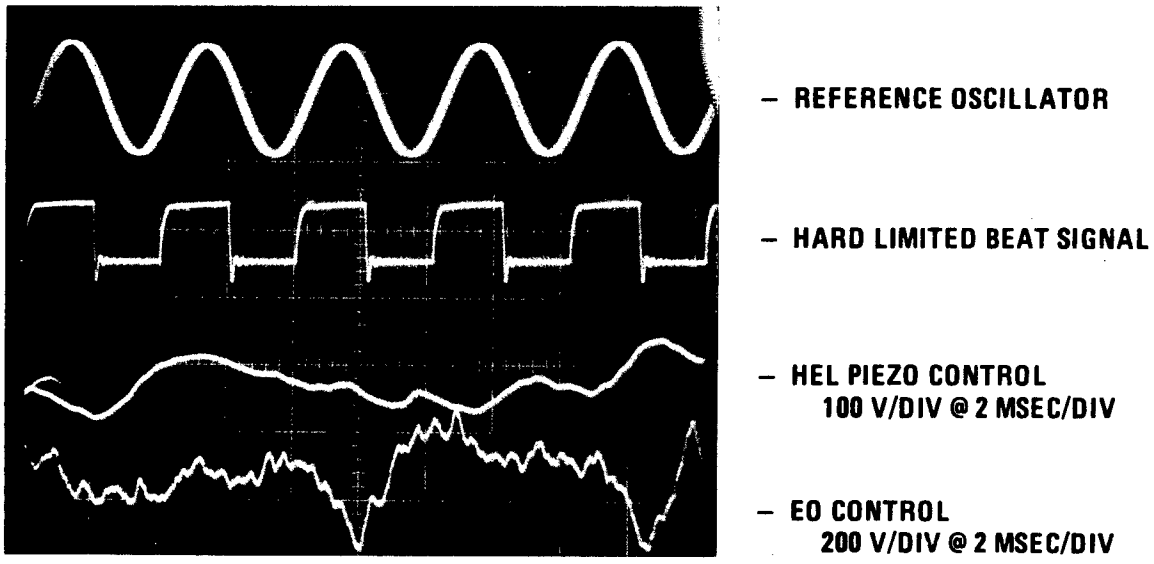

Figure 60. Phase Lock Tests HEL Locked to Low Power Laser

signals. Consider the spectrum of the HEL mirror control signal of Figure 61. When compared with the frequency lock spectrum of Figure 58, qualitatively, there does not appear to be any significant differences. This leads to the conclusion that the higher frequencies are compensated by the E-O modulator as the means of achieving the phase lock condition.

In terms of frequency deviations present in the two-meter cavity, the 4 v rms piezo signal at 250 Hz corresponds to a frequency spread of about 33 KHz. The contribution of the E-O modulator/cavity control signal is about 90 KHz at 250 Hz (see Figure 62). Thus, a significant portion of the control function has been "picked-up" by the wide band system. This is further accentuated at frequencies approaching 500 Hz.

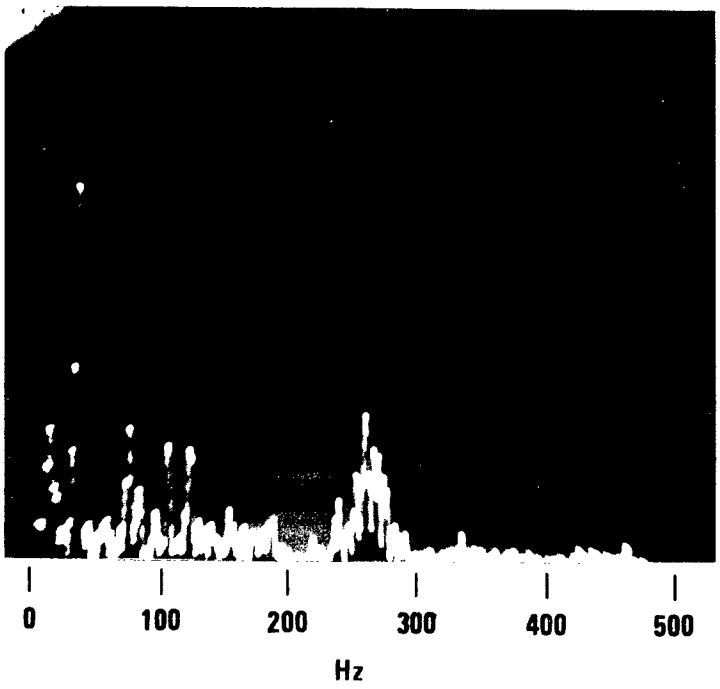

2 V RMS/DIV

Figure 61. Phase Lock Tests Spectrum of HEL Mirror Signals

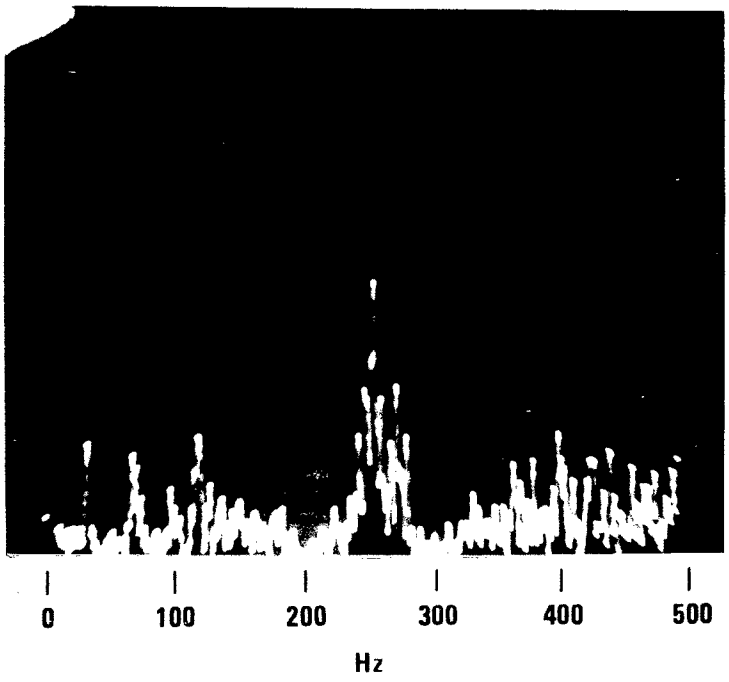

10 V RMS/DIV

CAVITY SENSITIVITY - 800 Hz/VOLT

Figure 62. Phase Lock Tests Spectrum of E-O Signal

In summary, these final sequence of tests conclusively demonstrate the viability of generating high power outputs through use of phase control technology. Control of the present system is limited by the response (bandwidth) of the movable cavity mirror. Time did not permit the redesign of the present mirror for extended response. As an alternative, elimination of the basic error sources within the system may permit operation with the present design. In either case, the results show the high power system to be within the realm of complete phase control.

VII. CONCLUSIONS

Previous to this program, studies were conducted to assess the feasibility of delivering substantial quantities (5 Mw) of power to satellites from a ground-based station. Four candidate systems were considered and one, a multielement array of phase locked laser oscillators, was selected for detailed analysis (NASA CR-134952). The principal conclusion of that study was that a system for transmitting large amounts of power to satellites can be developed to operate with reasonable efficiency using, for the most part, components and devices which are reasonable extensions of the state of the art.

This program has been directed toward answering some of the basic issues which arise in mechanizing an array of high power laser oscillators. The basic tool for answering some of the operational questions has been the closed-cycle, multiple channel, electrical discharge laser (EDL) with unstable resonator optics situated at the NASA Lewis Research Center. Among the topics which have been addressed are:

1. Phase lock operation of unstable resonators.
2. Frequency characteristics of the LeRC HEL.
3. Power/polarization characteristics of the LeRC HEL.
4. Multiple cavity interaction.
5. Analysis and design of a piezo-driven, water-cooled mirror, and
6. Phase lock operation of one channel of the LeRC HEL.

Initial tests conducted with low power unstable resonator optics demonstrated that previously developed control techniques were applicable. The phase of two resonators were locked to about 5° rms and formed the basis for design of the LeRC HEL processing system.

Additional data were collected to characterize the operational limitations imposed by the high power system. These data show the NASA laser to be a well designed device suitable for phase lock operation. As is to be expected with a system of this magnitude, various perturbations are present which can degrade loop performance.

Phase lock operation by cavity length control, based on a water-cooled, piezo-driven mirror, has been demonstrated when augmented with a wideband control loop. The aforementioned error sources and/or the limited mirror response lead to this mode of operation. However, with engineering, the effect of both these limitations can be overcome and neither detracts in any way from the proof of concept demonstration. Extension to a multiple channel system can be considered as a viable technique.

To pursue this program further, it is recommended that both additional component and system developments be considered. At the component level, as mentioned previously, a mirror possessing more bandwidth is desirable. One feature to incorporate into the design of such a unit would be the means of providing a polarized output. Alignment sensitivity would then be eliminated as a possible error source in the processing algorithm.

At the system level, it is necessary, at this time, to bring all channels of the system up to full power. In that way, any cavity interactions which might be present in the total system could be evaluated (e.g., effects of reduced down-stream gain). At the same time, isolation of mechanical perturbations due to the blower drive can be considered. The observed effect of power/frequency fluctuations can then be eliminated.

With these modifications, the testing program can proceed to a full power evaluation. Phased array operation through the atmosphere with compensation for turbulence can be implemented based on techniques which have already been demonstrated. Such a program is recommended at this time.

With these modifications, the testing program can proceed to a full power evaluation. Phased array operation through the atmosphere with compensation for turbulence can be implemented based on techniques which have already been demonstrated. Such a program is recommended at this time.